DENSITY FUNCTIONAL THEORY STUDY OF ELECTRONIC BAND STRUCTURES OF FLUORENE-BASED CONUGATED POLYMERS

LIN LING

Density Functional Theory Study of Electronic Band Structures of Fluorene-based Conjugated Polymers

by

© Lin Ling

A thesis submitted to the
School of Graduate Studies
in partial fulfillment of the
requirements for the degree of
Master of Science.

Department of Physics and Physical Oceanography
Memorial University of Newfoundland

Nov 2007

St. John's Newfoundland

Contents

Abbreviations

- **1D** One Dimension(al)
- **AOs** Atomic Orbitals
- **BLA** Bond Length Alternation
- **BZ** Brillouin Zone
- **BW** Band Width
- **DFT** Density Functional Theory
- **EA** Electron affinity
- **Egap** Energy Band Gap
- **EL** Electronluminesence
- **GGA** Generalized Gradient Approximation
- **HF** Hartree-Fock
- **HOCO** Highest Occupied Crystal Orbital
- **IP** Ionization Potential
- **LSDA** Local Spin Density Approximation

- **LCAO** Linear Combination of Atmoic Orbitals
- **LCMO** Linear Combination of Molecular Orbitals
- **LDA** Local Density Approximation
- **LUCO** Lowest Unoccupied Crystal Orbital
- **MOs** Molecular Orbitals
- **MM** Molecular Mechanics
- **MP2** Møller-Plesset Second-order Perturbation Theory
- **OxF**$_n$ Alternating Fluorene Oxadiazole Copolymers
- **OLED** Organic Light-Emitting Diode
- **PEDOT** Poly(ethylenedioxythiophene)
- **PLED** Polymeric Light Emitting Diode
- **PFs** Polyfluorenes
- **PA** Polyacetylene
- **PBC** Periodic Boundary Condition
- **PES** Potential Energy Surface
- **PL** Photoluminescence(fluorescence)
- **SCF** Self Consistent Field
- **STO** Slater Type Orbital

- **TPAF**$_n$ Alternating Triphenylamine-Fluorene Copolymer
- **TBPA** Tris(4-dihydroxyboranylphenyl)amine Polymer
- **Tv** Translation Vector

Abstract

Alternating triphenylamine-fluorene, $TPAF_n$ (n=2,3), and fluorene-oxadiazole copolymers OxF_n (n=2,3) are important components of novel high-efficiency multilayer polymeric blue light-emitting diodes [1]. In this work we investigate their electronic structure properties using a computational approach. For comparison and calibration purposes we also perform the calculations for poly(acetylene) (PA). The band gaps (E_{gap}'s) and band widths (E_{width}'s) are studied with the Hartree-Fock (HF) and density functional theory (DFT) approaches. The polymers are treated as one-dimensional (1D) infinite conjugated chains with periodic boundary condition. We consider a number of DFT exchange correlation functionals: B3LYP, O3LYP, OB95, PBEPBE, PBE1PBE and TPSSTPSS and employ the 6-31G* basis set and 32 k points in most of our calculations. We compare our results with experimental values whenever possible. The results show that HF method overestimates the band gap of trans-PA by 2.0 eV while the DFT theory underestimates it by 0.20 eV or more. In all DFT calculations with various functionals, B3LYP, O3LYP, OB95, PBEPBE, PBE1PBE and TPSSTPSS, all band gaps are direct and the best agreement with experiment is obtained with the B3LYP and O3LYP functionals for the fluorene-based polymers. The variation of bond length alternations (BLA's) and dipole moments as related to band gaps are discussed.

Acknowledgements

I would first like to thank my supervisor, Dr. J. B. Lagowski, for being extremely helpful and understanding during my graduate study. I would not be able to go so far in my research career without her help and encouragement over the two years. And I appreciate so much her encouragement for my personal growth and maturity.

I would also like to thank Dr. Michael Morrow for his help during my graduate studies.

Also, I appreciate the financial support from the National Science and Engineering Research Council of Canada for their partial funding in this research. The computations were performed on the computational facilities at ACE-net, Westgrid and CVC at MUN. I would like to convey my thanks to Mr. Fred Perry and Mr. Mark Staveley for their computational help.

Finally I would like to thank my parents and my husband Luc Beaulieu for giving me support and being good listeners when I met difficulties in Canada.

List of Tables

List of Figures

Chapter 1

Introduction

1.1 Electroluminescent Polymers

Electroluminescence (EL) is a phenomenon often observed in amorphous, disordered organic semiconducting materials. It was first observed in inorganic compounds (ZnS phosphors) in 1936 [2]. We confine the description of light-emitting polymers to the unique aromatic organic molecules that exhibit semiconducting behavior and give off light when electrically stimulated [3]. The majority of conjugated semiconductors exhibit good hole-transporting properties [4, 5]. Conjugated polymers have a framework of alternating single and double carbo-carbon (sometimes carbon-nitrogen) bonds that are formed by a overlapping π molecular orbitals that are delocalized along a polymer chain backbone. Organic conjugated polymers are also known for the photoluminescent (PL) properties which are displayed when they are stimulated by long-wave ultraviolet (UV) irradiation. Light is produced in the polymer by the fast decay of excited molecular states.

EL efficiency can be measured by the number of photons emitted per electron injected.

Light emitting layers are usually deposited by spin coating (a procedure that involves the application of a uniform thin film to a flat substrate). Usually, the organic light-emitting device (OLED) is operated on with the use of a continuous DC or AC power. The efficiency of the basic OLED (one consisting of one light-emitting layer in combination with a anode and a cathode) is usually improved by the multilayered device design [6].

The performance of polymeric light-emitting diodes (PLEDs) has been considerably improved over the past twenty years. For example, a Japanese group recently designed a three-layer PLED [7]. In general, PLEDs offer a low-cost, thin-film approach with reduced manufacturing process complexity. Polyacetylene (PA) is the simplest of the organic conjugated polymers and it is known to produce low PL upon $\pi - \pi*$ transitions. However, one of the most studied polymers for PLEDs is poly(phenylenevinylene) (PPV). In 1990, the Cambridge group led by Friend announced that they have achieved green-yellow EL using PPV in a single-layer device structure [8]. In 1991, Heeger and co-workers at the University of California reported the EL application of a soluble derivative of PPV [9, 10]. More recently, K. Yoshino and co-workers prepared the wide-band-gap polymer polyfluorene (PF) using the ferric chloride oxidative route [11] which is known to emit blue light. Many other reports of advances in the field of PLEDs have been made [12, 13, 14, 15, 16, 17, 18, 19]. Over the years a number of derivatives of PPV and other polymers (such as PFs) have been proposed for use in PLEDs.

In a light-emitting device, optimal efficiency is achieved where the respective electrode work functions closely match the valence (ground) and conduction (excited state) energy levels in the polymer. Charge imbalance in the emissive layers is one of the main reasons for low luminous efficiency and high operating voltage. Tang and co-workers

employed a transparent hole-injecting electrode of mixed-metal oxide indium tin oxide (ITO) on glass to improve the extraction of light [20]. ITO has a high work-function, which matches the HOMO energy level of PPV and makes it convenient for hole injection. The new technique of constructing multilayered assembly by consecutively alternating absorption of polyelectrolyte has been developed recently [21, 22].

Over the past decade, fluorene-based conjugated polymers have emerged as a promising class of blue light-emitting materials because of their high PL and EL quantum efficiencies. Moreover, their thermal stability, good solubility and ease of processability are of great importance during their synthesis. PFs and other fluorene-based polymers are excellent film formers and are soluble in conventional organic solvents. Their lowest unoccupied crystal orbital (LUCO) and highest occupied crystal orbital (HOCO) energy levels can be obtained by Cyclic Voltammetry in conjunction with UV/vis spectrometry [23].

As shown in Figure 1.1, a basic light-emitting device mainly includes electron transport layers such as OxF_2, OxF_3 and hole transport layers such as $TPAF_2$ and $TPAF_3$. These thin-film structures of layers are typically no more than 0.1 μm thick. In addition, optically transparent anode and metallic cathode and DC or AC power sources are used. The conducting polymer layers are deposited on ITO by spin-coating in solution. EL occurs when a singlet exciton, formed by the Coulombic combination of electron and hole pairs with opposite spin states, decays to the ground state of the molecule.

Given the brief history of PLEDs above, computer simulations may play an important role in the understanding of materials behavior at a microscopic level, provided a certain level of reliability of the modeling and theoretical approach is guaranteed [25, 26, 27, 28]. However, the theoretical models that describe the complete and

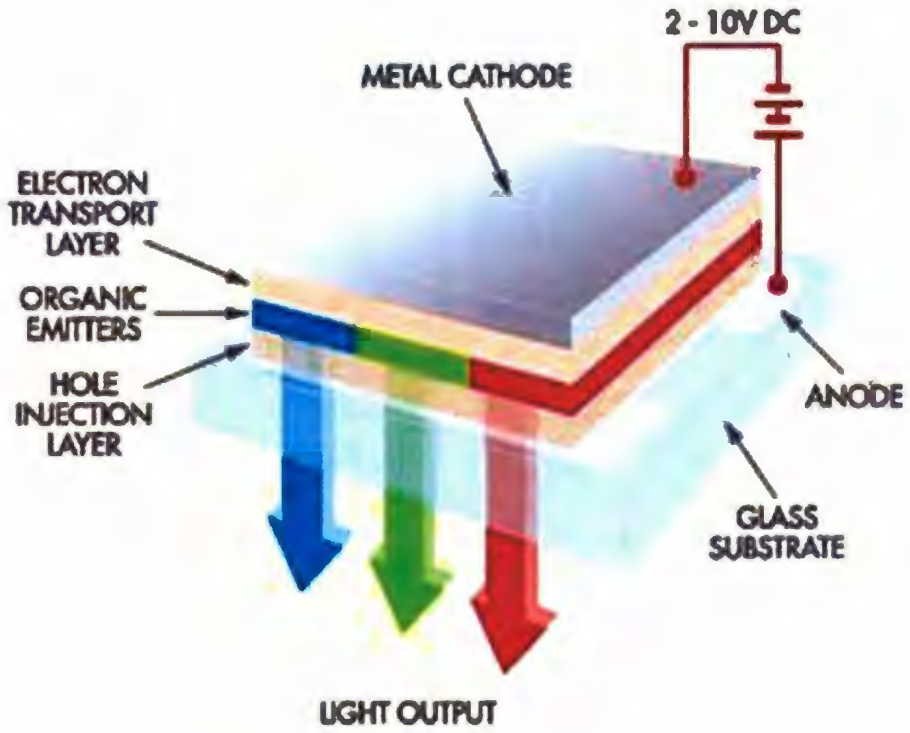

Figure 1.1: Typical design of an OLED showing optional electron and hole transport layers [24].

detailed physics of operation do not yet exist. Unlike crystalline inorganic semiconductor material, organic semiconductors are not well suited to the electronic energy band structure calculations. It is the main aim of this thesis to test the current computational approaches on the organic polymers. That is, we compare computational results as obtained from the electronic structure calculations with the corresponding experimental values and determine which computational approach is best suited for the electronic structure studies of these materials.

1.2 Current Research

In this thesis, we consider a typical PLED device as designed in 2005 by Lu et al. [1]. The energy diagram of this PLED device is shown in Figure 1.2. On the left, $TPAF_n$ and PEDOT are called hole-transport materials while the other three layers refer to electron-transport and light emitting materials. The upper energy levels (around 2 eV) are electron affinities (EA) and the lower ones (around 5 eV) are ionization potentials (IP). Electrons are injected from the low work function Mg/Ag cathode, go through all layers and then flow out from the high work function ITO anode. The light-emitting efficiency is closely tied to the energy gap of $\pi - \pi*$ (LUCO-HOCO) transitions. The color of the emitted light is controlled by E_{gap} which is the energy difference between IP and EA. Experimentally, the E_{gap} is related to the wavelength of the first absorption band in the electron spectrum of the substance. Charge recombination within the chromophilic polymer results in excited states which decay and emit photons. Unless the energy barriers between the anode (cathode) IP (EA) and the HOCO (LUCO) energy level of the polymers are closely matched, one type of charge carrier (either holes or electrons) will be preferentially transported and the recombination of a hole with an electron will decrease, resulting in the lower

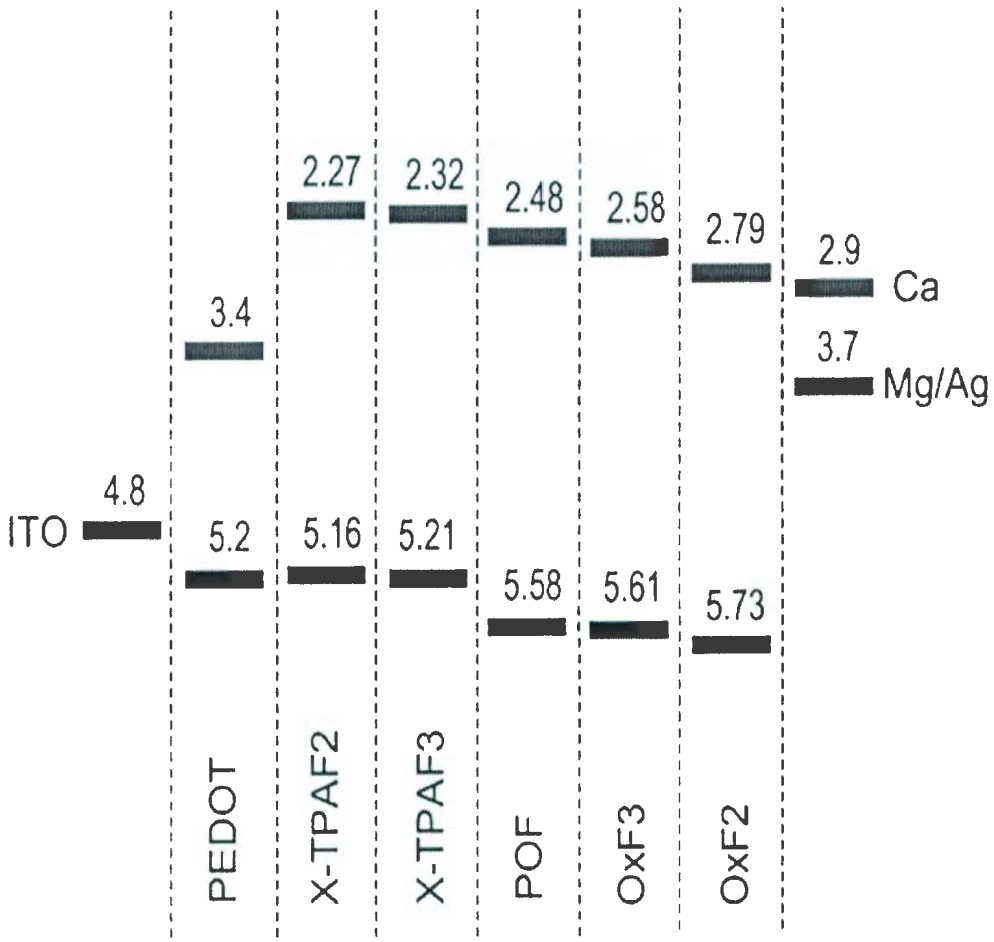

Figure 1.2: The energy diagram of the PLED compounds [1].

efficiency of the device.

The theoretical/computational approach applied to conjugated polymers involves many methods, from the simple free-electron molecular orbital approach to *ab initio* methods. For extended systems such as polymers, one-dimensional, infinite π-conjugated chains with periodic boundary condition (PBC) are used in solid state calculations. More recently, some research has been presented on the effect of disorder, the inter-chain and three-dimensional effect, lattice quantum fluctuations, doping effects and the semiconductor-metal transitions [29, 30, 31, 32].

The properties of PAs and PFs have been well studied [33, 34, 35]. The latest experimental investigations report considerable improvement of EL and PL efficiency in PFs [36]. The computational approach is a promising aid in the synthesis of materials with low band gap or desired IP and EA. For fluorene-based polymers investigated in this thesis, the novel aspect is the inclusion of oxadiazole group in the fluorene chain (which increases its PL efficiency significantly) and the hydroxyl end groups (which improves the cross linkage between the chains) in the fluorene side chains.

We have employed density functional theory (DFT) for all the calculations. We calculated the electronic band structures of 1D infinite conjugated organic chains. The calculated results show a reasonably good agreement with experimental values.

The outline of this thesis is as follows. Chapter 2 introduces the general history and basic concepts of molecule orbital theory, HF and DFT methods. Major theorems and equations have been listed, such as Born-Oppenheimer approximation, basis set, variational principle, and DFT exchange-correlation functionals etc.

Chapter 3 lists the computational details of Gaussian 03 calculations. The major parameters discussed include theory level, DFT functional, optimization process, k-point and basis set.

Chapter 4 discusses the band structures of 1D PA isomers: trans-PA, cis-PA and meta-PA. These calculations are used as a simple test of DFT calculations before we apply them to fluorene-based polymers. In the case of trans-PA, we also obtain the E_{gap} of infinite chain from finite oligomers. All calculations show that DFT gives more accurate results than HF. In particular, amongst DFT functionals, PBE1PBE gives the best agreement between the calculated and the experimental E_{gap} in trans-PA.

Chapter 5 and Chapter 6 present the energy and geometry results of OxF_n and $TPAF_n$. The calculated fluorene-based polymers' band structures can be directly compared to experimental results in four cases. For these systems, O3LYP and B3LYP give the best agreement with the experimental data (O3LYP underestimates the E_{gap} and B3LYP overestimates it). The E_{width} of fluorene-based polymers are much less than those of PA and are very narrow.

Chapter 7 summarizes the conclusions of this thesis.

Chapter 2

Theoretical Approach

In this chapter, we briefly summarize the theoretical approaches used in this thesis. We review the molecular orbital theory with emphasis on HF approximation and DFT theory which are employed for atomic and molecular systems. The ultimate goal is to investigate the electronic band structure of conjugated 1D polymer chains in the gas phase. Hence, we also briefly discuss the application of HF and DFT methods to extended, infinite 1D systems.

2.1 Molecule Orbital Theory

Molecular orbital theory is concerned with obtaining properties of atomic and molecular systems [37]. The fundamental problem involves finding an accurate solution of non-relativistic Schrödinger equation [38, 39]. The Schrödinger equation is given as follows

$$\widehat{H}\Psi(\vec{r},\vec{R}) = E\Psi(\vec{r},\vec{R}) \tag{2.1}$$

where $\widehat{H}$ is the Hamiltonian, Ψ is the wave function, $\vec{R}$ and $\vec{r}$ stand for all nuclear and electron coordinates and E is the total energy of the system.

The non-relativistic Hamiltonian for a system containing N electrons and M nuclei can be written as

$$\widehat{H} = \widehat{T} + \widehat{V} \tag{2.2}$$

$$\widehat{H} = -\sum_{i=1}^{N} \frac{h^2 \nabla_i^2}{2m_e} - \sum_{A=1}^{M} \frac{h^2 \nabla_A^2}{2m_A} - \sum_{i=1}^{N} \sum_{A=1}^{M} \frac{Z_A e^2}{4\pi\epsilon_0 r_{iA}} + \sum_{i=1}^{N} \sum_{j>i}^{N} \frac{e^2}{4\pi\epsilon_0 r_{ij}} + \sum_{A=1}^{M} \sum_{B>A}^{M} \frac{Z_A Z_B e^2}{R_{AB}} \tag{2.3}$$

where $\widehat{T}$ is the kinetic energy operator that consists of the electron and nuclei kinetic energy terms, and $\widehat{V}$ is the potential energy operator that contains the nuclei-electron attraction, the electron-electron repulsion and the nuclei-nuclei repulsion terms. In the Eq. 2.3, Z_A and m_A are, respectively, the charge and mass of the A_{th} nucleus and m_e is the electron mass. The R_{AB} and r_{iA} are the relative nuclear distance between the A_{th} and B_{th} nucleus and the distance between the i_{th} electron and A_{th} nucleus, respectively. The r_{ij} is the relative distance between the i_{th} and j_{th} electrons. h is *Planck's constant* and ϵ_0 is the permittivity of free space constant.

2.1.1 Hartree-Fock Method

HF is an *ab initio* method, the beginning of which was first introduced to atoms by Hartree in 1928 [40]. In this approximation, the total energy for a molecular system is given by

$$E^{total} = E_{HF} + E_{NN} \tag{2.4}$$

where E_{HF} is the electronic HF energy and E_{NN} is the internuclear Coulumbic repulsion energy. The HF approach serves as an essential zeroth-order approximation to the ground state of interacting electrons. The total electronic energy will be obtained by applying the Born-Oppenheimer (BO) approximation. BO is the first of several approximations used to simplify the solution of the Schrödinger equation (Eq. 2.1). The full many-body electronic wave functions can be expressed as a product of single-particle wave functions (which becomes a Slater determinant when the Fermi statistics of the electrons is taken into account). This leads to a separation of electronic variables and to the complete diagonalization of H in terms of single particle molecular orbitals for the system. Since the mass of a nucleus is 1836 times than that of an electron, it is assumed that nuclei move much slower than electrons. In the Born-Oppenheimer approximation, the nuclear and electronic motions are separated. Correspondingly, the total wave function can be written as a product of electronic and nuclear wave functions

$$\Psi = \Psi_{electrons} \times \Psi_{nuclei}. \tag{2.5}$$

In this BO approximation, the electronic Hamiltonian then becomes

$$\widehat{H} = -\sum_{i=1}^{N} \frac{\hbar^2 \nabla_i^2}{2m_e} - \sum_{i=1}^{N} \sum_{A=1}^{M} \frac{Z_A e^2}{4\pi\epsilon_0 r_{iA}} + \sum_{i=1}^{N} \sum_{j>i}^{N} \frac{e^2}{4\pi\epsilon_0 r_{ij}}. \tag{2.6}$$

Since electrons are fermions, they obey the Pauli exclusion principle. This requires that the total electronic wave function $\Psi_{electrons}$ be antisymmetric with respect to the interchange of the coordinates of the electrons and can be written as a Slater determinant for a $2n$-electron system [41]

$$\Psi(r,s) = (\frac{1}{\sqrt{2n!}}) \begin{pmatrix} \Psi_1(1)\alpha(1) & \Psi_1(1)\beta(1) & \dots & \Psi_n(1)\beta(1) \\ \Psi_1(2)\alpha(2) & \Psi_1(2)\beta(2) & \dots & \Psi_n(2)\beta(2) \\ \vdots & \vdots & \ddots & \vdots \\ \Psi_1(2n)\alpha(2n) & \Psi_1(2n)\beta(2n) & \dots & \Psi_n(2n)\beta(2n). \end{pmatrix} \tag{2.7}$$

The factor $(1/\sqrt{2n!})$ ensures the wave function to be normalized. Here the $\Psi(i)$ is a function of the coordinates of ith electron with the spin α ($\uparrow$) or β ($\downarrow$). The function $\Psi(i)$ is called molecular orbital (MO), and $\Psi(i,\xi)$ ($\xi = \alpha$ *or* β) is referred to as spin-orbital for the i$_{th}$ electron. In this thesis, we are considering the close-shell systems for which all spin orbitals are doubly occupied [42].

2.1.2 The Rayleigh-Ritz Variational Theorem

Given the electronic Hamiltonian (Eq. 2.6) and the electronic wave function (Eq. 2.7), the total electronic energy is given by the following general equation [43]

$$E[\Psi] = \frac{\int \Psi^* \hat{H} \Psi d\tau}{\int \Psi^* \Psi d\tau} \tag{2.8}$$

where $d\tau$ stands for spatial and spin coordinate, $dxdydzd\xi$, for all electrons.

The variational theorem states that the energy calculated with any arbitrary wave functions must be greater than or equal to the exact HF ground-state (gs) energy

calculated with the true ground-state HF wave function [42]

$$E[\Psi'] \geq E[\Psi_{gs}^{HF}]. \tag{2.9}$$

Applying the variational principle to Eq. 2.8, we obtain the n integro-differential HF equations

$$\hat{\mathbf{F}}(\mathbf{r})\Psi_i(\mathbf{r}) = \epsilon(\mathbf{r})\Psi_i(\mathbf{r}) \tag{2.10}$$

where $\hat{\mathbf{F}}(\mathbf{r})$ is defined as

$$\hat{\mathbf{F}}(\mathbf{r_1}) = \hat{H}^{core}(\mathbf{r_1}) + \sum_{i=1}^{n}(2\hat{J}_i(\mathbf{r_1}) - \hat{K}_i(\mathbf{r_1})). \tag{2.11}$$

The $\hat{\mathbf{J}}(\mathbf{r})$ is the coulomb operator and $\hat{\mathbf{K}}(\mathbf{r})$ is the exchange operator (which we shall discuss next).

2.1.3 The HF Electronic Energy and Equations

Substituting the Slater determinant for Ψ and the explicit form of the Hamiltonian operator $\widehat{H}$ into Eq. 2.6 gave the following equation for the energy

$$E = 2\sum_{i=1}^{n} H_{ii} + \sum_{i=1}^{n}\sum_{j=1}^{n}(2J_{ij} - K_{ij}). \tag{2.12}$$

H_{ii} presents the electronic energy of a single electron in the surrounding force field of a nuclear core and is given by

$$H_{ii} = \int \Psi_i^*(1)\hat{H}^{core}\Psi_i(1)d\nu \tag{2.13}$$

where $d\nu = dxdydz$. The next two terms in Eq. 2.9 account for the electron-electron interactions [44, 45]. J_{ij} is called the coulomb integral and it represents the electronic repulsion between the electrons in states Ψ_i and Ψ_j, and it is given by

$$J_{ij} = \int \Psi_i^*(1)\Psi_i(1)(\frac{1}{r_{ij}})\Psi_j^*(2)\Psi_j(2)d\nu_1 d\nu_2. \tag{2.14}$$

K_{ij} is referred to as an exchange integral and it accounts for the exchange correlation between electrons of the same spin. It is given by the following equation [42]

$$K_{ij} = \int \Psi_i^*(1)\Psi_i(2)(\frac{1}{r_{ij}})\Psi_j^*(2)\Psi_j(1)d\nu_1 d\nu_2. \tag{2.15}$$

2.1.4 Basis Set

In 1951, Roothaan and Hall independently pointed out that MO's, $\Psi(i)$, can be expanded as a linear combination of basis functions, (often refer to as a linear combination of atomic orbital (LCAO)) [46], that is,

$$\Psi_i = \sum_{s=1}^{m} C_{si}\phi_{si} \qquad i = 1, 2, 3 \ldots, m \qquad (m = MO) \tag{2.16}$$

where C_{si} are the molecular orbital expansion coefficients and ϕ_{si} denotes the basis functions. The widely used basis functions are Slater-type or Gaussian-type functions. In our calculation, we are using the Gaussian-type basis functions [47].

2.1.5 The Roothaan-Hall Equations

Substituting the basis functions' expansions for the MO's into the HF equations (Eq. 2.10), we obtain a total of $m \times m$ equations,

$$\sum_{s=1}^{m} F_{rs} C_{si} = \epsilon \sum_{s=1}^{m} S_{rs} C_{si} \tag{2.17}$$

where the Fock matrix elements F_{rs} are

$$F_{rs} = \int \phi_r \hat{F} \phi_s d\nu \tag{2.18}$$

and the overlap matrix elements S_{rs} are

$$S_{rs} = \int \phi_r \phi_s d\nu. \tag{2.19}$$

In the Roothaan-Hall approach, the matrix form of algebraic HF equations is

$$\mathbf{FC} = \mathbf{SC}\epsilon. \tag{2.20}$$

The total HF energy is given by

$$\begin{aligned} E_{HF} &= 2\sum_{s=1}^{m} F_{rs} C_{si} + \sum_{s=1}^{m} S_{rs} C_{si} \epsilon_{ij} \\ r &= 1, 2, 3, \ldots, m \quad \text{(for each } i = 1, 2, 3, \ldots, m) \end{aligned} \tag{2.21}$$

where ϵ_{ij} are the elements of the Lagrange multiplier matrix (introduced during the constrained minimization of the total energy) that are related to the molecular orbital

energies. The Roothaan-Hall-Hartree-Fock equations are solved iteratively in a self consistent way. The process starts from initial guess for the molecular orbital MO's Ψ and then the matrix elements F_{rs} and S_{rs} are calculated. The eigenvalues ϵ_{ij} and eigenfunctions C_{ij} of equation Eq. 2.17 are obtained. This process is repeated until the initial and final MO's are the same within the convergence criteria [48].

2.2 DFT Method

The main weakness of HF approximation is that it only accounts for part of electron-electron interactions. The HF approximation is a type of a mesn field theory that treats the exchange interaction between the electrons exactly, but it neglects the interactions between the electrons with the same spin. The DFT is one of the post-HF approaches that includes the electron correlations beyond the HF approximation. The main variable in DFT is the electron density $\rho = \Psi * \Psi$ rather than the electronic wave function Ψ [49, 50, 51].

2.2.1 Hohenberg-Kohn Theorems

The basis of the DFT theory was formulated by Hohenberg and Kohn in 1964 [52]. They stated two theorems. The first Hohenberg-Kohn theorem is an existence theorem that says that any ground state energy of a molecular system is a functional of the ground state electron density, ρ_0, moving in the presence of a external potential v(r),

$$E_0 = E[\rho_0]. \tag{2.22}$$

The exact ground state energy functional form is not known. The second Hohenberg-

Kohn theorem uses the variational principle that says that any trial electron density gives energy higher than the true ground state energy calculated with the ground-state electron density function, that is,

$$E_v[\rho_t] \geq E_0[\rho_0] \tag{2.23}$$

where the E_v is the electronic energy of the system.

2.2.2 Kohn-Sham Equations

The ground state electronic energy in DFT theory can be written as follows

$$E_0 = \int \rho_0(\mathbf{r})\nu(\mathbf{r})d\mathbf{r} + < T[\rho_0] > + < V_{ee}[\rho_0] > \tag{2.24}$$

where the $< T[\rho_0] >$ is the kinetic energy of electrons, $\int \rho_0(\mathbf{r})\nu(\mathbf{r})d\mathbf{r}$ is the potential energy due to electron-nucleus interactions, and $V_{ee}[\rho_0]$ is the potential energy due to the electron-electron interactions. The exchange-correlation energy functional E_{xc} is defined as the sum of the kinetic energy deviation from the reference system and the electron-electron repulsion energy deviation from the classical system

$$E_{xc}[\rho_0] = \Delta < T[\rho_0] > + \Delta < V_{ee}[\rho_0] >. \tag{2.25}$$

The use of the variational principle leads to the formulation of Kohn-Sham equations [53]

$$[-\frac{1}{2}\nabla^2 + \nu_{eff}(r)]\psi(\mathbf{r}) = \varepsilon_i\psi(\mathbf{r}) \tag{2.26}$$

which are similar to HF equations, except that the effective potential $\nu_{eff}(r)$ is given

by

$$\nu_{eff}(r) = V_c + \nu_{xc}(\mathbf{r}) = \nu(\mathbf{r}) + \int \frac{\rho(\mathbf{r}')}{|\mathbf{r} - \mathbf{r}'|} d\mathbf{r}' + \frac{\delta E_{xc}}{\delta \rho(\mathbf{r})},$$

an expression that includes an additional exchange-correlation potential ν_{xc} which is the functional derivative of exchange-correlation energy functional E_{xc}. The V_c is the classic term including the first two terms in the above equation.

2.2.3 The Exchange-Correlation Energy Functionals

The form of the exchange-correlation energy functional is unknown, and various approximations are used for E_{xc}, for example, local spin density approximation LSDA functional [54], generalized gradient approximation (GGA) or hybrid functionals [55]. In general, the exchange-correlation energy term can be separated into two terms, exchange and correlation energies: $E_{xc} = E_x + E_c$.

The simplest approximation of E_{xc} is the local density approximation (LDA) [56] or local spin density approximation LSDA functional [54]

$$E_{xc}[\rho] = \int \epsilon_{xc}[\rho]\rho d\mathbf{r} \tag{2.27}$$

where ϵ_{xc} is the exchange-correlation energy for a homogeneous electron gas with density ρ [57]. It applies to a uniform electron gas with the nuclei fixed. An improvement to LSDA functional involves GGA and hybrid functionals [55]. In most recent applications, the hybrid functionals have given the most accurate results [58]. In this work, we focus on the hybrid functionals.

In the hybrid methods, the exchange functional is a linear combination of the HF

exchange and a functional integral of the density and the density gradient [59]

$$E_{hybrid}^{XC} = c_{HF}E_{HF}^{X} + c_{DFT}E_{DFT}^{XC} \tag{2.28}$$

where the c_{HF} and c_{DFT} are adjustable coefficients. One of the most often used hybrid functionals is one due to Becke called B3LYP. It includes HF and DFT exchange along with DFT correlation energies and has the form

$$\begin{aligned} E_{xc}[B3LYP] &= (1 - a_0 - a_x)E_x[LSDA] + a_0E_x[HF] \\ &+a_xE_x[B88] + (1 - a_c)E_c[VWN] + a_cE_c[LYP]. \end{aligned} \tag{2.29}$$

The $E_x[LSDA]$ is the LSDA non-gradient-corrected exchange functional, $E_x[HF]$ is the KS-orbital-based HF exchange energy function, $E_x[B88]$ is the Becke88 exchange functional, $E_c[VWN]$ is the VWM term (VWN is the Vosko, Wilk and Nusair functional introduced in 1980 [57]) and $E_c[LYP]$ is the LYP correlation functional (due to Lee, Yang and Parr which includes both local and non-local terms [60]). The a_0, Ra_x, a_c are parameters that give the best fit of the calculated energies to experimental molecular energies [61].

In 2001, Handy and Cohen introduced a new exchange functional called optimized exchange functional (OPTX) that meant to correct the failures of the current exchange functionals in describing the π-conjugated systems. The OLYP functional as defined by Handy and Cohen [62] essentially replaces B88 by OPTX in Eq. 2.29. The optimized exchange O3LYP is claimed to be superior by Garcia [63, 64]. It is similar to B3LYP but with slightly different mixing coefficients (in particular, the coefficient for HF exchange is reduced from 0.20 to 0.1161) Both B3LYP and O3LYP can be

written as

$$\begin{aligned} B3LYP &= 0.2 * XHF + 0.8 * XS + 0.72 * XB88 + 0.19 * VWN + 0.81 * LYP \\ O3LYP &= 0.1661 * XHF + 0.9262 * XS + 0.8133 * OPTX \\ &\quad +0.19 * VWN5 + 0.81 * LYP \end{aligned} \tag{2.30}$$

where the XHF is the HF exchange, XS is the Dirac-Slater exchange, other terms are defined as before in Eq. 2.29 [64]. Compared with B3LYP, O3LYP has a reduced HF-exchange contribution, a larger coefficient multiplying OPTX compared to B88, and a different local correlation functional, VWN5 compared to VWN. Other functionals that we have employed in our calculations are: the B95 correlation functional that stands for Becke's τ-dependent gradient-corrected correlation functional [65]; PBEPBE which is the exchange functional proposed by Perdew, Burke and Ernzerhof in 1996 [66]; and the TPSSTPSS (meta-GGA) [67] and PBE1PBE [68].

2.3 Solid State Electronic Band Structure Calculation

In solid state physics, energy bands are formed by splitting the atomic energy levels when the atoms approach one another in a crystal or a polymer [69] (see Figure 2.1). The band gap (E_{gap}) is defined as the energy required for one electron to jump from the top of valence band to the bottom of conduction band. In this way, we can divide materials into insulators, semiconductors and conductors. Most semiconductors have band gaps less than 2.0 eV. For conducting polymers, the latest research reports the

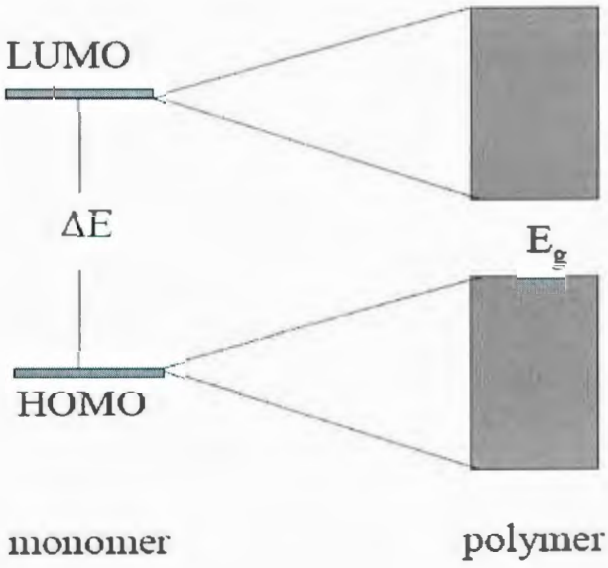

Figure 2.1: The band structure in solid state [71].

smallest band gap to be 0.5 eV [72].

Both HF and DFT method can be applied to the solid state calculations. For a periodic arrangement of nuclei, the single electron wave functions $\Psi_n(\mathbf{r})$ (where n corresponds to a given atomic level with eigenvalue E_n) can be expressed with the help of the Bloch's Theorem [73]. That is, in the periodic potential, each atomic wave function $\Psi_n(\mathbf{r})$ would yield N levels wave functions $\Psi_n(\mathbf{r}+\mathbf{R})$ where $\mathbf{R}$ is the Bravais lattice vectors such that they satisfy the Bloch condition

$$\Psi(\mathbf{r}+\mathbf{R}) = e^{i\mathbf{k}\cdot\mathbf{R}}\Psi(\mathbf{r}). \tag{2.31}$$

Given the above equation, the single electron wave function can be written

$$\Psi_{n\mathbf{k}}(\mathbf{r}) = \sum_{\mathbf{k}} e^{i\mathbf{k}\cdot\mathbf{R}}\phi(\mathbf{r}+\mathbf{R}) \tag{2.32}$$

where $\mathbf{k}$ ranges through the N values in the first Brillouin zone, and the $\phi(\mathbf{r}+\mathbf{R})$ can be atomic or molecular spin orbital. The atomic orbital can then be expanded in terms of a linear combination of N basis functions. This approximation is referred to as LCAO method in solid state [69]. The substitution of expanded wave function into the Schrödinger equation results in HF or KS like eigenvalue-eigenfunction equations depending on the level of approximation used [70]. Because of the translational symmetry in 1D polymer case, the HF or KS like equations are solved in a self-consistent way in the first Brillouin zone with $-\pi/a \leq k \leq \pi/a$ where the a is the translational vector along the chain backbone [71, 72, 73].

In addition to the solid state approach, the band gaps can be approximated as the energy differences between EA and IP energies, where the values of IP and EA energies are obtained by taking the negative of the highest occupied (HOMO) and lowest unoccupied (LUMO) molecular orbital eigenvalues in molecular system calculations.

Chapter 3

Computational Details

All calculations in this thesis have been performed with Gaussian 03 software package [74] available on the cluster of **Silicon Graphics, Inc** (SGI) machines at Memorial University ACEnet facilities and the computers at Westgrid at University of Calgary. The average CPU usage on Ace-net machines is 4 CPUs per job and the requirement of the memory is 128-200 MB for each CPU. The ACEnet machines support parallel jobs which can speed up our calculations. For PA isomers, it normally takes two hours or half a day, while it may take a week or even weeks for fluorene-based polymers calculations to complete.

We have performed both HF and DFT solid state calculations for trans-PA. For other polymers only DFT calculations were performed [75]. As was discussed in Chapter 2, the following DFT exchange functionals were used: B3LYP, O3LYP, OB95, PBEPBE, PBE1PBE and TPSSTPSS. The basis sets 3-21G, 6-31G and 6-31G* were employed in this thesis. The main basis set used in this work is the polarized split-valence basis set 6-31G*. It comprises a linear combination of six gaussian primitives for the inner-shell functions, and three and one gaussian primitives for the two valence shells

[76, 77]. The asterisk * indicates the addition of the six d-type primitives to 6-31G basis set to take into account the polarization effect [78].

We use the keyword PBC to specify the 1D solid state calculations in the Gaussian 03 input files. This requires that in addition to the nuclei coordinates, the translational vector (Tv) must be included in the input files. We also specify the number of k points to be used in integration in reciprocal space. We have found that the minimal requirement for k points is 32 in the band structure calculations. Total energy (E_{total}) is the sum of all kinetic energies and potential energies. All the E_{total} mentioned in the thesis refers to the total energy per unit cell. For the purpose of displaying the top occupied and unoccupied bands in the first Brillouin zone, we use the keyword **IOp**. This keyword **IOp(5/103= -1)** writes five occupied and unoccupied eigenvalues into the output files which can then be plotted as functions of k points. The analysis of the band structure focuses on the E_{gap} and E_{width} properties. There are two types of band gaps in solid state: direct and indirect gaps. The former one refers to the band gap where LUCO and HOCO occur at the same k point in the reciprocal lattice space; the indirect one occurs at different k points. The E_{gap} is obtained as the minimal energy difference between two bands: HOCO and LUCO, and it is related to the energy barriers for electron transport. The E_{width} is the difference between maximum and minimum for a particular band, the width of which indicates the degree of delocalization inside the system.

All PBC calculations were geometry optimized (mostly using the keyword fopt) in order to find the lowest energy state for the ground state. This involves searching for the global minimum on the potential energy surface (PES) which is satisfied when the gradient of energy with respect to the nuclear coordinates is zero. That is, the stable point or the lowest energy point is obtained from the first- and second-order

derivatives of energy with respect of the nuclear coordinates [48] that satisfy the following conditions

$$\frac{\partial E}{\partial R} = 0 \tag{3.1}$$

$$\frac{\partial^2 E}{\partial^2 R} > 0. \tag{3.2}$$

In fopt approach, both the first- and second-order gradients of energy are determined, while the keyword opt which we used occasionally specifies the calculation of the first-order gradient of energy only.

The criteria of the self consistent force (SCF) convergence are defined as follows: the maximum component of the force is below the cutoff value 0.00045 N; the root-mean-square of the force is below 0.0003 N; the calculated displacement for the next step is smaller than the cutoff value 0.0018 Å; and the root-mean-square of the displacement for the next step is below 0.0012 Å [48].

Both the input and output geometries of the systems have been obtained with the use of Gauss View 3.0 software [79]. This visualization software can be used to set up or measure the bond lengths, bond angles, dihedral angles, and symmetries. As well for the PBC calculation, it aids in setting up the size (Tv) of the unit cell.

The bond length alternation (BLA) measures the degree of the conjugation along the chain. BLA (Δr) of trans-PA system is defined as

$$BLA = \Delta r = R_{c-c} - r_{c=c} \tag{3.3}$$

where the R_{c-c} is the longer single carbon-carbon bond and the $r_{c=c}$ is the shorter

double bond. For larger monomers, BLA is calculated from the average value of $R_{c\ c}$ - r_{c-c} pairs along the fixed direction of Tv,

$$BLA = \Delta r = 1/m(\sum_{i=1}^{m}(R_{c-c} - r_{c=c})) \tag{3.4}$$

where m is the number of R_{c-c} - $r_{c=c}$ pairs. In OxF_1 m=5, in OxF_2 m=9 and in OxF_3 m=13. For the $TPAF_n$, m is 8, 12 and 16 for n=1, 2, 3, respectively.

The magnitude and direction of dipole moment give the information about the charge polarizations in the polymer. The dipole moment is defined as the sum of the products of the charge and the distance between the two charges

$$\mu = \sum_{i=1}^{n} Q_i R_i. \tag{3.5}$$

It is expected that the biggest component of the total dipole moment is along the Tv due to the charge redistribution along the chain backbone. All the calculations are dealing with the close-shell neutral polymer systems. The symmetry for all systems is C1 point group.

Chapter 4

The Electronic Structures of PA

In this chapter we apply 1D solid state DFT method to obtain the electronic band structures of PA isomers: trans-PA, meta-PA and cis-PA. In the case of trans-PA, we also include 1D solid state HF calculations, and briefly discuss the finite system approach of extrapolating the infinite chain band gap from the oligomers. Since all band structures are closely related to geometries of the systems, we discuss the geometrical parameters such as bond lengths, bond angles and dihedral angles including BLA and Tv. The dipole moment trends are also investigated.

4.1 trans-PA

Trans-PA is the simplest zig-zag conjugated carbon-carbon chain [80]. Two unit cells consisting of four CH units of trans-PA are shown in Figure 4.1. In this figure, each carbon atom is connected with two adjacent carbon atoms and one hydrogen atom. In the initial structure, all bonds are set to be equal along the chain backbone. The geometry optimization modifies the intra-cell and inter-cell bonds to achieve the lowest energy state. The resulting structure has alternating shorter and longer bonds

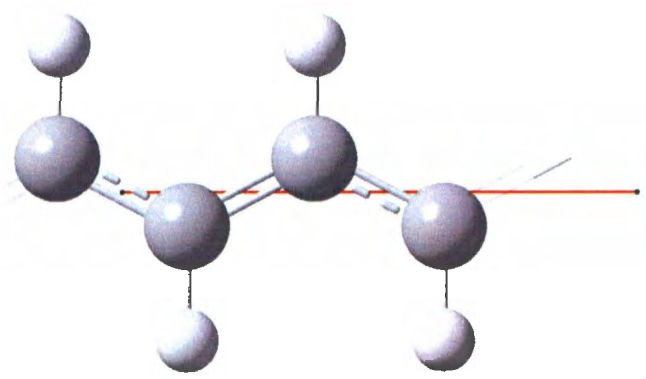

Figure 4.1: Molecular structure of trans-PA (two unit cells are displayed).

along the backbone.

4.1.1 k Points Analysis

Ideally, the number of k points for an extended system is equal to the number of the primitive unit cells [69]. Typically, this is a very large number for bulk systems. For the purpose of computing, smaller number of k points is used. For example, Pino and Scuseria [36] employed 1024 k points for 1D PA system. The number of k points determines the accuracy of reciprocal lattice integrations in solid state computations. However, since we are dealing with relatively large molecular unit cells, it is not feasible to perform computations with a large number of k points for fluorene-based polymers. In Table 4.1 (whose data are also plotted in Figure 4.2), we show how the E_{gap} changes as a function of k points for B3LYP and O3LYP DFT approximations for PA. This table illustrates that even for a very small molecular unit cell such as the one corresponding to PA, a relatively small number of k points is sufficient for (reasonably) accurate calculations of most of its solid state properties.

Table 4.1 and Figure 4.2 show that, for PA, even 32 or 64 k points calculation produces

Table 4.1: IPs, EAs and E_{gap}'s (in eVs) are given as a function of number of k points for B3LYP and O3LYP approximations for trans-PA.

DFT	B3LYP			O3LYP		
no. of k points	**IP**	**EA**	$\mathbf{E_{gap}}$	**IP**	**EA**	$\mathbf{E_{gap}}$
4	5.46	1.60	3.86	5.07	1.85	3.22
12	4.31	2.69	1.62	4.01	2.90	1.12
32	4.12	2.88	1.24	3.86	3.06	0.80
64	4.12	2.87	1.25	3.86	3.18	0.68
128	4.11	2.89	1.22	3.81	3.10	0.71
256	4.11	2.90	1.21	3.81	3.10	0.71
512	4.11	2.90	1.21	3.81	3.10	0.71

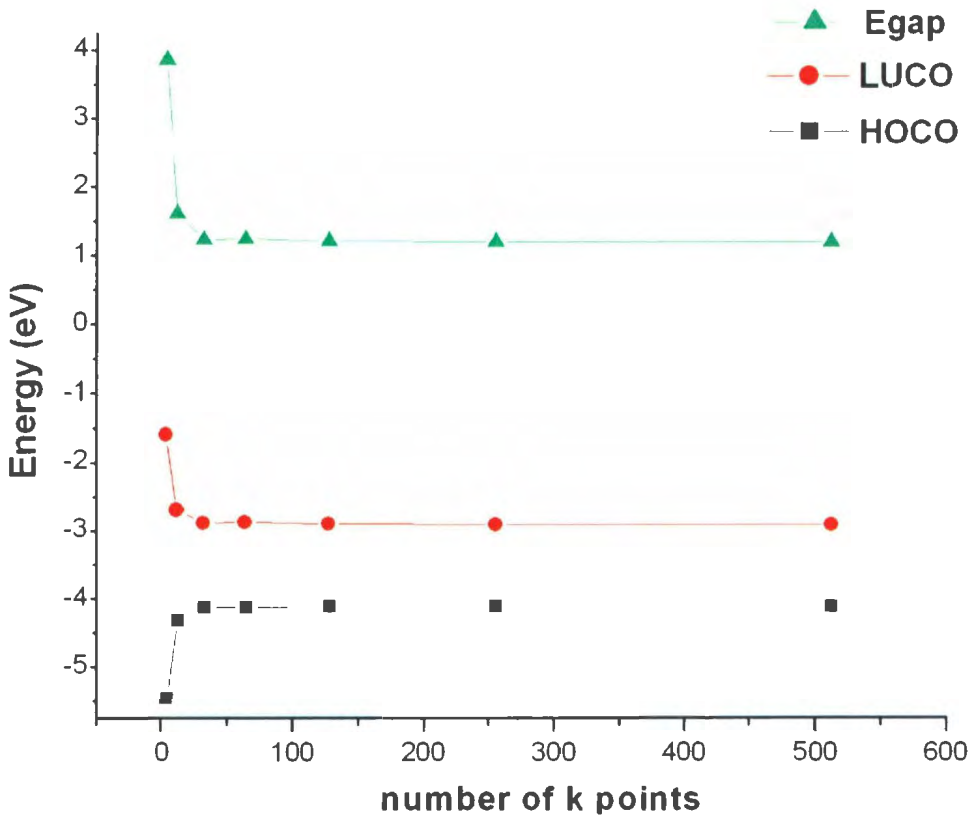

Figure 4.2: HOCO and LUCO energy levels and E_{gap}'s of trans-PA as a function of number of k points at B3LYP/6-31G* theory (DFT) level.

Table 4.1 and Figure 4.2 show that, for PA, even 32 or 64 k points calculation produces E_{gap} to within 0.1 eV of the final converged value. Considering the size of the fluorene-based polymers' unit cells, we will use 12 and 32 k points for their band structure calculations since 12 or 32 k points produce results that are accurate enough for the purpose of this thesis.

4.1.2 HF 1D Solid State Calculations

The 1D solid state HF energy results are given in Table 4.3. The HF E_{total} is 0.9 hartrees higher than DFT E_{total}. The HF E_{gap} is 7.24 eV which is approximately 5 times larger than the experimental value of 1.5 eV for bulk PA. The reason for this is the fact that the IP (negative of HOCO eigenvalue) is overestimated by approximated 1.7 eV whereas EA (negative of LUCO eigenvalue) is underestimated by 3.0 eV. Hence, there is no error cancelation which occurs in DFT calculations. The result is that E_{gap} has a big deviation from the experimental value at the HF level. The inclusion of perturbation correction at a MP2 (MØller-Plesset second-order perturbation theory) level [83], gives the E_{gap} for trans-PA to be 3.0 eV. The inclusion of further correlation effects deceases E_{gap} even more [84].

HF geometry optimization gives C=C bond equal to 1.33 Å and C-C equal to 1.45 Å along the PA chain backbone (see Table 4.2). This results in 0.12 Å for BLA which is 0.04 Å higher than experimental value of 0.08 Å [85] (with C=C bond equal to 1.36 Å and C-C equal to 1.44 Å). HF optimized Tv is 2.46 Å. In summary, the HF calculation clearly illustrates that the inclusion of correlation effects beyond HF level is essential for more accurate electronic band gap calculations [86, 87, 88, 89]. For the remaining of this thesis, we employ DFT in the calculations.

4.1.3 DFT 1D Solid State Calculations

Table 4.2 lists the Tv, BLA and bond length values for trans-PA for the DFT (32 k-point) 1D solid state calculations.

Table 4.2: Geometry parameters of trans-PA as obtained from 32 k-point 1D solid state DFT calculations. Tv's, CC bond lengths and BLA's (all in Å) are listed.

Method	Tv	C-C	C=C	BLA
HF/6-31G*	2.464	1.450	1.330	0.120
B3LYP/6-31G*	2.473	1.423	1.371	0.053
O3LYP/6-31G*	2.476	1.419	1.377	0.042
OB95/6-31G*	2.476	1.397	1.398	0.001
PBEPBE/6-31G*	2.481	1.403	1.400	0.003
PBE1PBE/6-31G*	2.466	1.423	1.365	0.058
TPSSTPSS/6-31G*	2.480	1.406	1.397	0.010
Expt [85]		1.44	1.36	0.08

The structure of the electronic energy bands are determined by the systems' optimized geometries. As shown in Table 4.2, the carbon-carbon bonds as obtained at the B3LYP level with 32 k points are 1.42 Å and 1.37 Å which are somewhat closer to the experimental 1.44 Å and 1.36 Å bonds than the HF values. Similarly, O3LYP gives BLA of 0.042 Å with the corresponding bonds, 1.42 Å and 1.38 Å. The best agreement with the experimental data is given by PBE1PBE approximation which gives 1.42 Å and 1.37 Å for bond lengths. Other DFT approximations give BLA's close to zero since their optimized carbon-carbon bonds along the chain backbone are nearly equal (all are approximately 1.40 A). This result does not compare well with the experimental observation. The corresponding Tv's are also listed in Table 4.2.

Table 4.3 gives the results of energy calculations at the DFT level. As expected, the E_{total} is rather insensitive to various DFT functionals and is close to -77.4 hartrees. The six DFT functionals give different values for band gap. BE1PBE gives the best

Table 4.3: E_{total}, IP, EA, E_{gap} and max-gap values for trans-PA. E_{total} is in hartree, all other energies are in eV.

Method	E_{total}	IP	EA	E_{gap}	max-gap
12 k points					
B3LYP/6-31G*	-77.41	4.31	2.69	1.62	12.03
O3LYP/6-31G*	-77.38	4.01	2.90	1.12	11.39
32 k points					
HF/6-31G*	-76.89	6.20	-1.04	7.24	19.41
B3LYP/6-31G*	-77.41	4.12	2.88	1.24	12.03
O3LYP/6-31G*	-77.38	3.86	3.06	0.80	11.39
OB95/6-31G*	-77.39	3.66	3.37	0.29	10.17
PBEPBE/6-31G*	-77.31	3.71	3.42	0.29	10.21
PBE1PBE/6-31G*	-77.31	4.35	2.83	1.52	12.72
TPSSTPSS/6-31G*	-77.42	3.64	3.32	0.31	10.61
Expt [85, 91]		4.50	3.00	1.50	10.00

agreement (1.52 eV) with the experimental value of 1.5 eV for E_{gap}. It should be noted that, for an appropriate comparison of 1D solid state calculations with experimental values, it is necessary to correct them for the bulk 3D effects. It has been shown that the experimental value for E_{gap} for 1D trans-PA is closer to 1.83 eV [90] rather than 1.5 eV. The B3LYP gives a 1.24 eV E_{gap} and O3LYP gives a 0.80 eV E_{gap}. The band gaps with OB95, PBEPBE and TPSSTPSS are around 0.3 eV. In general, DFT calculations underestimate the observed band gap. This is in contrast to HF which overestimates them. However, the DFT deviations are not as large. The main reason for this improvement is the better agreement of IP and EA with their corresponding experimental values. This is due to the fact that, in most cases in DFT, both IP and EA are underestimated (with EA more than the IP) and the difference between the underestimations reduced the deviation of calculated band gaps with experimental data for DFT versus HF. Typically, the max-gap is 5-8 times larger than the minimum E_{gap}. The max-gap can be used to estimate the band width of the IP and EA bands

since max-gap minus E_{gap} is approximately the sum of the two band widths. In the DFT calculations, it can be seen from Table 4.3 that that top band widths are of the order of 5 - 6 eV. For example for B3LYP, IP band width is 5.4 eV and EA band width is 5.7 eV. All approximations, including HF, give similar band widths.

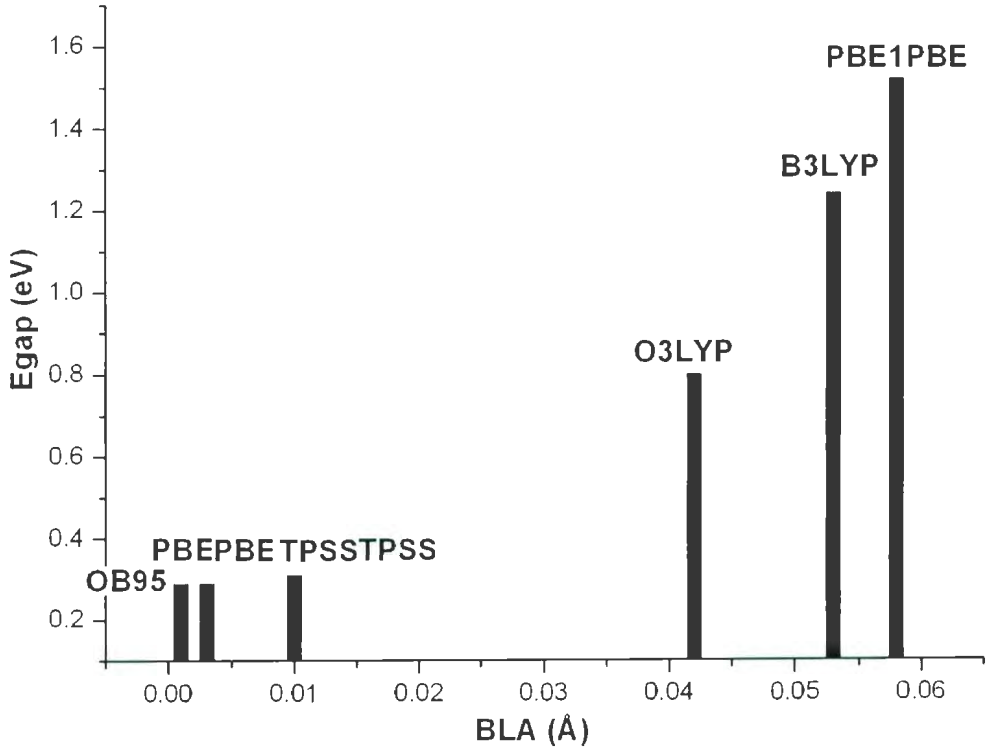

Figure 4.3: E_{gap}'s of trans-PA as a function of BLA's as obtained from various DFT functionals (with 6-31G* basis set and 32 k points).

In addition to the above, the variation of DFT results for E_{gap} with BLA's and Tv's are plotted. Figure 4.3 displays the E_{gap} values as a function of BLA's. As expected, larger BLA corresponds to larger E_{gap}. This is because the occurrence of the band gap is a direct consequence of the presence of unequal bond lengths. Figure 4.4 illustrates the variation of band gaps with Tv. This figure shows that smaller units cells correspond to larger E_{gap}'s.

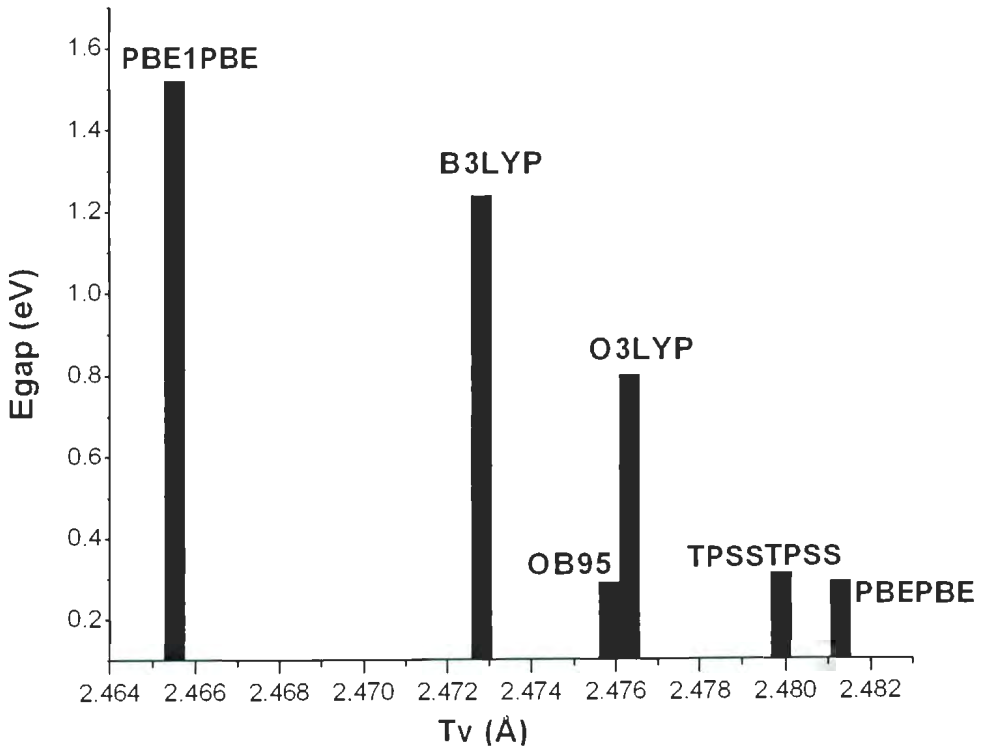

Figure 4.4: E_{gap}'s of trans-PA as a function of Tv's as obtained from various DFT functionals (with 6-31G* basis set and 32 k points).

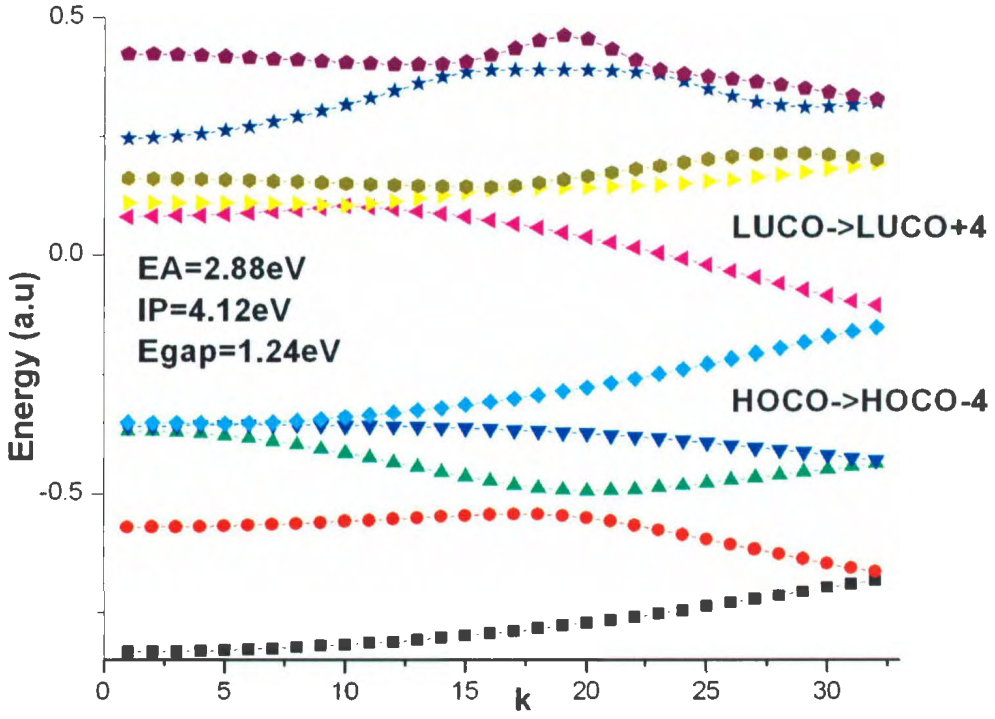

Figure 4.5: The DFT/B3LYP 1D band structure of trans-PA with 6-31G* basis set and 32 k points. For clarity, different colors have been used for different energy bands corresponding to the top 10 bands (HOCO-4 to LUCO+4).

Finally, a typical example of the band structure is displayed in Figure 4.5 for the trans-PA in the B3LYP approximation. Figure 4.5 shows five HOCO and LUCO top bands: HOCO-1, HOCO-2, ... HOCO-5 and the LUCO+1, LUCO+2, ... LUCO+5. The max-gap minus E_{gap} is of the order of 11 eV for trans-PA as shown in figure 4.5. Then it follows that the two top E_{width}'s are of the order of 5.5 eV.

4.1.4 Finite System Method

In addition to the solid state approach, there are alternative methods to compute the band gaps (see for example, references [92, 93, 94, 95]). In one study [93], the HOMO-LUMO gaps were plotted against the inverse chain length for $C_{10}H_{12}$ through $C_{24}H_{26}$. The extrapolated infinite chain band gap of 1.57 eV was obtained which, in turn, compared relatively well with the extrapolated experimental value of 1.83 eV for 1D trans-PA. In this thesis, as an example, we consider oligomers from C_4H_8 through $C_{18}H_{22}$ to perform similar analysis.

Table 4.4: BLA's and dipole moments for C_nH_{n+4} (with $n = 4-18$) at B3LYP/6-31G* level. BLA's (in Å) and dipole moments (in debye) are listed.

Molecule	BLA	Dipole
C4H8	0.57	-0.18,-0.19,0.00
C6H10	0.46	0.07,-0.04,0.00
C8H12	0.37	0.00,-0.16,0.00
C10H14	0.33	-0.07,-0.17,0.00
C14H18	0.19	0.13,-0.15,0.11
C16H20	0.18	0.14,-0.49,0.09
C18H22	0.18	0.22,-0.16,0.08
CnH2n	0.05	0.00,0.00,0.00
Expt [85]	0.08	0,0,0

Table 4.4 shows that the BLA's decrease with the increasing oligomer size, indicating strong finite system effects for these rather short oligomers. The oligomers also have

finite dipole moments. The three components of dipole moments stand for the three directions along the backbone, perpendicular and out of the polymer plane. Table 4.5 shows that the band gaps decrease with increasing number of carbon atoms. The C_nH_{2n} is the estimated result with 1D PBC calculation with trans-PA unit cell (n stands for the number of carbon atoms in the chain). These E_{gap} values are plotted as function of $1/n$ in Figure 4.6. The extrapolated value as obtained from Figure 4.6 gives a band gap of approximately 3 eV for an infinite chain which differs by more than 1 eV in comparison to the expected experimental value 1.8 eV for 1D trans-PA.

Table 4.5: E_{total}, IP, EA and E_{gap} values for 1D acetylene oligomers at B3LYP/6-31G* level. E_{total} is in hartree, all other energies are in eV.

Molecule	$\mathbf{E}_{total}$	**IP**	**EA**	$\mathbf{E}_{gap}$
C4H8	-157.22	6.35	-0.75	7.10
C6H10	-234.62	5.68	0.53	5.15
C8H12	-312.03	5.32	0.93	4.39
C10H14	-389.40	5.38	1.02	4.36
C14H18	-544.15	5.01	1.49	3.52
C16H20	-621.54	5.01	1.53	3.48
C18H22	-698.94	5.00	1.55	3.45
CnH2n	-77.41	4.12	2.88	1.24
Expt [91]		4.50	3.00	1.50

4.2 cis-PA

The two isomers, aromatic and quinoid, of cis-PA are presented in Figure 4.7 and Figure 4.8 respectively. There are four carbon atoms in each isomer's unit cell of cis-PA (only two carbon atoms are in the unit cell of trans-PA).

If one assumes that the experimental single bonds in cis-PA isomers are of the same length as in trans-PA and are 1.44 Å and the double bonds are 1.37 Å [85], then the

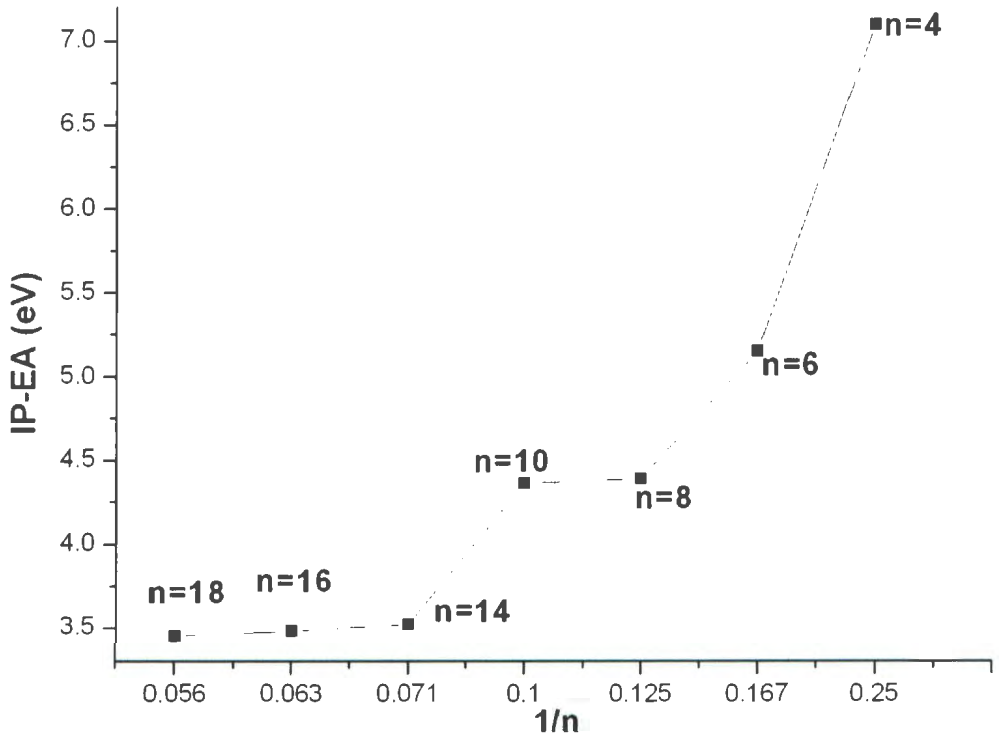

Figure 4.6: Energy differences, IP-EA (obtained with B3LYP/6-31G*) of acetylene oligomers as a function of 1/n, where n is the number of carbon atoms.

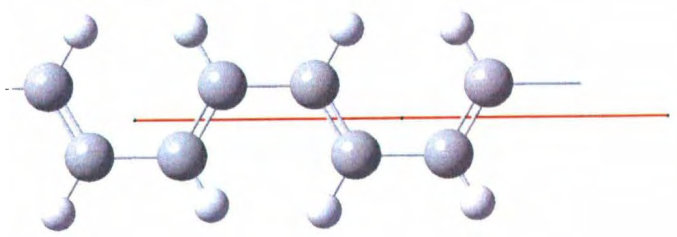

Figure 4.7: Molecular structure of an aromatic isomer of cis-PA (two unit cells are displayed).

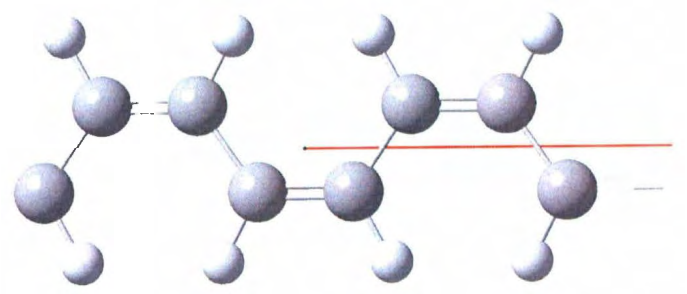

Figure 4.8: Molecular structure of quinoid isomer of cis-PA (two unit cells are displayed).

Table 4.6: Geometry parameters of cis-PA isomers as obtained from 32 k-point 1D solid state DFT calculations. Tv's, CC bond lengths and BLA's (in A), dipole moments (in debye) are listed.

Aromatic	**Tv**	**C-C**	**C=C**	**BLA**	**Dipole**
B3LYP/6-31G*	4.46	1.44	1.37	0.07	0,-0.0001,0
O3LYP/6-31G*	4.49	1.43	1.38	0.06	0,-0.0001,0
OB95/6-31G*	4.50	1.42	1.38	0.04	0,-0.0001,0
PBEPBE/6-31G*	4.48	1.43	1.39	0.04	0,-0.0002,0
PBE1PBE/6-31G*	4.50	1.42	1.37	0.05	0,0.0002,0
TPSSTPSS/6-31G*	4.48	1.43	1.38	0.05	0,-0.0001,0
Quinoid	**Tv**	**C-C**	**C=C**	**BLA**	**Dipole**
B3LYP/6-31G*	4.46	1.44	1.37	0.07	0,0.0002,0
O3LYP/6-31G*	4.49	1.43	1.38	0.06	0,0,0
OB95/6-31G*	4.50	1.42	1.38	0.04	0,0.0003,0
PBEPBE/6-31G*	4.48	1.43	1.39	0.04	0,0.0005,0
PBE1PBE/6-31G*	4.44	1.43	1.36	0.08	0,0.0003,0
TPSSTPSS/6-31G*	4.48	1.43	1.38	0.04	0,0.0004,0

experimental value for cis-PA's BLA is close to 0.07 Å. As shown in Table 4.6, most DFT approximations underestimate this BLA value somewhat. For both isomers, the BLA's are in the range of 0.04-0.09 A. The Tv for both isomers are also very similar. The reason for this closeness of structural results for both isomers is the fact that the quinoid isomer for cis-PA is not stable in nature and when geometry optimization is performed the final structure is an aromatic one for all DFT functionals (this can be clearly seen from the CC bonds in Table 4.6 where the inter-unit CC bond is more like a single bond). Not surprisingly, the dipole moments for both aromatic and quinoid isomers are also similar and are either zero or nearly zero which is the same result as for trans-PA.

Table 4.7 lists the energy results for cis-PA. The DFT/6-31G* with 32 k points has been applied in all the band gap calculations for the cis-PA isomers. The E_{total} of cis-PA isomers is close to -154.5 hartrees per unit cell. The two isomers give results that are nearly degenerate.

The values of E_{gap}'s range from 0.7 - 2.0 eV. These values are somewhat higher than the corresponding numbers for trans-PA (see Table 4.3). Since the difference between the max-gap and E_{gap} is approximately the sum of the valence and conduction band widths, Table 4.7 clearly illustrates that optimized band widths of the quinoid isomer are similar to that of aromatic isomer. The E_{width} affects the efficiency and mobility of electrons in the bands. The average band width of cis-PA isomers is smaller than that of trans-PA, which predicts lower conductivity for cis-PA in agreement with most experiments.

In summary, two cis-PA isomers give similar energy results. In fact, the experimental observations show that quinoid cis-PA is not stable and so far has not been observed in the lab [96]. The quinoid cis-PA isomer must change into aromatic structure.

Table 4.7: E_{total}, IP, EA, E_{gap} and max-gap values of 1D cis-PA as obtained from 32 k-point 1D solid state DFT calculations. E_{total} is in hartree and all other energies are in eV.

Aromatic	$\mathbf{E_{total}}$	**IP**	**EA**	$\mathbf{E_{gap}}$	**max-gap**
B3LYP/6-31G*	-154.81	4.49	2.63	1.86	9.42
O3LYP/6-31G*	-154.75	4.18	2.87	1.31	8.72
OB95/6-31G*	-154.76	3.91	3.26	0.65	7.59
PBEPBE/6-31G*	-154.60	3.97	3.27	0.71	7.55
PBE1PBE/6-31G*	-154.61	4.08	3.27	0.81	10.05
TPSSTPSS/6-31G*	-154.84	3.94	3.15	0.79	7.77
Quinoid	$\mathbf{E_{total}}$	**IP**	**EA**	$\mathbf{E_{gap}}$	**max-gap**
B3LYP/6-31G*	-154.81	4.49	2.63	1.86	9.42
O3LYP/6-31G*	-154.75	4.18	2.87	1.31	8.72
OB95/6-31G*	-154.76	3.91	3.26	0.65	7.59
PBEPBE/6-31G*	-154.60	3.97	3.27	0.71	7.55
PBE1PBE/6-31G*	-154.62	4.73	2.57	2.15	9.96
TPSSTPSS/6-31G*	-154.84	3.94	3.15	0.79	7.77

The average C=C distance along cis-PA chain agrees with the experimental 1.37 Å value. And the E_{gap}'s of cis-PA are slightly larger than that of trans-PA with larger BLA's as well. For completeness we display the variation of E_{gap}'s with BLA's and Tv's in Figure 4.9 and Figure 4.10 respectively as obtained for the various DFT approximations for the aromatic cis-PA. Also the typical band structures for the aromatic and quinoid cis-PA is displayed on Figure 4.11 and Figure 4.12.

4.3 meta-PA

The electronic and structural properties of trans-PA and to some extent cis-PA have been adequately explored. There is another structure of PA, called meta-PA, that has not been studied as extensively. The structure and energy of meta-PA are of interest primarily at a theoretical level. They have been observed experimentally, but

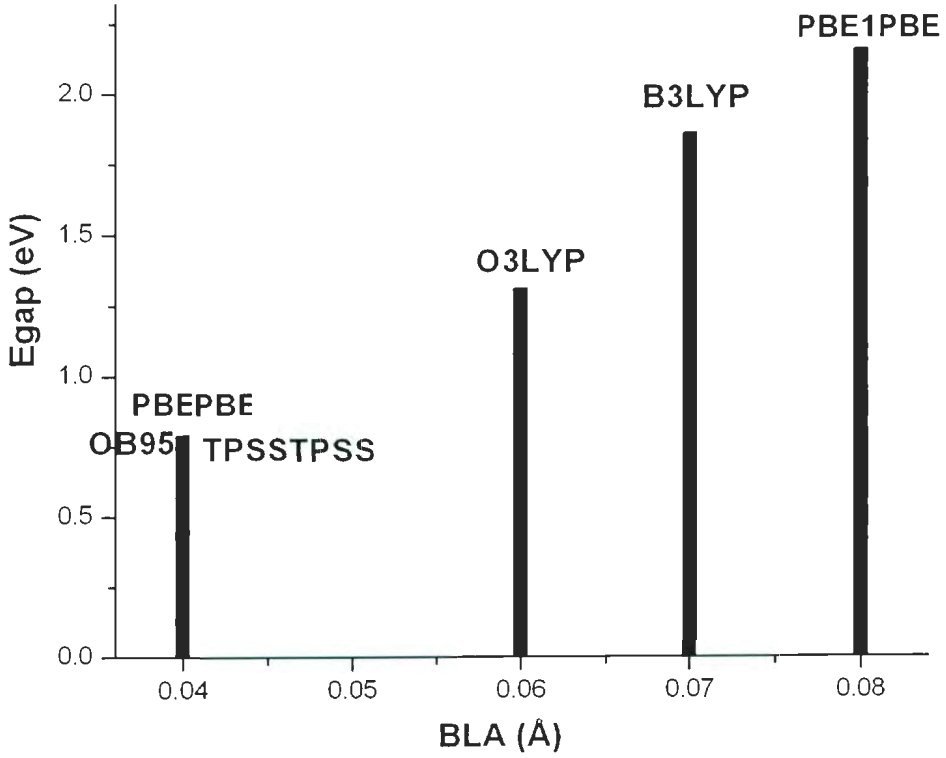

Figure 4.9: E_{gap}'s of aromatic cis-PA as a function of BLA's as obtained from various DFT functionals (with 6-31G* basis set and 32 k points).

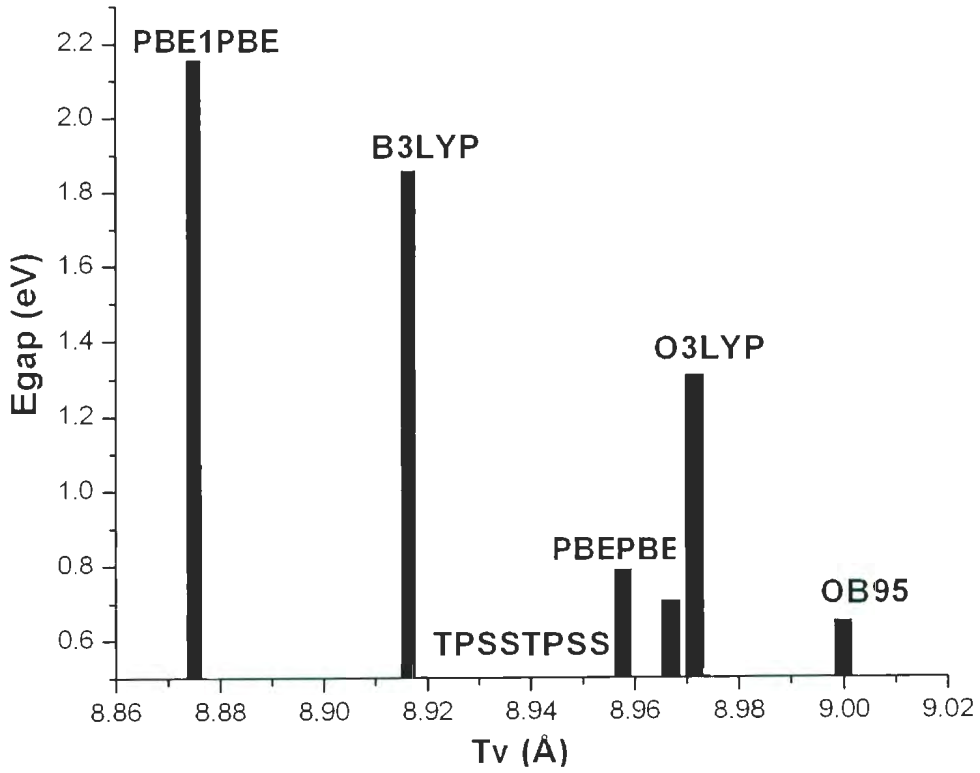

Figure 4.10: E_{gap}'s of aromatic cis-PA as a function of Tv's as obtained from various DFT functionals (with 6-31G* basis set and 32 k points).

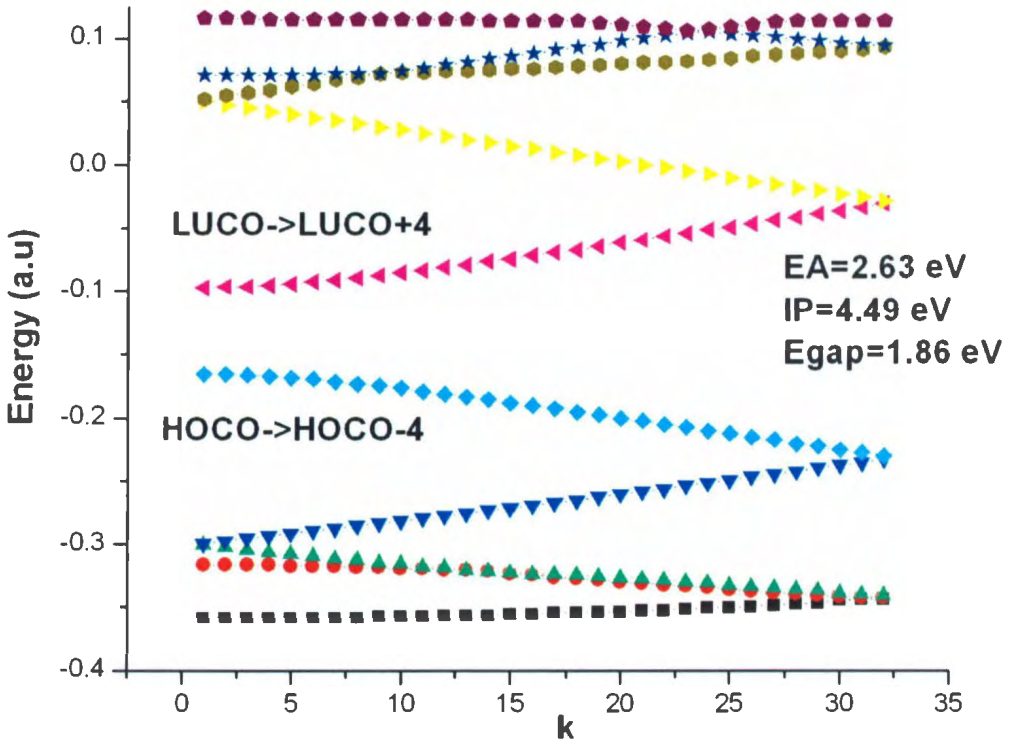

Figure 4.11: The DFT/B3LYP 1D band structure of aromatic cis-PA with 6-31G* basis set and 32 k points. For clarity, different colors have been used for different energy bands corresponding to the top 10 bands (HOCO-4 to LUCO+4).

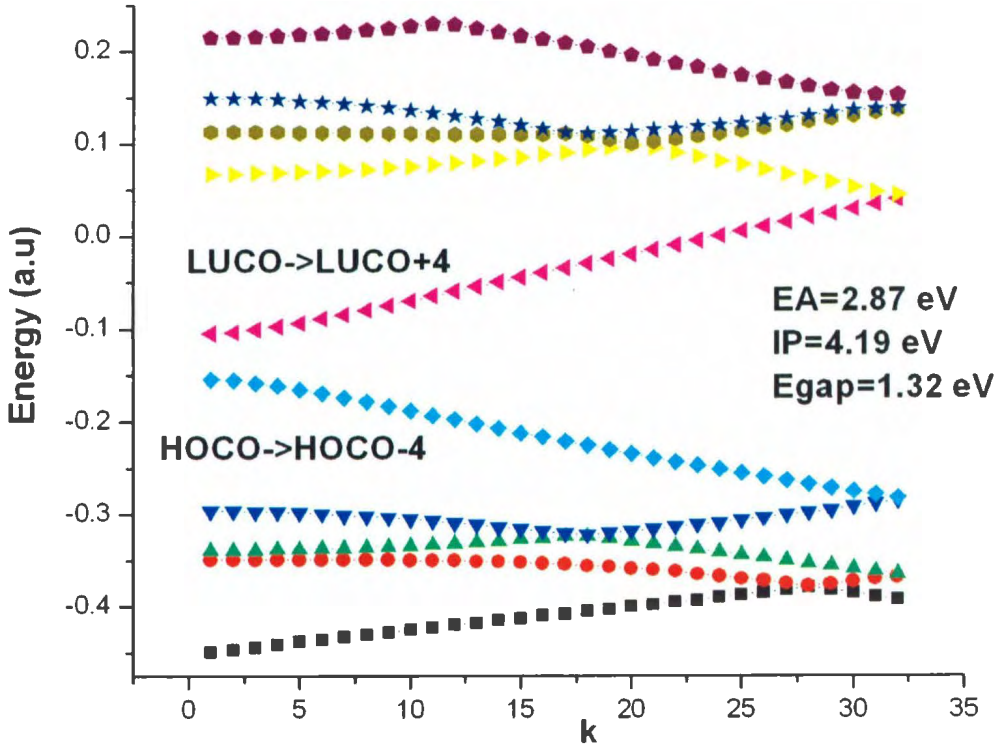

Figure 4.12: The DFT/B3LYP 1D band structure of quinoid cis-PA with 6-31G* basis set and 32 k points. For clarity, different colors have been used for different energy bands corresponding to the top 10 bands (HOCO-4 to LUCO+4).

Tv's are also similar to those obtained for cis-PA. Both BLA's and Tv's are relatively insensitive to the various DFT functionals. Similar to cis-PA and trans-PA, meta-PA has a vanishing dipole moment.

Table 4.9: E_{total}, IP, EA, E_{gap} and max-gap values for 1D meta-PA as obtained from 32 k-point 1D solid state DFT calculations. E_{total} is in hartree and other energies are in eV.

Method	$\mathbf{E_{total}}$	**IP**	**EA**	$\mathbf{E_{gap}}$	**max-gap**
B3LYP/6-31G*	-309.624	4.31	2.78	1.53	5.66
O3LYP/6-31G*	-309.510	4.00	3.00	1.01	5.09
OB95/6-31G*	-309.532	3.76	3.35	0.41	4.24
PBEPBE/6-31G*	-309.215	3.82	3.38	0.44	4.24
PBE1PBE/6-31G*	-309.243	4.53	2.73	1.81	6.06
TPSSTPSS/6-31G*	-309.684	3.77	3.27	0.50	4.36

In Table 4.9, the E_{total} for a repeat unit cell of meta-PA consisting of 8 CH units is around -309.00 hartree which is 4 times than that of the value obtained for trans-PA (-77.00 hartree) since four unit cells of trans-PA consist of 8 CH units. The B3LYP and O3LYP, together with PBEPBE show that the E_{gap} is close to 1 eV or is greater than 1 eV. With the same basis set, 6-31G*, and 32 k points, the O3LYP gives a E_{gap} 1.007 eV, B3LYP 1.530 eV and PBEPBE 1.805 eV. The other three functionals give values of order 0.5 eV for the E_{gap}. The OB95 gives 0.411 eV E_{gap}, PBE1PBE gives 0.441 eV and TPSSTPSS gives 0.50 eV E_{gap}. The HOCO and LUCO bands shift to narrow the energy gaps in these cases. In Figure 4.13, E_{gap} is plotted as a function of BLA. The BLA's for OB95 and TPSSTPSS are much smaller than that with B3LYP and O3LYP which in turn correspond to lower energy gaps for OB95 and TPSSTPSS than for B3LYP and O3LYP. The band gaps of meta-PA and cis-PA are slightly larger than those of trans-PA. For completeness we also include a plot of E_{gap} as a function of Tv's (see Figure 4.15).

As can be seen from Table 4.9 (also from Figure 4.16), the max-gap of meta-PA is roughly 3-4 times the E_{gap}, while the trans-PA is 8 times the E_{gap}. This indicates that the top band widths of meta-PA are smaller than those of trans-PA by a factor of two. That is, the E_{width} of meta-PA is of the order of 2 eV in comparison to 4-5 eV for trans-PA. The typical band structure for cis-PA is displayed in Figure 4.16.

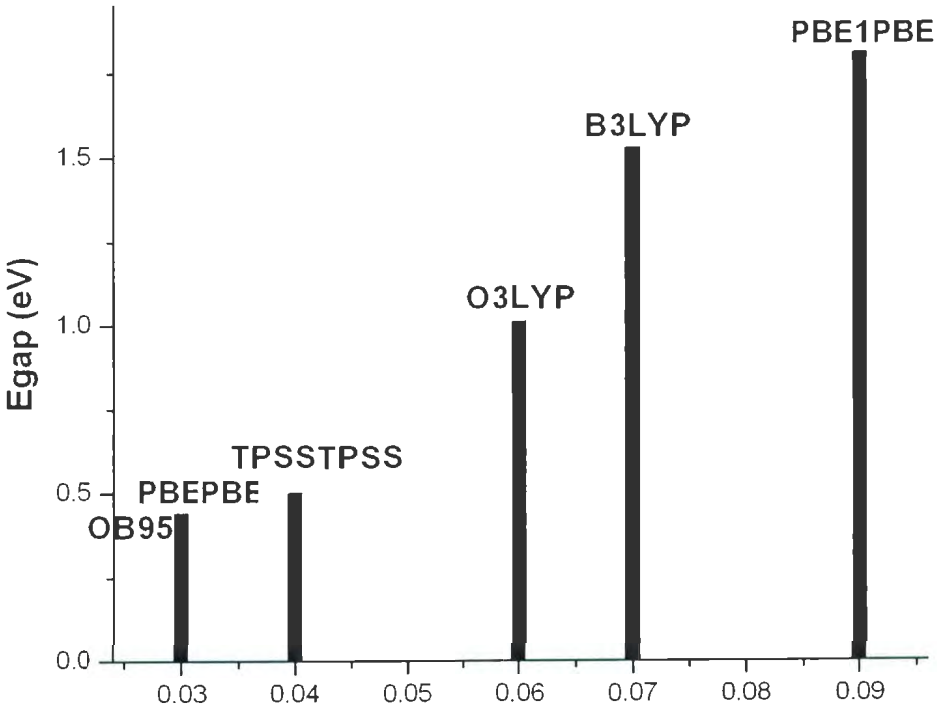

Figure 4.14: E_{gap}'s of meta-PA as a function of BLA's as obtained from various DFT functionals (with 6-31G* basis set and 32 k points).

4.4 Conclusions

In this Chapter the structure and the electronic band structure of the various isomers of PA were investigated using the 1D solid state calculation. Experimentally, it has

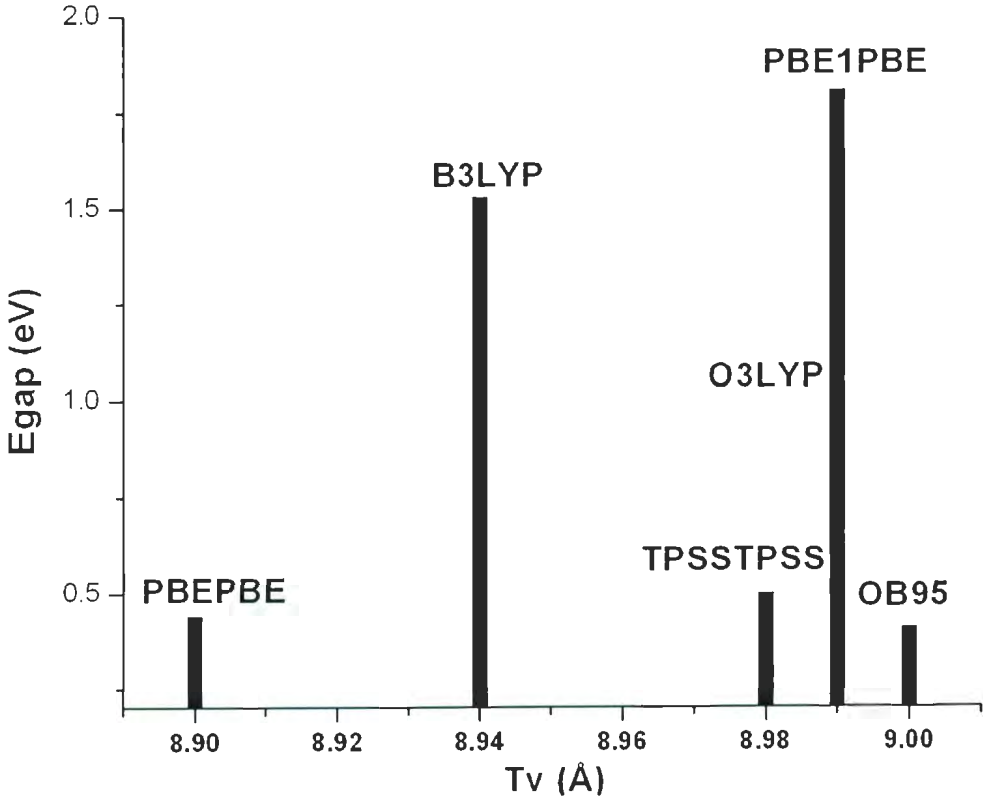

Figure 4.15: E_{gap}'s of meta-PA as a function of Tv's as obtained from various DFT functionals (with 6-31G* basis set and 32 k points).

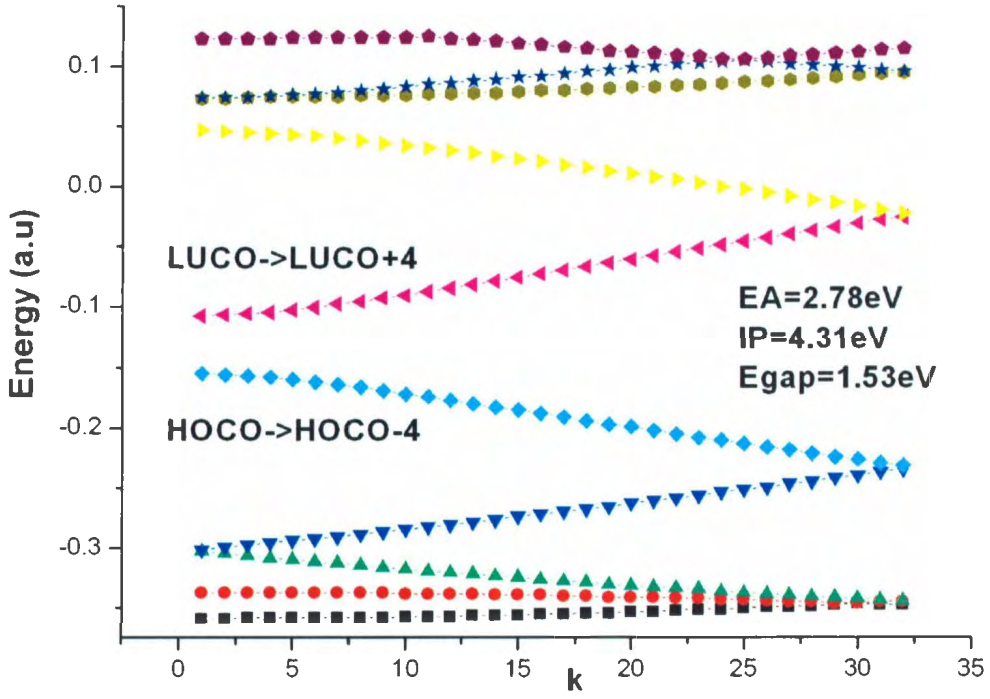

Figure 4.16: The DFT/B3LYP 1D band structure of meta-PA with 6-31G* basis set and 32 k points. For clarity, different colors have been used for different energy bands corresponding to the top 10 bands (HOCO-4 to LUCO+4).

been determined that the bond lengths for trans-PA are approximately in the range of 1.35-1.45 Å. These values are best reproduced by B3LYP, O3LYP and PBE1PBE functionals. In general, it has been found that the greater BLA's produce larger energy gaps. The E_{gap}'s of all PA isomers are in the range of 0.3 - 1.8 eV. The PBE1PBE, B3LYP and O3LYP functionals give results that agree best with experimental value of 1.8 eV for 1D trans-PA. In order of agreement with experimental E_{gap} for trans-PA we have: PBE1PBE > B3LYP, O3LYP, TPSSTPSS > PBEPBE > OB95. For meta-PA from largest to smallest band gaps we obtain the following order: PBEPBE > B3LYP > O3LYP > TPSSTPSS > PBE1PBE > OB95. For aromatic cis-PA, the same order (from largest to smallest band gaps) is PBE1PBE > B3LYP > O3LYP > TPSSTPSS > PBEPBE > OB95, and from largest to smallest band gaps for quinoid cis-PA, it is B3LYP > O3LYP > PBE1PBE > TPSSTPSS > PBEPBE > OB95. OB95 gives the smallest E_{gap} in all cases. The different performance of DFT functionals are due to their differences between the various approximations of exchange-correlation energy functionals. The above results are summarized on Figure 4.17 where results of 1D solid state DFT calculations with B3LYP and O3LYP functionals with 6-31G* and 32 k points are displayed.

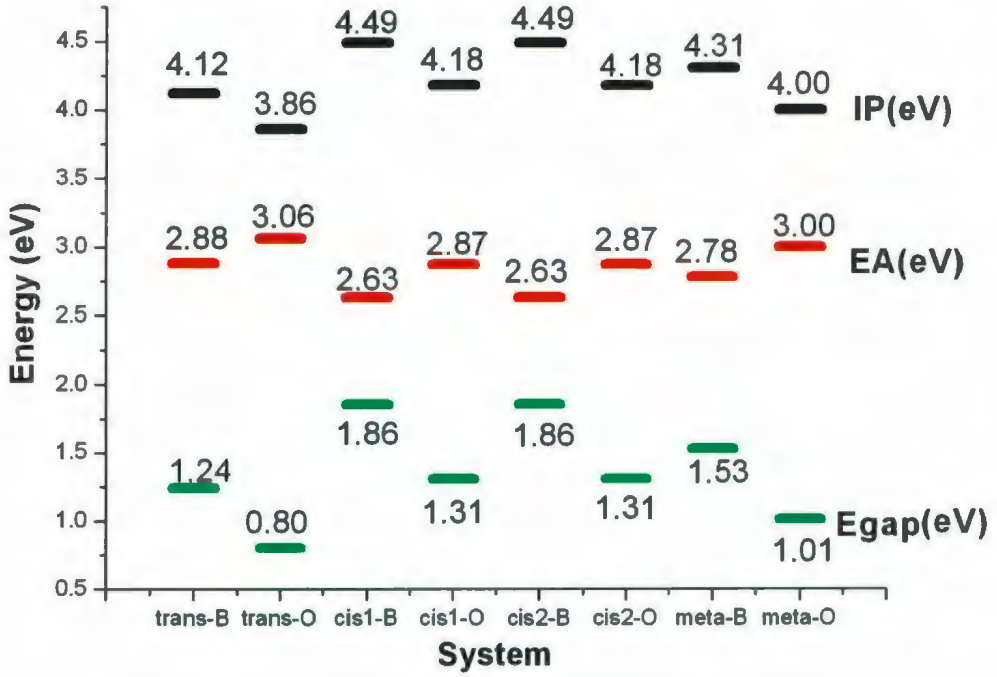

Figure 4.17: E_{gap}'s, IPs and EAs of PA isomers with B(O)3LYP/6-31G* and 32 k-points. trans-B stands for trans-PA with B3LYP/6-31G* method and trans-O stands for trans-PA with O3LYP/6-31G* method. cis1 and cis2 stand for the quinoid and aromatic isomers of cis-PA.

Chapter 5

The Electronic Band Structures of OxF_n

A typical multilayer PLED device may be composed of a hole transport layer such as triphenylamine-fluorene alternating copolymer ($TPAF_n$) and electron transport and emitting layer such as fluorene-oxadiazole alternating copolymer (OxF_n) together with anode such as Induim Tin Oxide (ITO) and cathode such as Mg-Ag alloy [1]. To increase the PL and EL efficiency, PLEDs may also employ additional hole and electron transport layers. The main role of these additional layers is to better match the IP and EA energies of these materials with the anode and cathode top energy levels respectively. As discussed in the introduction, Cyclic Voltammetry is one of the methods that can be used to determine the top energy levels of the organic polymers and cathode and anode materials [98, 99, 100, 101] (see Figure 2.2 for example).

In chapter 5, we investigate the electronic structure properties of OxF_n (n=1,2,3) with the use of 1D solid state DFT calculations. We compare the computational results with the experimental observations as given in reference [1]. The bond lengths for OxF_n (n=1,2,3) are given in the Appendix.

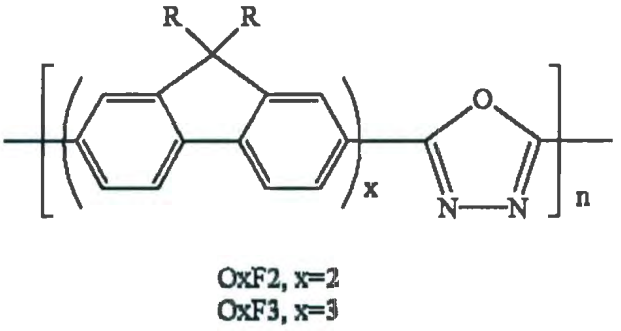

Figure 5.1: Chemical structure of OxF_n unit cell.

5.1 OxF_1

It has been found that all OxF_n (n=1,2,3) have direct band gaps and their band structures are closely related to their geometries. We begin the investigation of OxF_n with the simplest compound OxF_1. As shown in Figure 5.1, OxF_1 consists of one fluorene and one oxadiazole group. In our computations, the fluorene side groups (R's) are made of short ethyl groups (C_2H_5) instead of the longer C_8H_{17} chains to reduce the computation time. This replacement did not significantly change computational results for band structure of OxF_1. OxF_1 unit cells are not planar due to rotation around the bond joining fluorene with oxadiazole ring.

Tables 5.1 and 5.2 clearly illustrate that for a large unit cell like that for OxF_1, 12 and 32 k-point DFT (with 6-31G* basis set) calculations give very similar results for the geometry parameters and energies. BLA's are computed for the fluorene group. Table 5.1 shows that all Tv's are of the order of 11.8 Å. Depending on the DFT approximation, BLA varies from -0.003 Å to -0.009 Å. Figures 5.3 and 5.4 display the variation of E_{gap} with BLA's and Tv's. Band gaps increase with the increasing magnitude of the BLA's. There does not seem to be much correlation between the

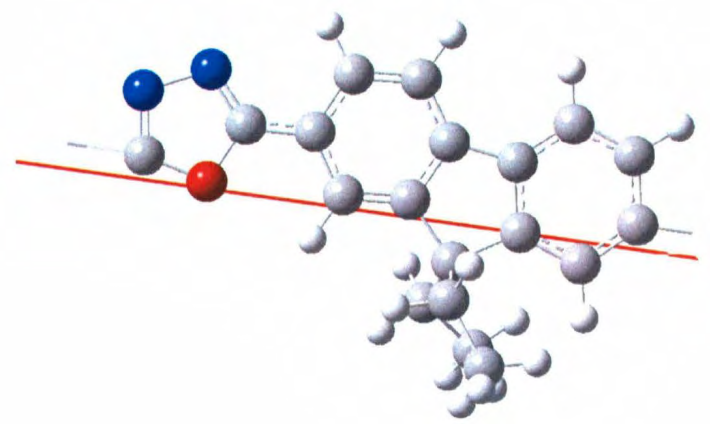

Figure 5.2: Molecular structure of OxF_1 (one unit cell is displayed).

Table 5.1: Geometry parameters of OxF_1 isomers as obtained from 12 and 32 k-point 1D solid state DFT calculations. Tv's and BLA's (in Å), dipole moments (in debye) are listed.

Method	**Tv**	**BLA**	**Dipole**
12 k points			
B3LYP/6-31G*	11.86	-0.0075	0.00,2.02,0.05
O3LYP/6-31G*	11.79	-0.0062	0.00,1.95,0.04
OB95/6-31G*	11.84	-0.0058	0.00,1.77,0.05
32 k points			
B3LYP/6-31G*	11.86	-0.0075	0.00,2.02,0.05
O3LYP/6-31G*	11.79	-0.0062	0.00,1.95,0.04
OB95/6-31G*	11.84	-0.0058	0.00,1.77,0.05
PBEPBE/6-31G*	11.89	-0.0030	0.00,1.88,0.04
PBE1PBE/6-31G*	11.81	-0.0086	0.00,2.04,0.05
TPSSTPSS/6-31G*	11.89	-0.0042	0.00,1.95,0.05

Table 5.2: E_{total}, IP, EA, E_{gap} and max-gap values of OxF_1 as obtained from 12 and 32 k-point 1D solid state DFT calculations. E_{total} is in hartree and all other energies are in eV.

Method	E_{total}	IP	EA	E_{gap}	max-gap
12 k points					
B3LYP/6-31G*	-918.40	5.50	2.30	3.20	4.92
O3LYP/6-31G*	-916.45	5.24	2.53	2.70	4.43
OB95/6-31G*	-918.18	4.82	2.83	2.00	3.60
32 k points					
B3LYP/6-31G*	-918.40	5.50	2.30	3.20	4.95
O3LYP/6-31G*	-916.45	5.24	2.53	2.70	4.47
OB95/6-31G*	-918.18	4.82	2.83	2.00	3.64
PBEPBE/6-31G*	-917.27	4.89	2.92	1.97	3.60
PBE1PBE/6-31G*	-917.35	5.74	2.22	3.52	5.34
TPSSTPSS/6-31G*	-918.57	4.89	2.82	2.06	3.70

size of the band gap and the magnitude of Tv. Actually, not unexpectedly, for all systems, there is no obvious correlation between band gaps and Tv's. There is a finite dipole moment along the chain backbone.

Table 5.2 shows the energy results of OxF_1 at DFT level. E_{total} varies from -918.6 hartrees to -916.5 hartrees per OxF_1 unit cell. E_{gap} ranges from 2.0 to 3.5 eV. It will be shown below that B3LYP and O3LYP DFT functionals give the best agreement with experiment values for E_{gap} for OxF_2 and OxF_3. The E_{gap} of OxF_1 at O3LYP (B3LYP) is 2.70 (3.20) eV with IP and EA as 5.24 (5.50) eV and 2.53 (2.30) eV respectively. Compared to these values PBE1PBE overestimates E_{gap} at 3.52 eV. Other functionals like OB95, PBEPBE and TPSSTPSS all underestimate the band gap and give its value at approximate 2.0 eV. The max-gap values (which are approximately equal to sum of the HOCO and LUCO band widths plus the band gap) of O3LYP and B3LYP differ by 0.05 eV and indicate that E_{width}'s of the top levels of OxF_1 are less than 0.9 eV and hence the band widths are a lot narrower than those of PA isomers

(which are of the order of 4-5 eV). That is, the HOCO and LUCO bands are very flat, almost parallel to each other. In general, fluorene-based polymers are known to present flatter energy band structure due to large unit cells as clearly illustrated in Figure 5.5.

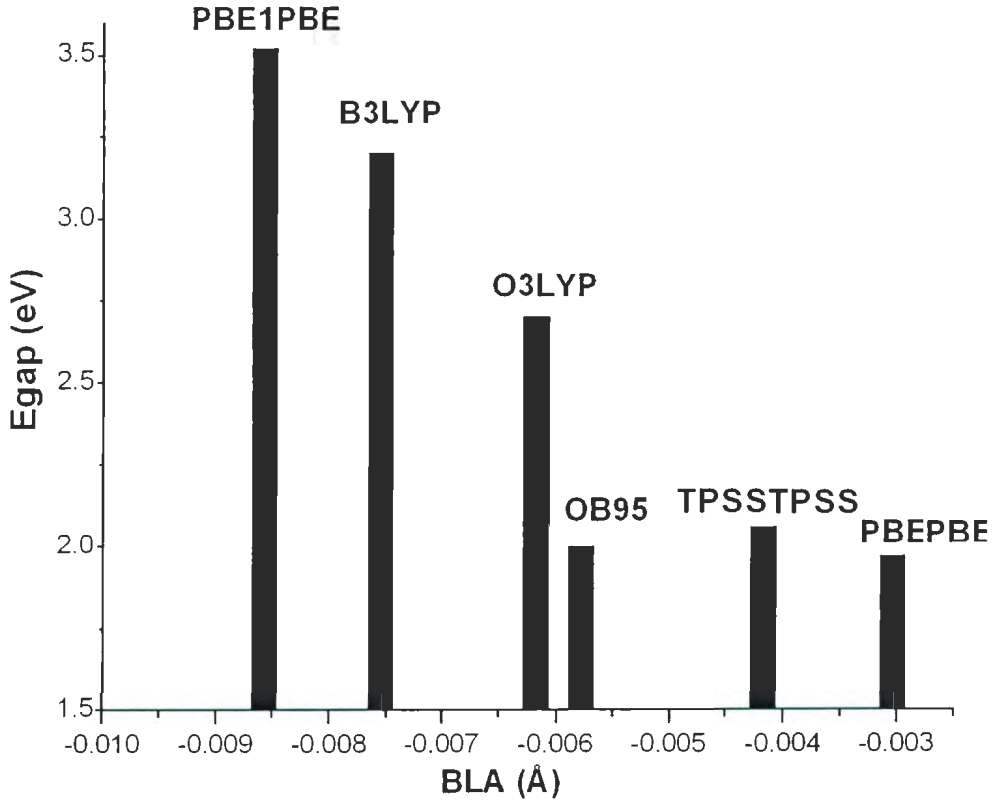

Figure 5.3: E_{gap}'s of OxF_1 as a function of BLA's as obtained from various DFT functionals (with 6-31G* basis set and 32 k points).

5.2 OxF_2

The molecular structure of OxF_2 unit cell is shown in Figure 5.6. In this case, one more fluorene group is added to improve the electron transport efficiency.

Table 5.3 shows the geometry properties of OxF_2. The optimized Tv at O3LYP is

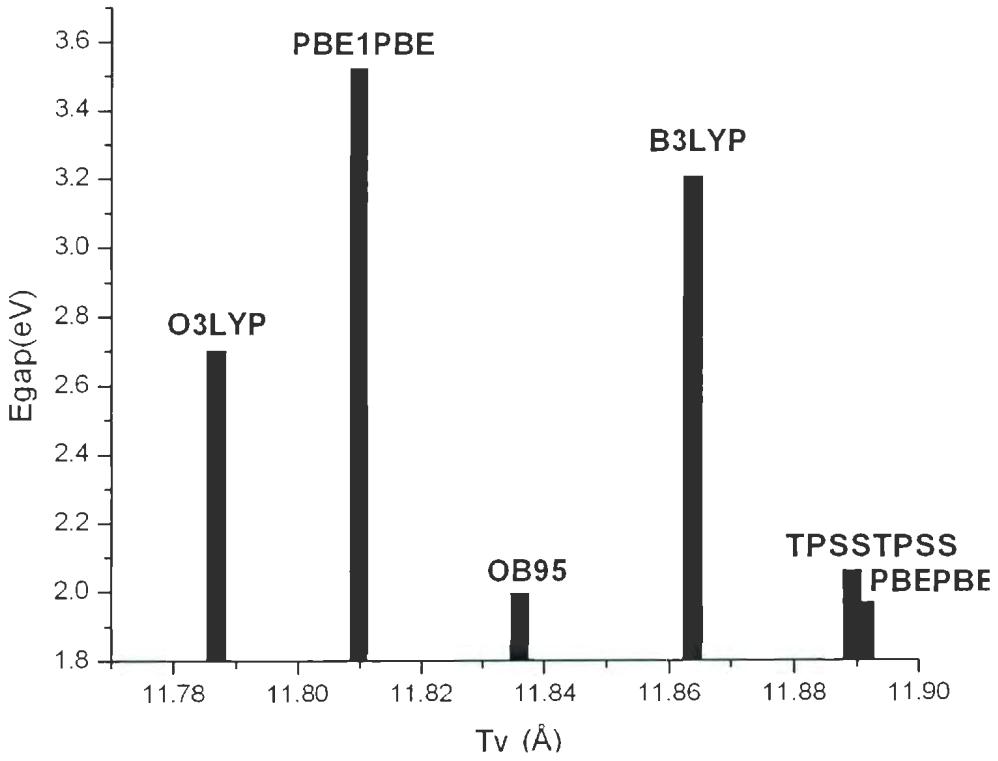

Figure 5.4: E_{gap}'s of OxF_1 as a function of Tv's as obtained from various DFT functionals (with 6-31G* basis set and 32 k points).

Table 5.3: Geometry parameters of OxF_2 isomers as obtained from 32 k-point 1D solid state DFT calculations. Tv's and BLA's (in Å), dipole moments (in debye) are listed.

Method	Tv	BLA	Dipole
B3LYP/6-31G*	20.00	-0.0162	-0.00,2.29,-0.30
O3LYP/6-31G*	20.00	-0.0143	-0.07,0.15,-2.16
OB95/6-31G*	19.96	-0.0138	0.02,1.70,-0.86
PBEPBE/6-31G*	20.05	-0.0104	-0.00,2.09,-0.29
PBE1PBE/6-31G*	19.91	-0.0173	-0.00,2.27,-0.28
TPSSTPSS/6-31G*	19.98	-0.0153	0.04,-0.65, 0.50

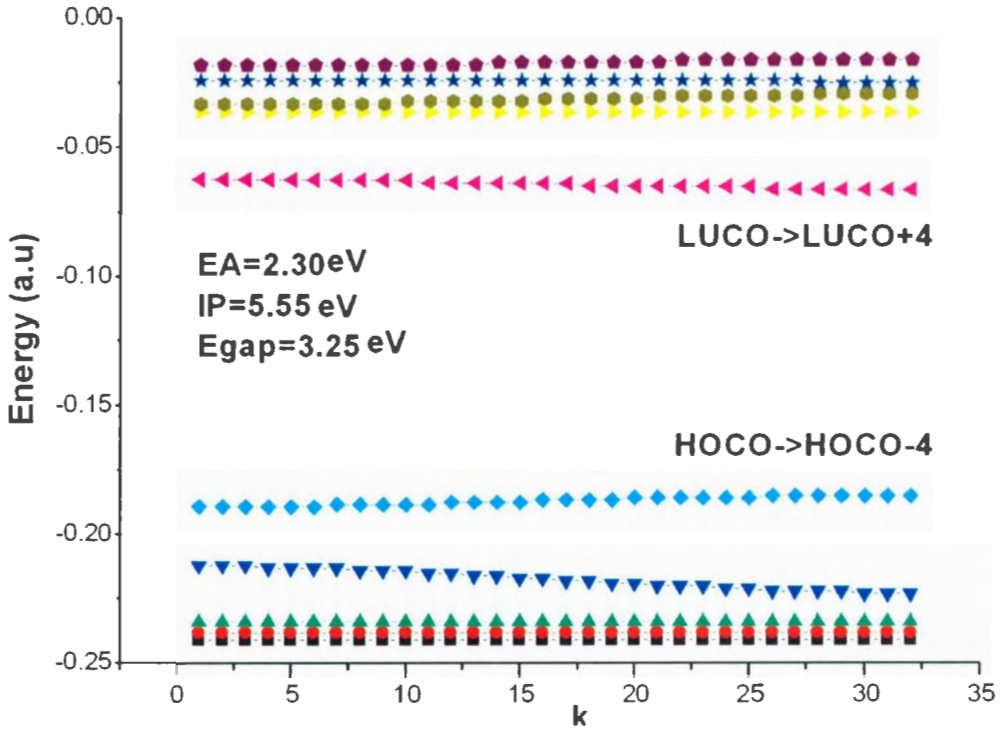

Figure 5.5: The DFT/B3LYP 1D band structure of OxF_1 with 6-31G* basis set and 32 k-points. For clarity, different colors have been used for different energy bands corresponding to the top 10 bands (HOCO-4 to LUCO+4).

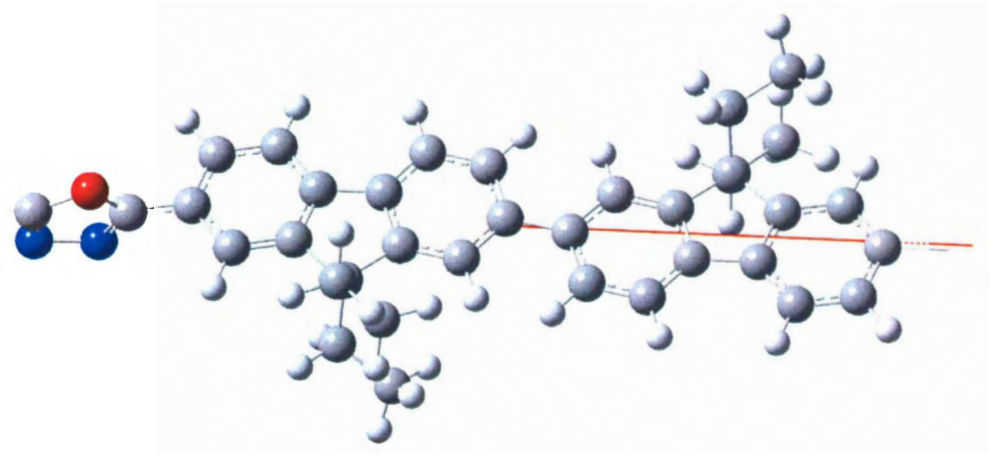

Figure 5.6: Molecular structure of OxF_2 (one unit cell is displayed).

20.00 Å which is approximately 8 Å larger than the corresponding value for OxF_1. This difference gives the length of fluorene group along the chain. Similar to OxF_1, the unit cell of OxF_2 is not planar. In fact OxF_2 is more distorted, for example, the inter-ring torsional angle between oxadiazole and fluorene groups is in the range of 29-34 degrees. O3LYP gives the largest magnitude of BLA of 0.017 Å and PBEPBE comes with the smallest magnitude of BLA of 0.010 Å. The average magnitude of BLA for OxF_2 is 0.0138 Å , roughly twice that of OxF_1. Figures 5.7 and 5.8 display the variation of E_{gap} with BLA's and Tv's. Similar to OxF_1, band gaps for OxF_2 still increase with the increasing magnitude of the BLA's in most cases. There are exceptions, for example, E_{gap} of B3LYP is 0.48 eV larger than that of O3LYP however its BLA is 0.0008 Å smaller. Again, there does not seem to be much correlation between the size of the band gap and the magnitude of Tv. As before, there is a finite dipole moment of the order of 2.0 D along the chain backbone.

Table 5.4: E_{total}, IP, EA, E_{gap} and max-gap values of OxF_2 as obtained from 32 k-point 1D solid state DFT calculations. E_{total} is in hartree and all other energies are in eV.

Method	$\mathbf{E}_{total}$	**IP**	**EA**	$\mathbf{E}_{gap}$	**max-gap**
B3LYP/6-31G*	-1575.88	5.31	2.02	3.28	4.03
O3LYP/6-31G*	-1572.46	5.06	2.26	2.80	3.57
OB95/6-31G*	-1575.47	4.68	2.55	2.13	2.85
PBEPBE/6-31G*	-1573.89	4.72	2.66	2.06	2.79
PBE1PBE/6-31G*	-1574.06	5.55	1.95	3.60	4.38
TPSSTPSS/6-31G*	-1576.16	4.73	2.49	2.24	2.93
Expt [1]		5.73	2.79	2.94	

Table 5.4 shows that the E_{total} of OxF_2 is -1575 hartrees, 660.0 hartrees larger than that of OxF_1. The E_{gap}'s of OxF_2 are approximately 0.1 eV larger than those of OxF_1. For this compound a direct comparison with experimental data can be made. Clearly, the B3LYP and O3LYP approximations give the best agreement with the

observed values for band gaps. B3LYP predicts 3.28 eV for E_{gap} (0.34 eV larger than the experimental value) and O3LYP predicts 2.80 eV for E_{gap} (0.14 eV smaller than the experimental value). With respect to experimental IP and EA values things are not as clear cut. Both B3LYP and O3LYP give reasonably good agreement with observed IPs, however PBE1PBE gives even better agreement. And for EAs, OB95, PBEPBE and TPSSPTSS all give better agreement with the experimental EA value than B3LYP and O3LYP. The E_{width}'s of OxF_2 are even smaller than those of OxF_1, for example, for B3LYP, the valance band is 0.14 eV and the conduction band is 0.08 eV as shown in Figure 5.9. Similar to OxF_1, all bands for OxF_2 are quite flat.

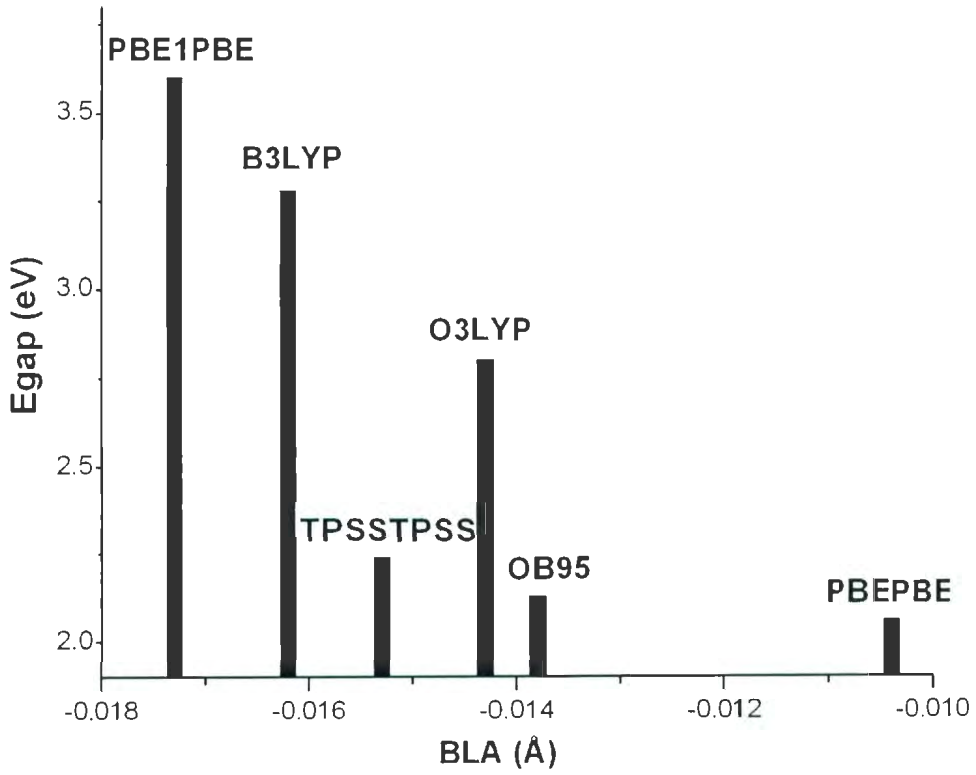

Figure 5.7: E_{gap}'s of OxF_2 as a function of BLA's as obtained from various DFT functionals (with 6-31G* basis set and 32 k points).

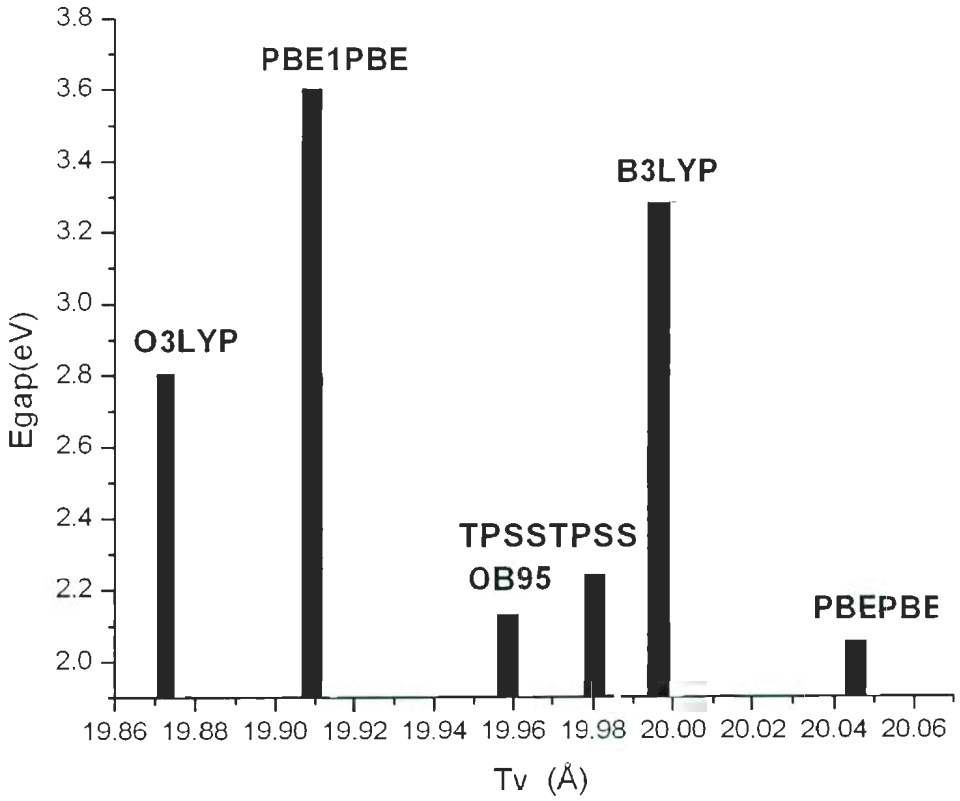

Figure 5.8: E_{gap}'s of OxF_2 as function of Tv's as obtained from various DFT functionals (with 6-31G* basis set and 32 k points).

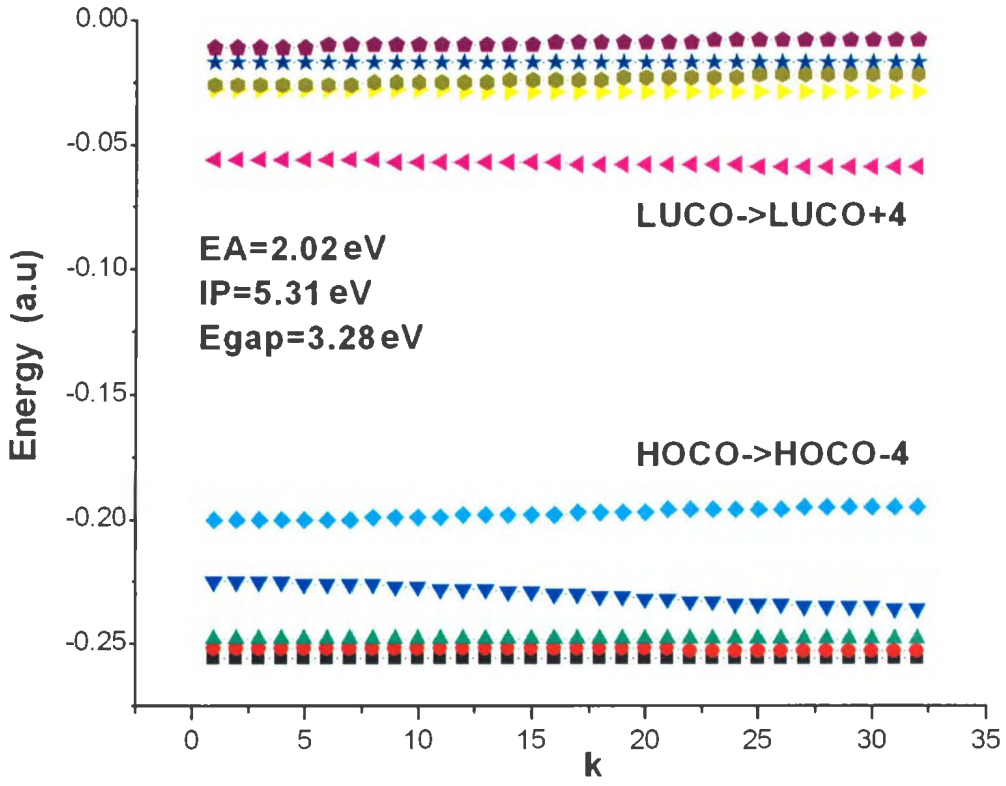

Figure 5.9: The DFT/B3LYP 1D band structure of OxF_2 with 6-31G* basis set and 32 k-points. For clarity, different colors have been used for different energy bands corresponding to the top 10 bands (HOCO-4 to LUCO+4).

5.3 OxF_3

In Figure 5.10, the OxF_3 unit cell is shown with one more fluorene group in comparison to OxF_2.

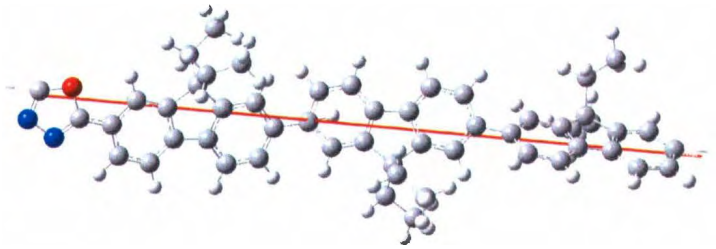

Figure 5.10: Molecular structure of OxF_3 (one unit cell is displayed).

Table 5.5: Geometry parameters of OxF_3 isomers as obtained from 32 k-point 1D solid state DFT calculations. Tv's and BLA's (in Å), dipole moments (in debye) are listed.

Method	Tv	BLA	Dipole
B3LYP/6-31G*	25.47	-0.0184	-0.01,2.49,-1.32
O3LYP/6-31G*	27.18	-0.0165	0.00,3.20,-1.18
OB95/6-31G*	27.29	-0.0162	0.01,3.16,-1.25
PBEPBE/6-31G*	27.42	-0.0134	0.00,3.19,-1.16
PBE1PBE/6-31G*	27.31	-0.0162	-0.01,3.19,-1.05
TPSSTPSS/6-31G*	27.39	-0.0150	0.00,3.30,-0.98

Tables 5.5 and Table 5.6 show the geometry parameters and energy results respectively. From Table 5.5 it can be seen that OxF_3 has a Tv equal to approximately 27 Å which is 7 Å larger than Tv for OxF_2 and 16 eV larger than Tv for OxF_1. As before the unit cell of OxF_3 is not planar. There is a rotation of the order of 36-45 degrees between fluorene groups and 29-34 degrees between oxadiazole and fluorene groups. This OxF_3 unit cell is more polar than unit cells of OxF_1 and OxF_2. This is

reflected in its increased dipole moment along the chain backbone (of the order of 3 D instead of 2 D as was seen for OxF_1 and OxF_2). Figures 5.11 and 5.12 display the variation of E_{gap} with BLA's and Tv's for OxF_3. Similar to OxF_1 and OxF_2, band gaps for OxF_3 increase with the increasing magnitude of the BLA's. And, there does not seem to be much correlation between the size of the band gap and the magnitude of Tv.

Table 5.6: E_{total}, IP, EA, E_{gap} and max-gap values of OxF_3 as obtained from 32 k-point 1D solid state DFT calculations. E_{total} is in hartree and all other energies are in eV.

Method	$\mathbf{E}_{total}$	**IP**	**EA**	$\mathbf{E}_{gap}$	**max-gap**
B3LYP/6-31G*	-2233.34	5.29	1.78	3.51	3.80
O3LYP/6-31G*	-2228.44	5.04	2.04	3.00	3.31
OB95/6-31G*	-2232.74	4.66	2.34	2.31	2.60
PBEPBE/6-31G*	-2230.50	4.69	2.46	2.23	2.53
PBE1PBE/6-31G*	-2232.74	4.65	2.35	2.29	2.59
TPSSTPSS/6-31G*	-2233.76	4.67	2.35	2.31	2.61
Expt [1]		5.61	2.58	3.03	

In Table 5.6, the E_{total} for OxF_3 is of the order of -2230 hartrees. The data for OxF_3 combined with the results for OxF_1 and OxF_2 indicate that the addition of a fluorene group adds approximately 660 hartrees to the magnitudes of their respective total energies.

For OxF_3, similar to OxF_2, a direct comparison with experimental data can be made. Again the B3LYP and O3LYP approximations give the best agreement with the observed values for band gaps. B3LYP predicts 3.51 eV for E_{gap} (0.48 eV larger than the experimental value) and O3LYP predicts 3.00 eV for E_{gap} (0.03 eV smaller than the experimental value). Also, with respect to experimental IP and EA values things are not as clear cut. Both B3LYP and O3LYP IPs give reasonably good agreement

with observed IPs, B3LYP gives the best agreement. And for EAs, OB95, PBEPBE, PBE1PBE and TPSSTPSS all give better agreement with the experimental EA value than B3LYP and O3LYP. The E_{width}'s of OxF_3 are even smaller than those of OxF_2 as shown in Figure 5.13. Similar to OxF_1 and OxF_2, all bands for OxF_3 are very flat.

Theoretically speaking, DFT can provide detailed theoretical prediction in simulating large molecules. B3LYP gives 3.51 eV E_{gap} with 1.78 eV EA and 5.29 eV IP. The 0.48 eV overestimates of E_{gap} occurs with 0.4 eV higher EA and 0.6 eV lower IP. Note that O3LYP ends with E_{gap} 2.99 eV, 0.04 eV less than experiment value. The best result is obtained at O3LYP level here. The experimental E_{gap} is 3.03 eV. O3LYP gives EA and IP deviations as 0.67 eV and 0.54 eV. However, individually, B3LYP of EA is better than O3LYP while O3LYP gives better IP result. It is proved that E_{gap} accuracy is less sensitive to k points for large molecular systems. OB95 and TPSSTPSS are still poor in giving reliable energy levels.

5.4 $OxF_{1.5}$

In order to investigate the effect of the benzene ring in the OxF_n polymer, we generated a new polymer labeled as $OxF_{1.5}$. The $OxF_{1.5}$ is formed by adding a benzene ring into the OxF_1 unit cell as shown in Figure 5.14. It is expected that $OxF_{1.5}$'s band structure will have properties between those of OxF_1 and OxF_2.

Isolated benzene is characterized by a six-member ring whose CC bonds are all equal [90]. After inserting the benzene ring into OxF_1 unit cell, charge delocalization leads to aromatic benzene structure (CC bonds are somewhat different). Table 5.7 lists the geometry parameters of $OxF_{1.5}$.

Not surprisingly, the Tv of $OxF_{1.5}$ is between those of OxF_1 and OxF_2. However, its

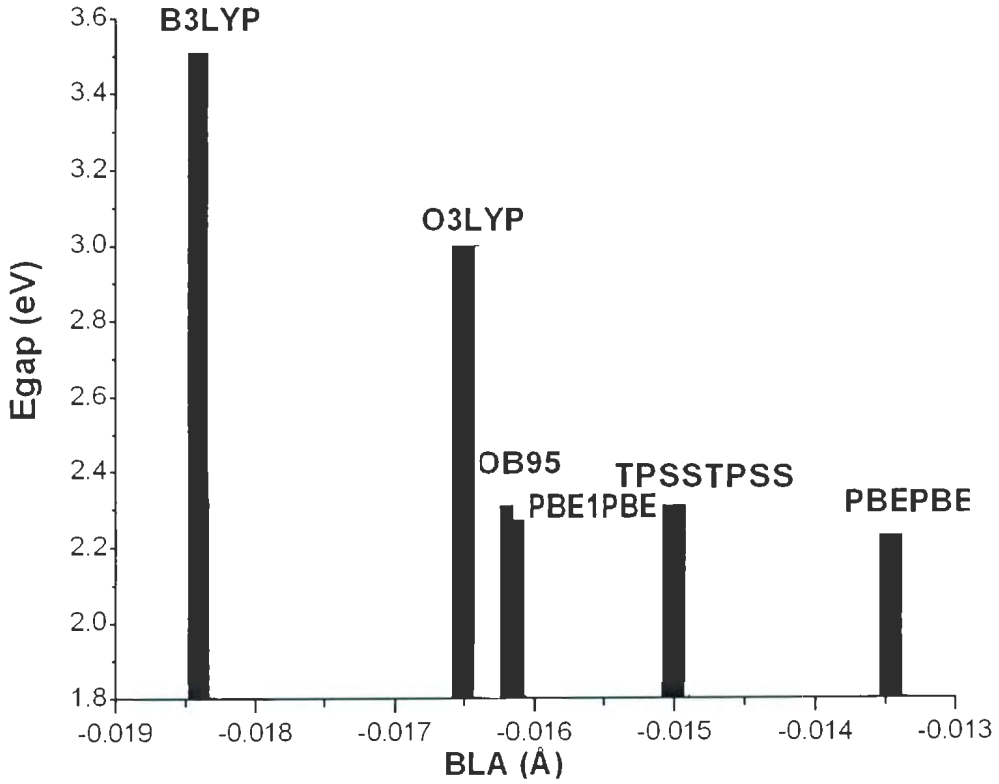

Figure 5.11: E_{gap}'s of OxF_3 as a function of BLA's as obtained from various DFT functionals (with 6-31G* basis set and 32 k points).

Table 5.7: Geometry parameters of $OxF_{1.5}$ isomers as obtained from 32 k-point 1D solid state DFT calculations. Tv's and BLA's (in A), dipole moments (in debye) are listed.

Method	Tv	BLA	Dipole
B3LYP/6-31G*	15.94	-0.0257	0.28,1.16,1.79
O3LYP/6-31G*	16.01	-0.0184	-0.02,-1.69,1.72
OB95/6-31G*	16.04	-0.0205	0.00,2.05,0.63
PBEPBE/6-31G*	15.94	-0.0269	0.00,-1.87,2.31
PBE1PBE/6-31G*	15.97	-0.0270	0.16,2.02,1.33
TPSSTPSS/6-31G*	15.95	-0.0285	0.00,-1.89,2.33

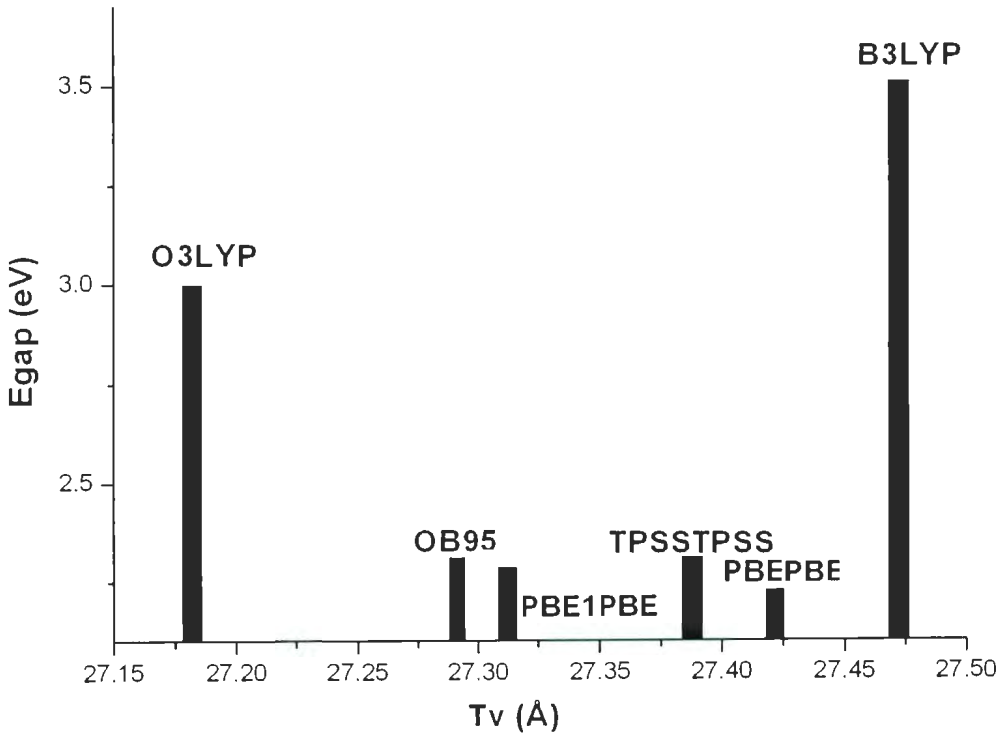

Figure 5.12: E_{gap}'s of OxF_3 as a function of Tv's as obtained from various DFT functionals (with 6-31G* basis set and 32 k points).

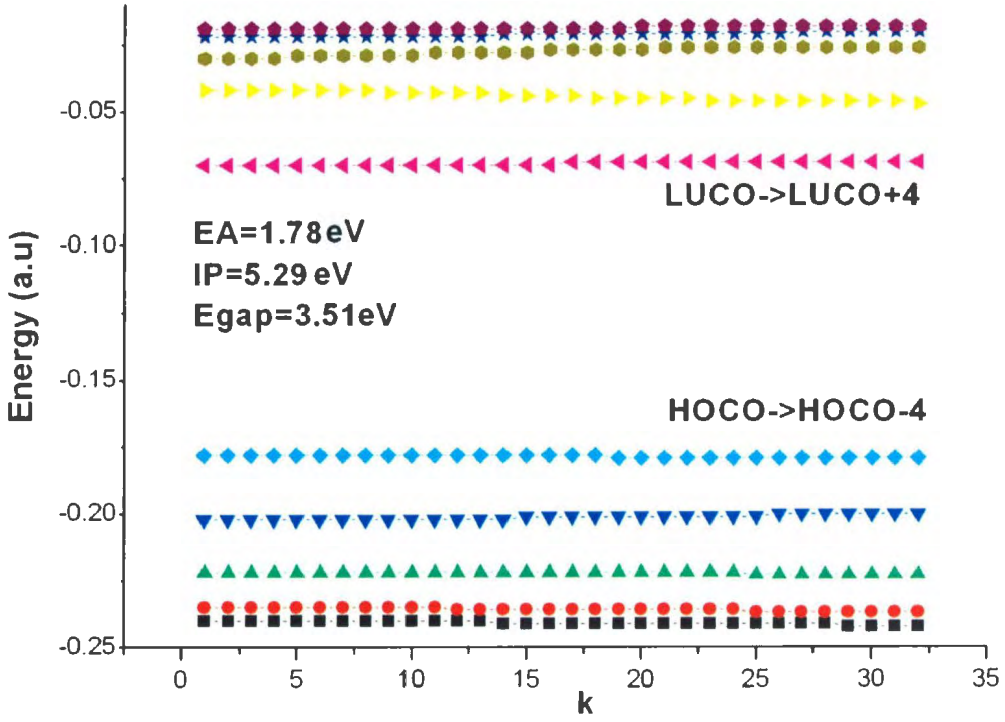

Figure 5.13: The DFT/B3LYP 1D band structure of OxF_3 with 6-31G* basis set and 32 k points. For clarity, different colors have been used for different energy bands corresponding to the top 10 bands (HOCO-4 to LUCO+4).

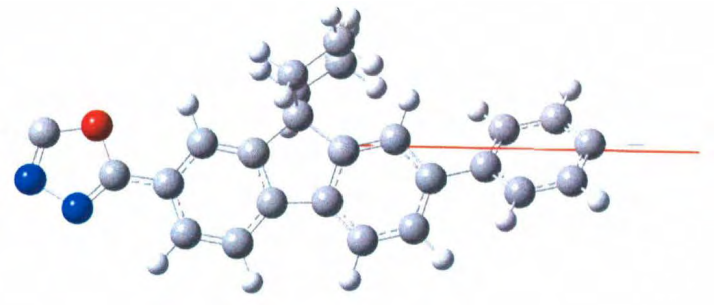

Figure 5.14: Molecular structure of $OxF_{1.5}$ (one unit cell is displayed).

BLA's are larger than those of either OxF_1 and OxF_2. This indicates that charge is more localized in this structure. Its dipole moment is similar (somewhat smaller) to those of OxF_1 and OxF_2.

Table 5.8: E_{total}, IP, EA, E_{gap} and max-gap values of $OxF_{1.5}$ as obtained from 32 k-point 1D solid state DFT calculations. E_{total} is in hartree and all other energies are in eV.

Method	E_{total}	IP	EA	E_{gap}	max-gap
B3LYP/6-31G*	-1149.45	5.49	2.12	3.37	4.40
O3LYP/6-31G*	-1147.00	5.22	2.39	2.83	3.92
OB95/6-31G*	-1149.17	4.84	2.67	2.17	3.14
PBEPBE/6-31G*	-1148.01	5.08	2.48	2.60	3.24
PBE1PBE/6-31G*	-1148.14	5.74	2.05	3.69	4.76
TPSSTPSS/6-31G*	-1148.65	5.07	2.38	2.70	3.34

As shown in Table 5.8, the E_{total} of $OxF_{1.5}$ is around -1148 hartrees. Its E_{gap}'s are nearly the same as those found for OxF_2. Figure 5.15 displays its band structure. As previously observed its bands are relatively flat. For example, the E_{width} of the valence band is 0.33 eV and the conduction band is 0.35 eV for the B3LYP functional.

5.5 Conclusions

OxF_n polymer layers are used to improve the electron transport of PLEDs by better matching their EA energy levels to the cathode one. Experimentally OxF_2 reduces the energy barrier with the cathode more than OxF_3. In general DFT calculations have been able to predict that trend. However the magnitudes of the EAs as obtained by the DFT calculations are off by 0.5-0.8 eV. The magnitudes of IPs show better agreement with experimental values (differences are of the order of 0.4-0.7 eV). Both O3LYP and B3LYP give the best agreement with experimental data for E_{gap}'s. As

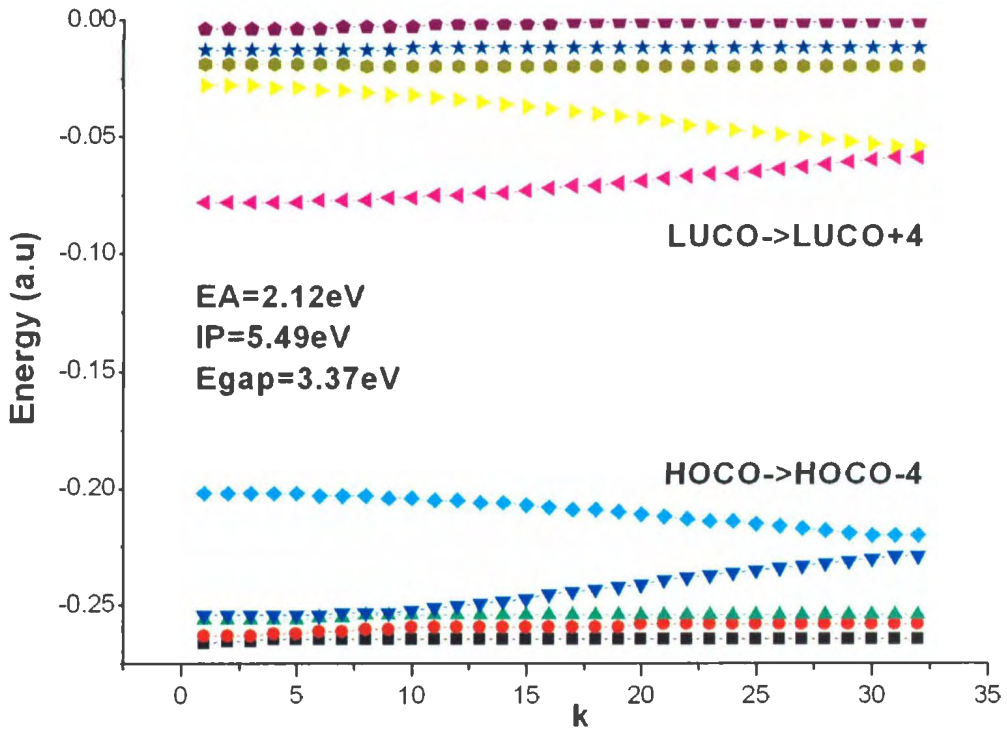

Figure 5.15: The DFT/B3LYP 1D band structure of $OxF_{1.5}$ with 6-31G* basis set and 32 k points. For clarity, different colors have been used for different energy bands corresponding to the top 10 bands (HOCO-4 to LUCO+4).

shown in Figure 5.16, the experimental E_{gap} value lies between the B3LYP and O3LYP results. The E_{gap}'s of OxF_n (n=1,2) obey the same order in energy, that is, from smallest to largest E_{gap} the order is: PBEPBE < OB95 < TPSSTPSS < O3LYP < B3LYP < PBE1PBE. This order for OxF_3 is as follows: PBEPBE < PBE1PBE < TPSSTPSS = OB95 < O3LYP < B3LYP. For $OxF_{1.5}$, the E_{gap}'s are in the order of: OB95 < PBEPBE < TPSSTPSS < B3LYP < O3LYP < PBE1PBE.

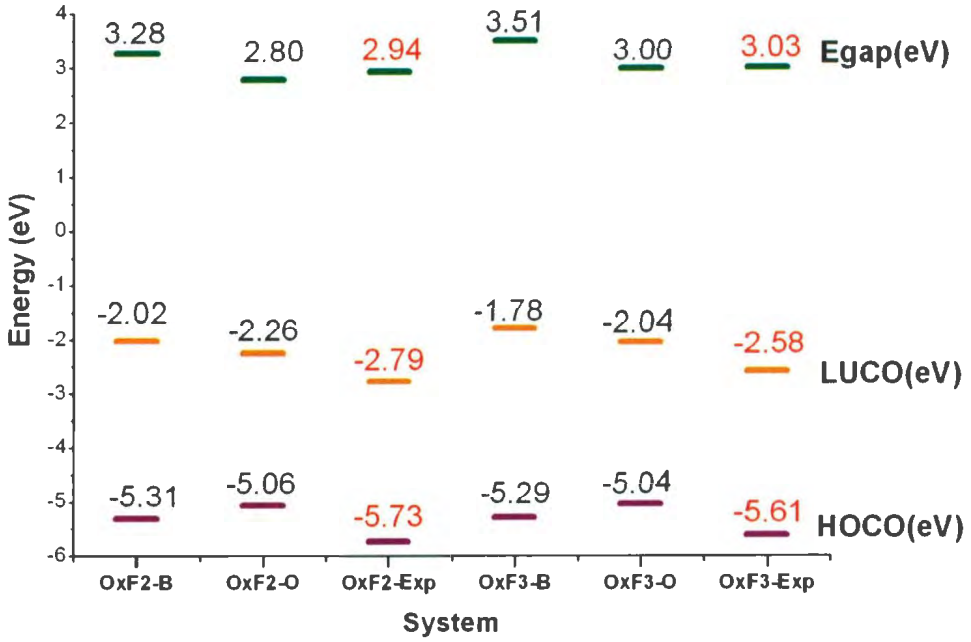

Figure 5.16: E_{gap}'s, IPs and EAs of OxF_n with B(O)3LYP/6-31G* and 32 k-points. OxF2-B stands for OxF_2 with B3LYP/6-31G* method and for and OxF2-O stands for OxF_2 with O3LYP/6-31G* method, the same for OxF_3.

Chapter 6

The Electronic Band Structures of $TPAF_n$

In this Chapter, we focus on investigating the electronic band structure properties of alternating triphenylamine-fluorene copolymers $TPAF_n$ (with $n = 1 - 3$) with the use of 1D solid state DFT calculations. As previously discussed in Chapter 5, we compare the computational results with the experimental observations as given in reference [1]. We also perform calculations for $TPAF_4$. However, because of its large size, the DFT calculation was performed on the finite oligomer instead of the infinite 1D $TPAF_4$ chain. $TPAF_n$ is typically used to improve the hole transport in PLED. This is because it has been found experimentally that its IP value matches the IP of ITO (the anode) better than other organic conjugated polymers. Experimentally $C_6H_{12}OH$ and C_8H_{17} chains have been used as side chains (R' and R respectively in Figure 6.1) on fluorene units in $TPAF_n$. The hydroxyl end group (-OH) reacts with a cross-linker (such as TBPA) to produce a cross-linked network that is very important for the formation of stable multilayer devices. In our calculations, similar to what was done in Chapter 5 we replace (with one exception) the long chains with shorter

Figure 6.1, the chemical structure (as used experimentally) of TPAF$_n$ is shown. The bond lengths for TPAF$_n$ (with $n = 1 - 4$) are given in the Appendix.

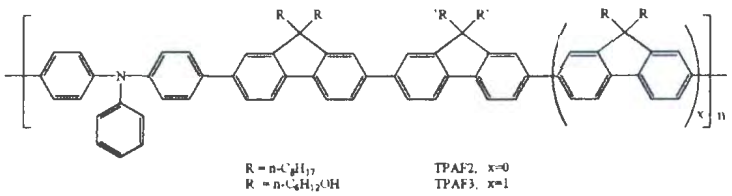

Figure 6.1: Chemistry structure of TPAF$_n$ unit cell.

6.1 TPAF$_1$

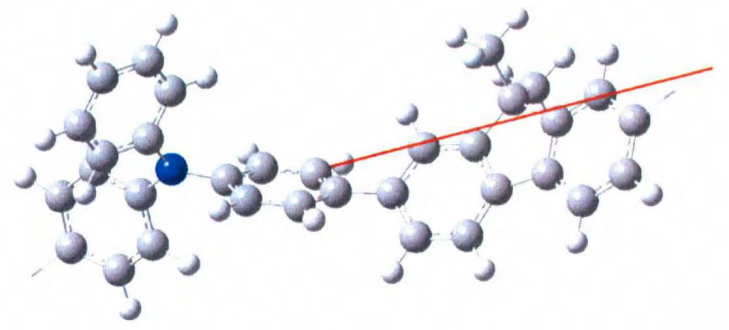

Figure 6.2: Molecular structure of TPAF$_1$ isomer 1 (one unit cell is displayed).

Figure 6.2 shows the molecular structure of TPAF$_1$ with CH_3 side chains which is designated as isomer 1. In this figure (as in all molecular structures of TPAF$_n$), the TBPA group is the one that includes three benzene rings attached to the nitrogen atom (N). The molecular structure of TPAF$_1$ with -OH group replacing one of the H in the methyl group is displayed in Figure 6.3. It is labeled as isomer 2.

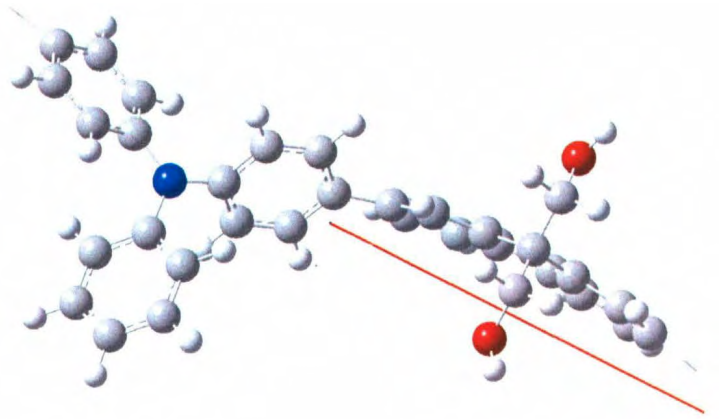

Figure 6.3: Molecular structure of $TPAF_1$ isomer 2 with hydroxy end group (one unit cell is displayed).

Table 6.1: Geometry parameters of $TPAF_1$ isomers as obtained from 32 k-point 1D solid state DFT calculations. Tv's and BLA's (in Å), dipole moments (in debye) are listed.

Method	**Tv**	**BLA**	**Dipole**
$TPAF_1$ isomer 1			
B3LYP/6-31G*	17.33	-0.0159	0.00,-0.61,-0.40
O3LYP/6-31G*	17.21	-0.0153	0.00,-0.67,-0.39
OB95/6-31G*	17.29	-0.0129	0.00,-0.81,-0.42
PBEPBE/6-31G*	17.35	-0.0100	0.00,-0.66,-0.36
PBE1PBE/6-31G*	17.24	-0.0165	0.00,-0.65,-0.44
TPSSTPSS/6-31G*	17.33	-0.0130	0.01,-2.57,1.26
$TPAF_1$ isomer 2			
B3LYP/6-31G*	17.33	-0.0158	0.02,-2.62,1.26
O3LYP/6-31G*	17.35	-0.0151	0.02,-2.76,1.15
OB95/6-31G*	17.30	-0.0129	0.02,-2.67,1.15
PBEPBE/6-31G*	17.35	-0.0162	0.01,-2.52,1.23
PBE1PBE/6-31G*	17.24	-0.0114	0.01,-2.66,1.23
TPSSTPSS/6-31G*	17.35	-0.0129	0.01,-2.57,1.26

Table 6.1: Geometry parameters of $TPAF_1$ isomers as obtained from 32 k-point 1D solid state DFT calculations. Tv's and BLA's (in Å), dipole moments (in debye) are listed.

Method	Tv	BLA	Dipole
$TPAF_1$ isomer 1			
B3LYP/6-31G*	17.33	-0.0159	0.00,-0.61,-0.40
O3LYP/6-31G*	17.21	-0.0153	0.00,-0.67,-0.39
OB95/6-31G*	17.29	-0.0129	0.00,-0.81,-0.42
PBEPBE/6-31G*	17.35	-0.0100	0.00,-0.66,-0.36
PBE1PBE/6-31G*	17.24	-0.0165	0.00,-0.65,-0.44
TPSSTPSS/6-31G*	17.33	-0.0130	0.01,-2.57,1.26
$TPAF_1$ isomer 2			
B3LYP/6-31G*	17.33	-0.0158	0.02,-2.62,1.26
O3LYP/6-31G*	17.35	-0.0151	0.02,-2.76,1.15
OB95/6-31G*	17.30	-0.0129	0.02,-2.67,1.15
PBEPBE/6-31G*	17.35	-0.0162	0.01,-2.52,1.23
PBE1PBE/6-31G*	17.24	-0.0114	0.01,-2.66,1.23
TPSSTPSS/6-31G*	17.35	-0.0129	0.01,-2.57,1.26

cells of the two isomers of TPAF are nonplanar.

Table 6.2 lists the energy results of $TPAF_1$. The E_{total} of $TPAF_1$ isomer 1 is around -1327 hartrees which is comparable OxF_2 total energy. The E_{total} of $TPAF_1$ isomer 2 is reduced by 150.0 hartrees because of the -OH end group is close to -1477 hartrees. $TPAF_1$ isomer 2 has a larger E_{gap} than $TPAF_1$ isomer 1. The difference ranges between 0.03 to 0.09 eV. For example, B3LYP gives BLA of -0.0168 Å for isomer 1 and -0.0158 Å for isomer 2 and the E_{gap} is 0.03 eV larger for isomer 2 than for isomer 1. In general, the presence of the hydroxyl end groups increase E_{gap} and decreases IP and EA by approximately 0.1 eV. The max-gaps of $TPAF_1$ are almost the same value as E_{gap}'s which means that E_{width}'s are very narrow. This is clearly illustrated in Figures 6.8 and 6.9 where the top bands for $TPAF_1$ isomers are plotted and are shown to be very flat.

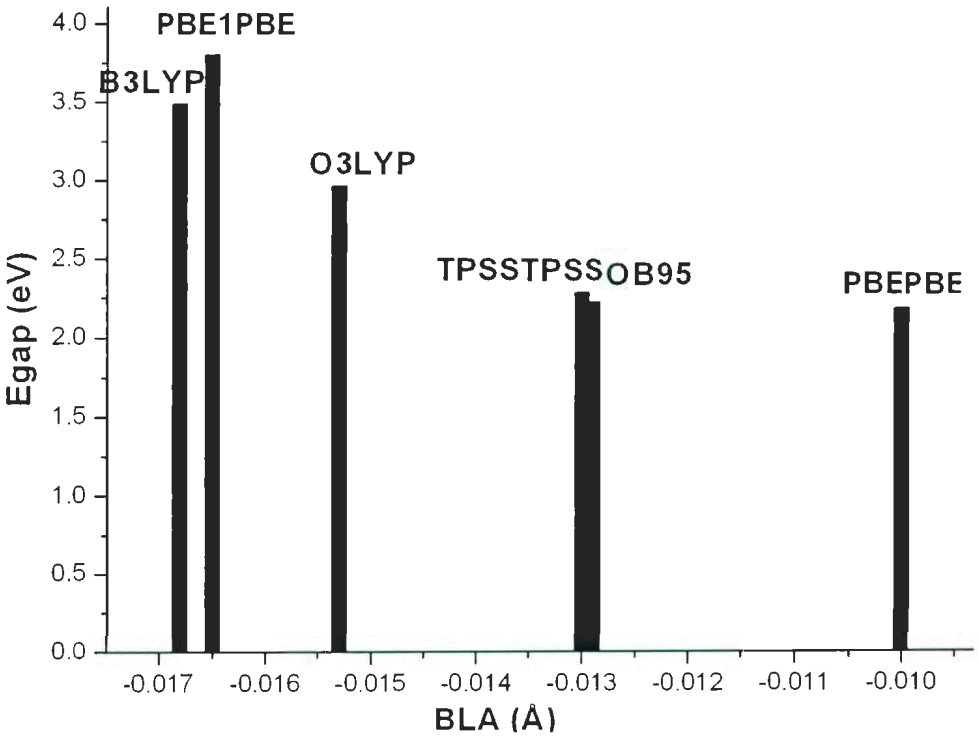

Figure 6.4: E_{gap}'s of $TPAF_1$ isomer 1 as a function of BLA's as obtained from various DFT functionals (with 6-31G* basis set and 32 k points).

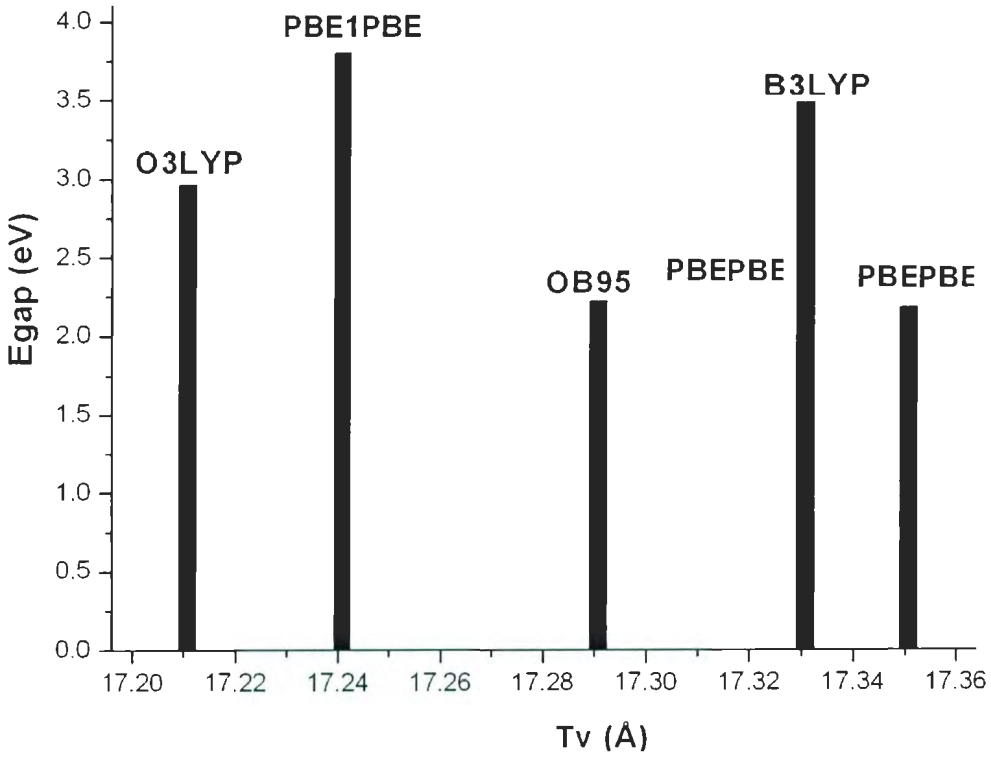

Figure 6.5: E_{gap}'s of $TPAF_1$ isomer 1 as a function of Tv's as obtained from various DFT functionals (with 6-31G* basis set and 32 k points).

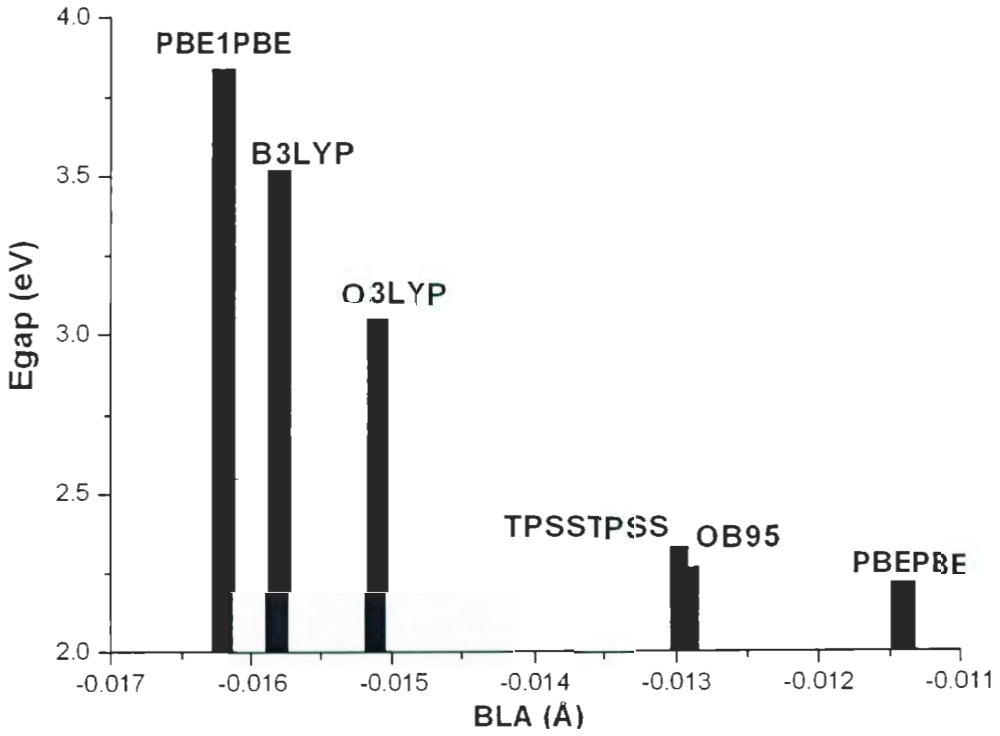

Figure 6.6: E_{gap}'s of $TPAF_1$ isomer 2 as a function of BLA's as obtained from various DFT functionals (with 6-31G* basis set and 32 k points).

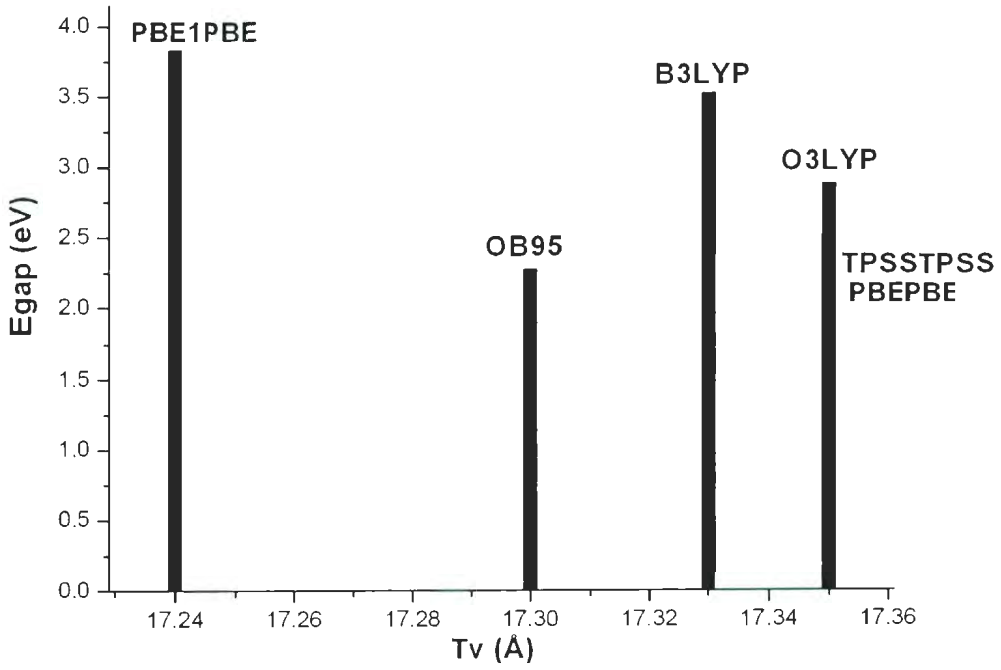

Figure 6.7: E_{gap}'s of $TPAF_1$ isomer 2 as a function of Tv's as obtained from various DFT functionals (with 6-31G* basis set and 32 k points).

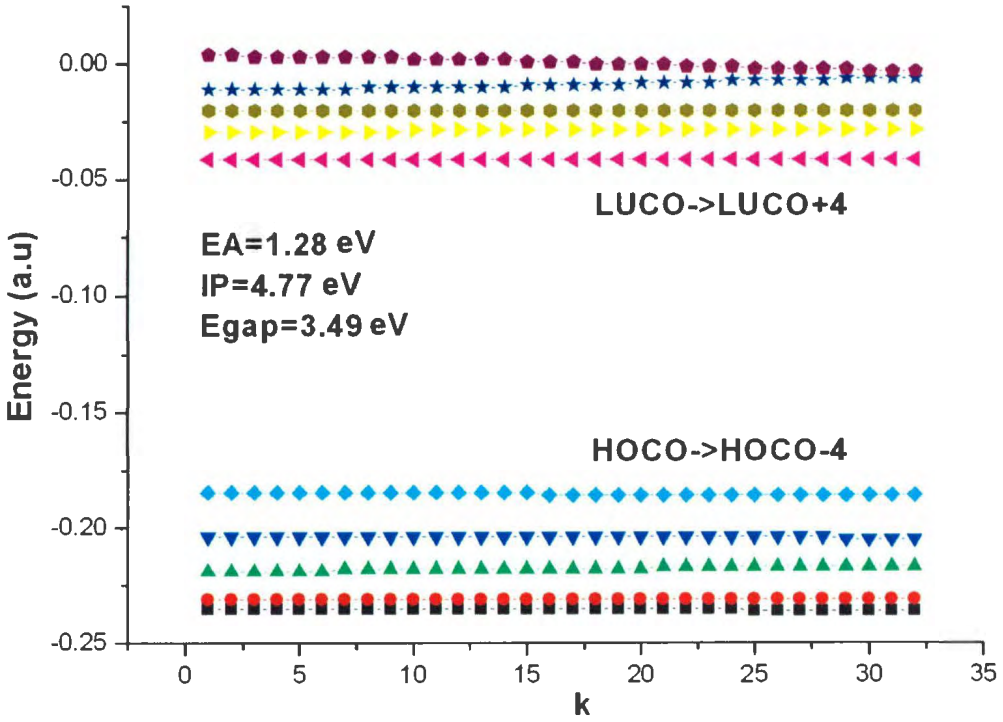

Figure 6.8: The DFT/B3LYP 1D band structure of $TPAF_1$ isomer 1 with 6-31G* basis set and 32 k points. For clarity, different colors have been used for different energy bands corresponding to the top 10 bands (HOCO-4 to LUCO+4).

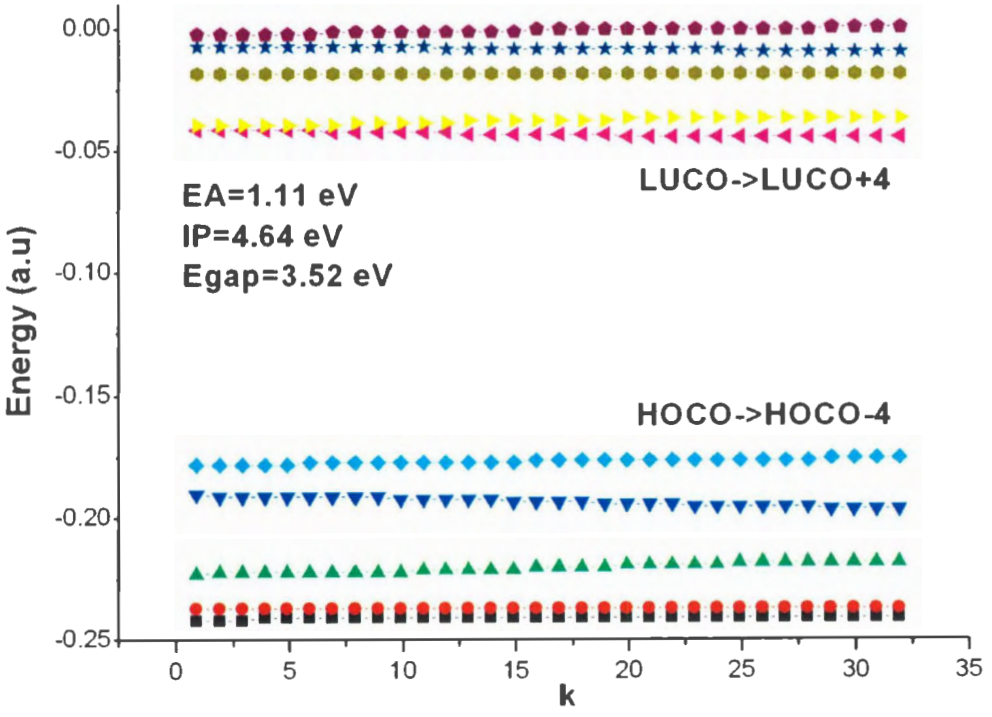

Figure 6.9: The DFT/B3LYP 1D band structure of $TPAF_1$ isomer 2 with 6-31G* basis set and 32 k points. For clarity, different colors have been used for different energy bands corresponding to the top 10 bands (HOCO-4 to LUCO+4).

Table 6.2: E_{total}, IP, EA, E_{gap} and max-gap values of $TPAF_1$ isomers as obtained from 32 k-point 1D solid state DFT calculations. E_{total} is in hartree and all other energies are in eV.

Method	E_{total}	IP	EA	E_{gap}	max-gap
$TPAF_1$-isomer 1					
B3LYP/6-31G*	-1327.36	4.77	1.28	3.49	3.84
O3LYP/6-31G*	-1324.44	4.50	1.53	2.96	3.31
OB95/6-31G*	-1327.02	4.10	1.87	2.22	2.53
PBEPBE/6-31G*	-1325.67	4.15	1.97	2.18	2.50
PBE1PBE/6-31G*	-1325.81	5.00	1.20	3.80	4.16
TPSSTPSS/6-31G*	-1327.61	4.12	1.84	2.28	2.61
$TPAF_1$-isomer 2					
B3LYP/6-31G*	-1477.76	4.64	1.11	3.52	3.89
O3LYP/6-31G*	-1477.23	4.33	1.28	3.05	3.40
OB95/6-31G*	-1477.39	3.98	1.71	2.27	2.58
PBEPBE/6-31G*	-1475.93	4.03	1.81	2.22	2.54
PBE1PBE/6-31G*	-1476.06	4.87	1.03	3.84	4.22
TPSSTPSS/6-31G*	-1478.02	4.01	1.68	2.33	2.65

6.2 $TPAF_2$

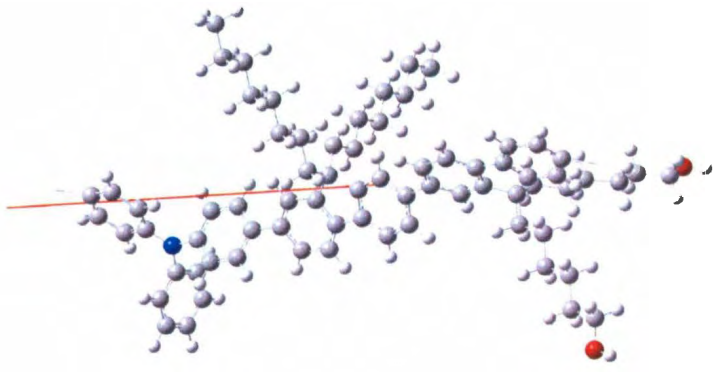

Figure 6.10: Molecular structure of $TPAF_2$ with side chain R (one unit cell is displayed).

Figure 6.10 shows the molecular structure of $TPAF_2$ unit cell with side chains R and

R'. In this figure, the R and R' side chains are of the same length as the ones used experimentally as discussed above.

Table 6.3: Geometry parameters of $TPAF_2$ as obtained from 32 k-point 1D solid state DFT calculations. Tv's and BLA's (in Å), dipole moments (in debye) are listed.

Method	Tv	BLA	Dipole
B3LYP/6-31G*	25.36	-0.0165	0.00,2.87,-1.24
O3LYP/6-31G*	25.38	-0.0154	0.00,2.73,-1.36
OB95/6-31G*	25.50	-0.0160	0.00,2.44,-1.37
PBEPBE/6-31G*	25.61	-0.0136	0.04,2.51,-1.59
PBE1PBE/6-31G*	25.58	-0.0189	-0.04,2.92,-1.19
TPSSTPSS/6-31G*	25.60	-0.0150	0.02,2.65,-1.40

In Table 6.3, the geometrical parameters of $TPAF_2$ are given. The average magnitude of BLA of $TPAF_2$ is 0.0159 Å, which is 0.0019 Å larger than the average value for $TPAF_1$ isomers. The optimized Tv is approximately 25.4 Å. The variation of BLA and Tv with E_{gap} for $TPAF_2$ is displayed in Figures 6.11 and 6.12. As noted above, in general larger magnitude of BLA is associated with larger E_{gap} there is no clear correlation between Tv and E_{gap}. Table 6.3 also shows that the dipole moment has two significant components. The larger one points along the chain backbone and the smaller one is associated with the presence of the hydroxyl groups. The magnitudes of the respective components are similar to those obtained for $TPAF_1$ isomer 2. This again illustrates that the results of our calculations are relatively insensitive to the length of the side chains R and R'.

Table 6.3 and Table 6.4 show the geometry and energy calculation results. Table 6.4 shows that the average E_{total} is -2055 hartrees. The experimental E_{gap} of $TPAF_2$ is 2.89 eV. Both B3LYP and O3LYP give the best agreement with this experimental result. B3LYP overestimates it by 0.44 eV and O3LYP underestimates it by 0.1 eV. Other functionals give larger deviations (except for PBE1PBE all underestimate E_{gap}). All

Table 6.4: E_{total}, IP, EA, E_{gap} and max-gap values of $TPAF_2$ as obtained from 32 k-point 1D solid state DFT calculations. E_{total} is in hartree and all other energies are in eV.

Method	E_{total}	IP	EA	E_{gap}	max-gap
B3LYP/6-31G*	-2056.63	4.82	1.49	3.33	3.44
O3LYP/6-31G*	-2052.19	4.53	1.74	2.79	2.92
OB95/6-31G*	-2056.10	4.12	2.08	2.05	2.17
PBEPBE/6-31G*	-2054.05	4.16	2.15	2.01	2.15
PBE1PBE/6-31G*	-2054.26	5.05	1.42	3.63	3.75
TPSSTPSS/6-31G*	-2057.00	4.14	2.04	2.10	2.24
Expt [1]		5.16	2.27	2.89	

DFT approximations also underestimate both the IP and EA when compared with the experimental results of 5.16 eV and 2.27 eV respectively. For example, for B3LYP, IP is underestimated by 0.34 eV and EA by 0.78 eV in comparison to the experimental values. In general the deviations for EA are larger than those for IP. In Figure 6.13, the band structure of top levels of $TPAF_2$ for B3LYP approximation is displayed. Once again all bands are very flat. This can also be deduced from the difference between max-gap and E_{gap} which gives an indication about the E_{width}'s (which must be of the order of 0.05 eV).

6.3 $TPAF_3$

The molecular structure of $TPAF_3$ is shown in Figure 6.14. In Table 6.5, the average Tv of $TPAF_3$ is 32.85 Å , comparable with OxF_3 case. The average magnitude of BLA for $TPAF_3$ is 0.0184 Å. The magnitude of BLA using O3LYP is 0.0185 Å and 0.0210 Å using B3LYP. For $TPAF_3$ calculation, BLA is still proportional to E_{gap} as seen in Figure 2.15. Tv does not correlate with E_{gap} (see Figure 2.16). The largest component of dipole moment is along the chain backbone and is of the order of 3 D.

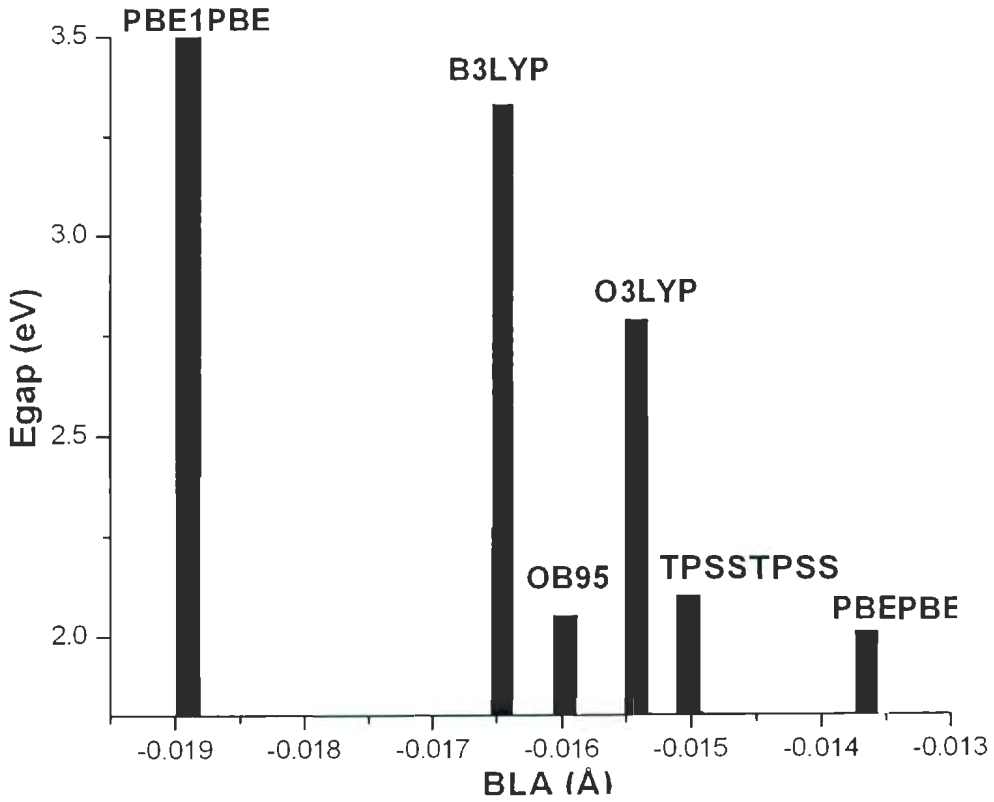

Figure 6.11: E_{gap}'s of $TPAF_2$ as a function of BLA's as obtained from various DFT functionals (with 6-31G* basis set and 32 k points).

Table 6.5: Geometry parameters of $TPAF_3$ as obtained from 32 k-point 1D solid state DFT calculations. Tv's and BLA's (in Å), dipole moments (in debye) are listed.

Method	Tv	BLA	Dipole
B3LYP/6-31G*	32.86	-0.0210	0.00,0.07,-3.04
O3LYP/6-31G*	32.67	-0.0185	0.00,0.15,-3.01
OB95/6-31G*	32.83	-0.0174	0.00,0.17,-2.95
PBEPBE/6-31G*	32.94	-0.0158	0.00,0.09,-3.11
PBE1PBE/6-31G*	32.95	-0.0211	0.00,-0.34,-3.02
TPSSTPSS/6-31G*	32.92	-0.0171	0.01,1.32,-2.84

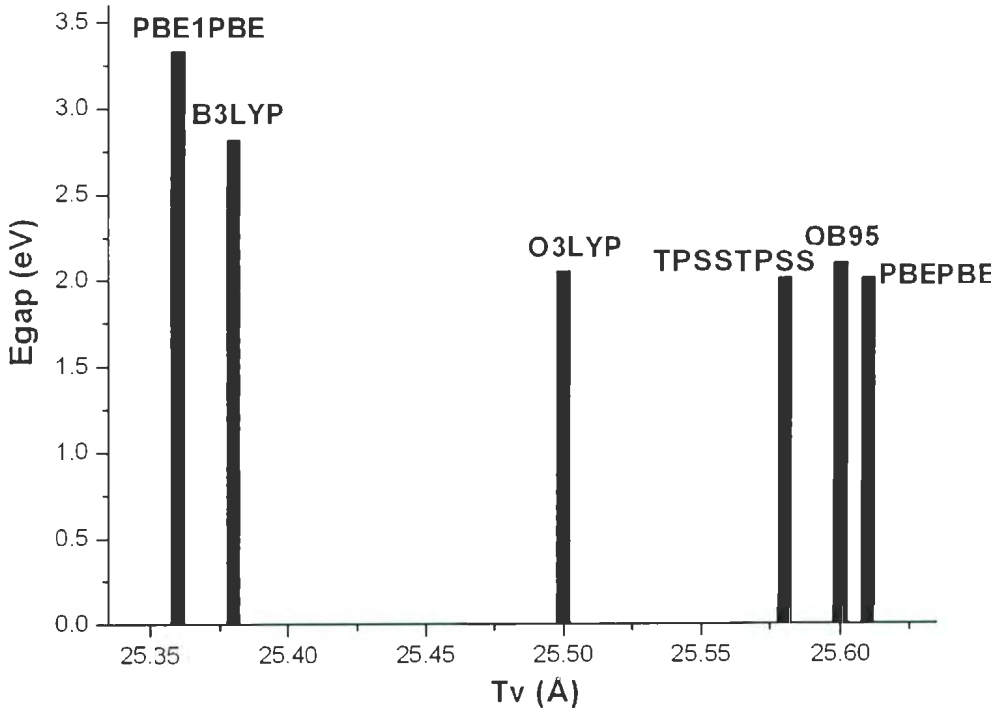

Figure 6.12: E_{gap}'s of $TPAF_2$ as a function of Tv's as obtained from various DFT functionals (with 6-31G* basis set and 32 k points).

Table 6.6: E_{total}, IP, EA, E_{gap} and max-gap values of $TPAF_3$ as obtained from 32 k-point 1D solid state DFT calculations. E_{total} is in hartree and all other energies are in eV.

Method	E_{total}	IP	EA	E_{gap}	max-gap
B3LYP/6-31G*	-2635.49	4.82	1.54	3.28	3.36
O3LYP/6-31G*	-2629.76	4.56	1.79	2.77	2.86
OB95/6-31G*	-2634.81	4.17	2.11	2.06	2.14
PBEPBE/6-31G*	-2632.16	4.22	2.21	2.01	2.09
PBE1PBE/6-31G*	-2632.44	5.05	1.48	3.58	3.67
TPSSTPSS/6-31G*	-2635.97	4.19	2.09	2.10	2.18
Expt. [1]		5.21	2.32	2.89	

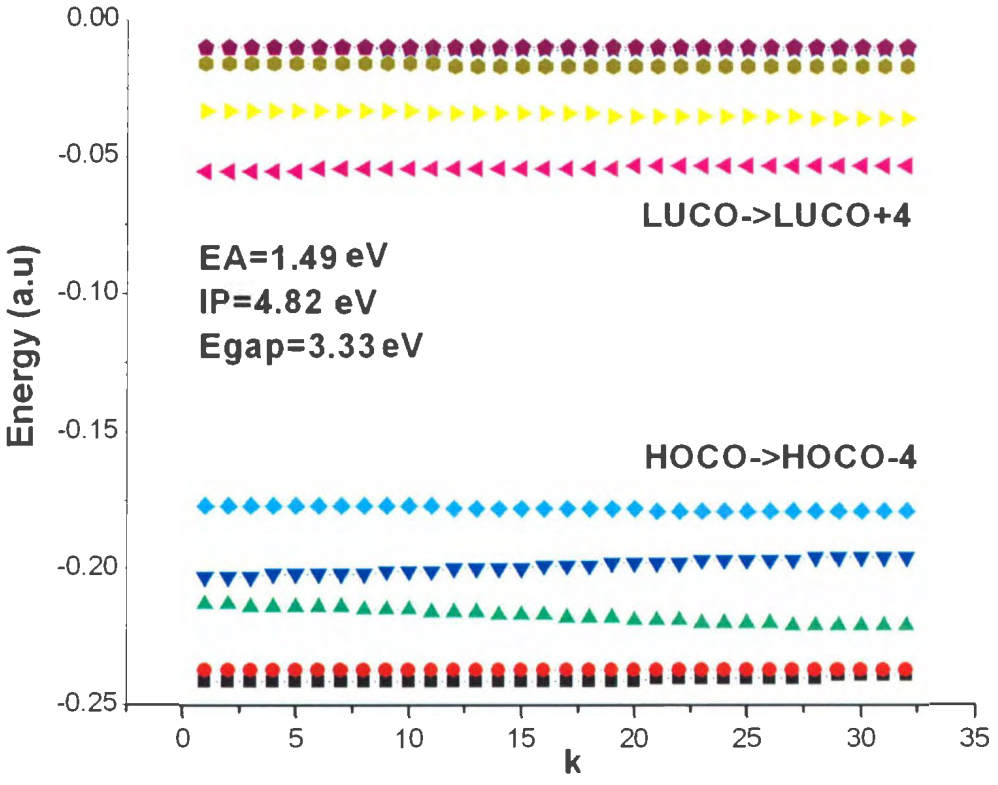

Figure 6.13: The DFT/B3LYP 1D band structure of $TPAF_2$ with 6-31G* basis set and 32 k points. For clarity, different colors have been used for different energy bands corresponding to the top 10 bands (HOCO-4 to LUCO+4).

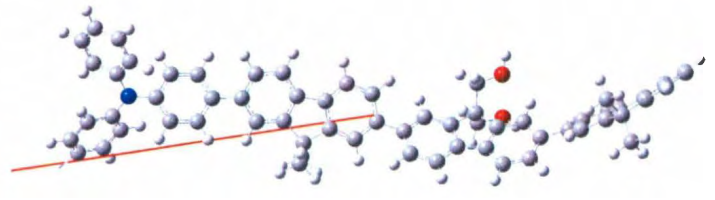

Figure 6.14: Molecular structure of $TPAF_3$ (one unit cell is displayed).

We follow the same discussion as with $TPAF_2$. Table 6.6 lists the energy results of $TPAF_3$. The average E_{total} of $TPAF_3$ is -2633 hartrees. The experimental E_{gap} of $TPAF_3$ is 2.89 eV. Both B3LYP and O3LYP give the best agreement with this experimental result. B3LYP overestimates it by 0.39 eV and O3LYP underestimates it by 0.12 eV. Other functionals give larger deviations (except for PBE1PBE all underestimate E_{gap}). All DFT approximations also underestimate both the IP and EA when compared with the experimental results of 5.21 and 2.32 eV respectively. For example, for B3LYP, IP is underestimated by 0.39 eV and EA by 0.78 eV in comparison to the experimental values. And again, in general the deviations for EA are larger than those for IP. In Figure 6.17, the band structure of top levels of $TPAF_3$ for B3LYP approximation is displayed. Once again all bands are very flat. This can also be deduced from the difference between max-gap and E_{gap} which gives an indication about the E_{width}'s (which must be less than 0.05 eV).

6.4 $TPAF_4$ Finite Molecule Calculations

Because of limited computational resource, $TPAF_4$ band structure is investigated using finite oligomer method. This is similar to our attempt for trans-PA oligomers. The molecular structure of $TPAF_4$ monomer is displayed in Figure 6.18.

Table 6.7: Energies of $TPAF_4$ oligomers at O3LYP/6-31G* level. E_{total} is in hartree, others are in eV.

No. of monomer	E_{total}	IP	EA	E_{gap}
1	-3208.52	4.61	1.72	2.89
2(b)	-6429.91	4.81	1.51	3.30

Energy results for $TPAF_4$'s E_{gap}'s are given in Table 6.7. IP band increases with the

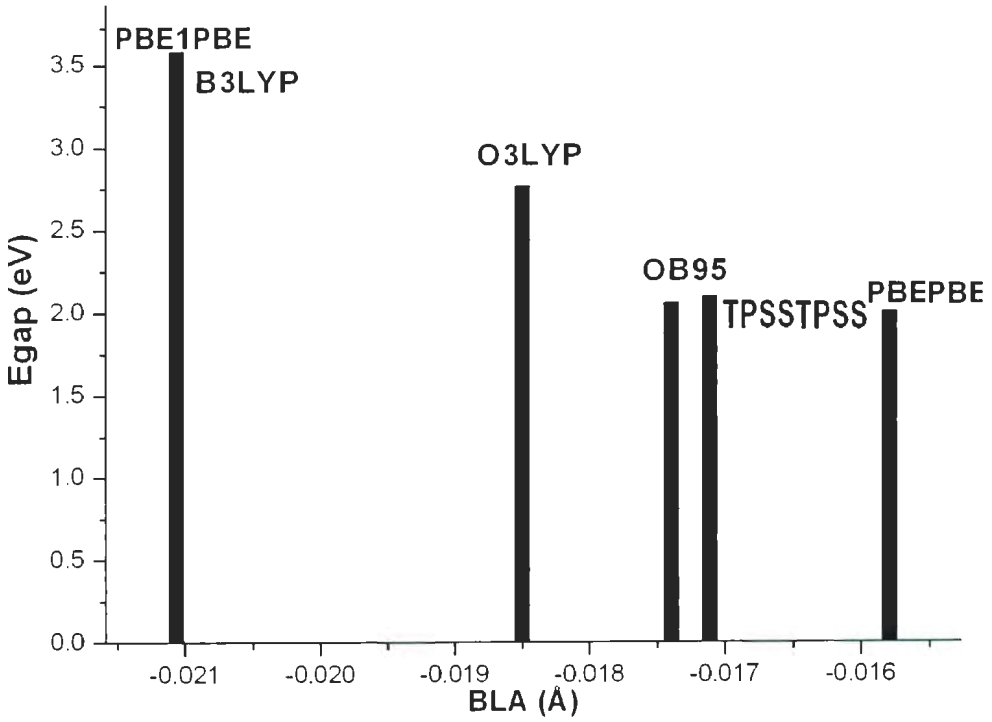

Figure 6.15: E_{gap}'s of $TPAF_3$ as a function of BLA's as obtained from various DFT functionals (with 6-31G* basis set and 32 k points).

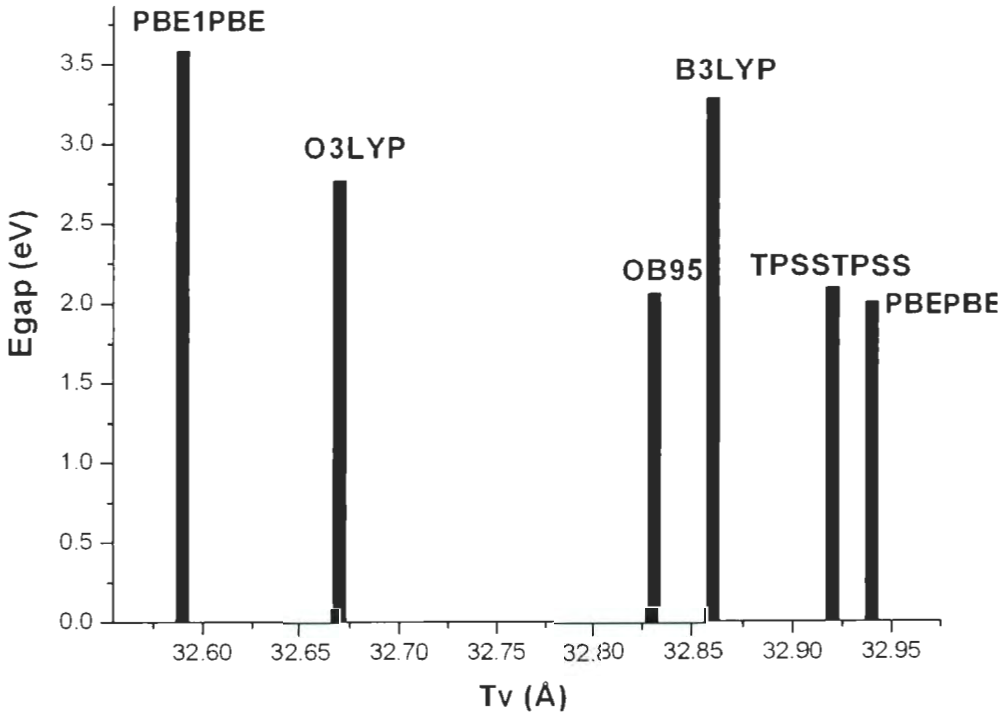

Figure 6.16: E_{gap}'s of $TPAF_3$ as a function of Tv's as obtained from various DFT functionals (with 6-31G* basis set and 32 k points).

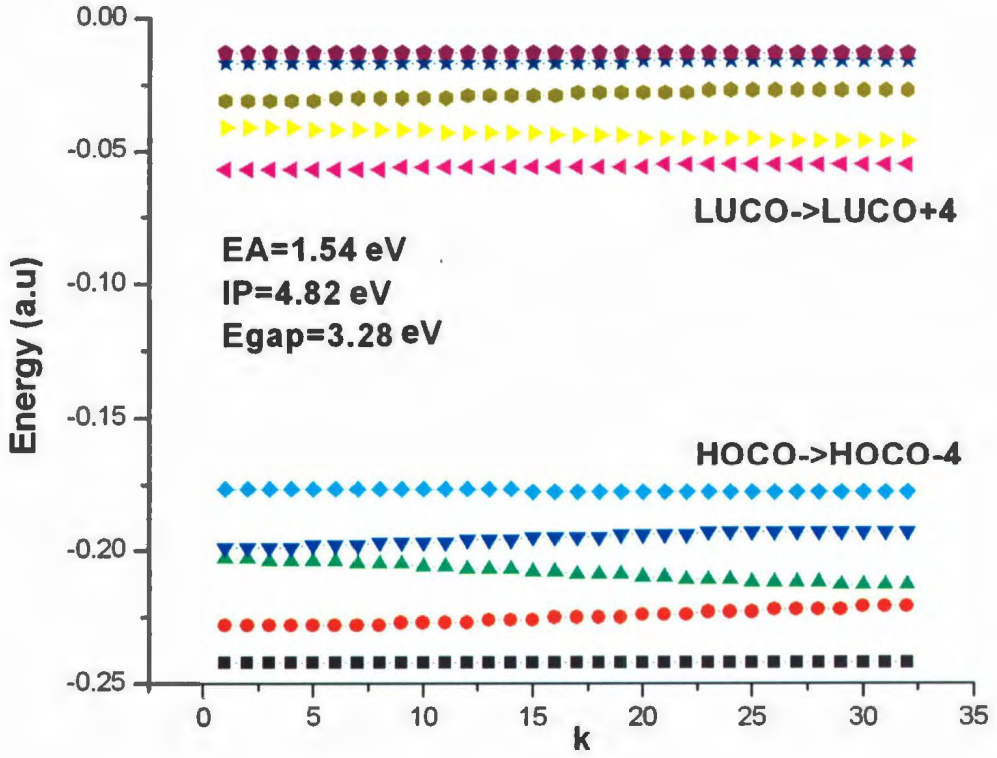

Figure 6.17: The DFT/B3LYP 1D band structure of $TPAF_3$ with 6-31G* basis set and 32 k points. For clarity, different colors have been used for different energy bands corresponding to the top 10 bands (HOCO-4 to LUCO+4).

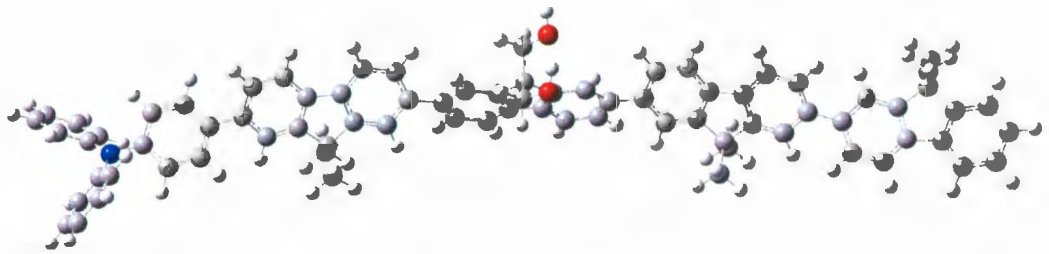

Figure 6.18: Molecular structure of $TPAF_4$ monomer.

oligomeric size while EA band decreases. $TPAF_4$ with one monomer produces E_{gap} 2.89 eV and it is close to that obtained for $TPAF_3$.

6.5 Conclusions

Experimental results show that two alternating triphenylamine-fluorene copolymers ($TPAF_n$, n=2,3) bearing hydroxyl groups on the side chains, and a cross-linker TBPA form twisted conjugated chains which in general agree with the corresponding computational results. All E_{gap}'s of $TPAF_n$ are of the same order of energy. From smallest to largest E_{gap} with various DFT functional is: PBEPBE < OB95 < TPSSTPSS < O3LYP < B3LYP < PBE1PBE. The experimental E_{gap} value always stays between the B3LYP result and O3LYP result. And PBE1PBE, as mentioned before, gives the largest E_{gap} among six functionals. The B3LYP and O3LYP energy results are summarized and compared with experimental values in Figure 6.19.

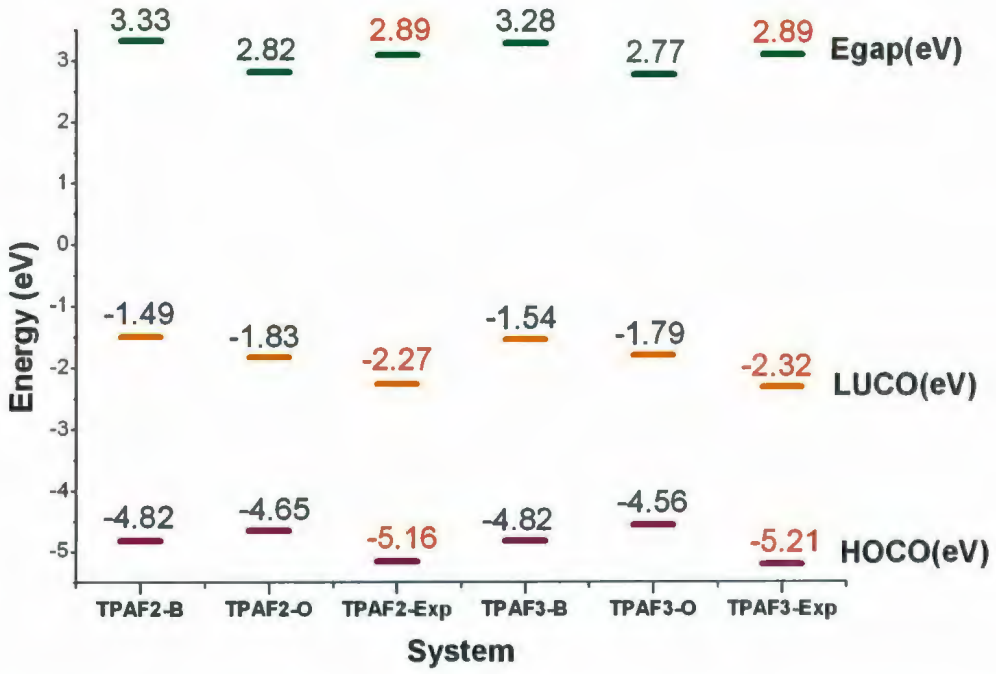

Figure 6.19: E_{gap}'s, IPs and EAs of $TPAF_n$ isomers with B(O)3LYP/6-31G* and 32 k-points. TPAF2-B stands for $TPAF_2$ with B3LYP/6-31G* method and TPAF2-O stands for $TPAF_2$ with O3LYP/6-31G* method, the same for $TPAF_3$.

Chapter 7

Summaries and Conclusions

Chapter 7 lists the major conclusions of this thesis. But first, because both B3LYP and O3LYP, on the whole, give the most accurate values for band gaps and reasonable values for IPs and EAs (as indicated above in chapters 5 and 6), they will be discussed in greater detail below before the main conclusions are stated.

7.1 B3LYP Calculations

The geometry parameters and energies as obtained from B3LYP computations are summarized in Table 7.1. The magnitudes of BLA's of PA isomers are larger than the OxF_n and $TPAF_n$ values. For all system, the magnitudes of BLA's increase with the size of the unit cell. For example, the addition of fluorene group changes BLA from -0.008 Å to -0.018 Å from OxF_1 to OxF_3. The negative sign of BLA's of fluorene-based polymers indicates the aromatic structure in fluorene-based unit cells. In contrast to the magnitudes of BLA's, E_{gap}'s of PA isomers are smaller than E_{gap}'s of fluorene-based polymers.

B3LYP underestimates the E_{gap} in comparison to the experimental value by 0.6 eV

Table 7.1: E_{total}, IP, EA, E_{gap}, max-gap and BLA values of PA and fluorene-based polymers at B3LYP/6-31G* level. E_{total} is in hartree , BLA is in Åand all other energies are in eV. Aromatic cis-PA and $TPAF_1$ isomer 1 are listed. The experimental values are available shown in the brackets.

Molecular	E_{total}	IP	EA	E_{gap}	max-gap	BLA
trans-PA	-77.41	4.12	2.88	1.24 (1.80)	12.03	0.050
cis-PA	-154.81	4.49	2.63	1.86	9.42	0.070
meta-PA	-309.62	4.31	2.78	1.53	5.66	0.070
OxF_1	-918.40	5.50	2.30	3.20	4.95	-0.008
OxF_2	-1575.88	5.31 (5.73)	2.02 (2.79)	3.28 (2.94)	4.03	-0.016
OxF_3	-2056.10	5.29 (5.61)	1.78 (2.58)	3.51 (3.03)	3.80	-0.018
$TPAF_1$	-1327.36	4.77	1.28	3.49	3.84	-0.017
$TPAF_2$	-2056.63	4.82 (5.16)	1.49 (2.27)	3.33 (2.89)	3.44	-0.017
$TPAF_3$	-2635.49	4.82 (5.21)	1.54 (2.32)	3.28 (2.89)	3.36	-0.021

for trans-PA and overestimates it by approximately 0.4 eV for OxF_2, OxF_3, $TPAF_2$, and $TPAF_3$. Compared to cis-PA and meta-PA, E_{gap} of trans-PA is smaller due to its raised IP and lowered EA. The E_{width}'s of trans-PA and cis-PA are similar in magnitude (4-5 eV) whereas the E_{width} of meta-PA is smaller (closer to 2 eV) due to its larger unit cell. For the fluorene-based polymers, the band widths are quite flat (less than 0.7 eV). The IP is 5.50 eV for OxF_1, 5.31 eV for OxF_2 and 5.29 eV for OxF_3 which should be compared with the experimental 5.73 eV and 5.61 eV for OxF_2 and OxF_3 respectively. The IP differences are of the order of 0.4 eV. EA is 2.30 eV for OxF_1, 2.02 eV for OxF_2 and 1.78 eV for OxF_3 which should be compared with the experimental 2.79 eV and 2.58 eV for OxF_2 and OxF_3 respectively. The EA differences are of the order of 0.8 eV which are larger than those for the IP by a factor of two or so. The IP is 4.77 eV for $TPAF_1$, 4.82 eV for $TPAF_2$ and 4.82 eV for $TPAF_3$ which should be compared with the experimental 5.16 eV and 5.21 eV for $TPAF_2$ and $TPAF_3$ respectively. Again, the IP differences are of the order of 0.4 eV. EA is 1.28 eV for $TPAF_1$, 1.49 eV for $TPAF_2$ and 1.54 eV for $TPAF_3$ which should be compared

with the experimental 2.27 eV and 2.32 eV for $TPAF_2$ and $TPAF_3$ respectively. As before, the EA differences are of the order of 0.8 eV which are larger than those for the IP by a factor of two or so.

7.2 O3LYP Calculations

The geometry parameters and energies as obtained from O3LYP computations are summarized in Table 7.2. As for B3LYP, the magnitudes of BLA's of PA isomers are larger than the OxF_n and $TPAF_n$ values. For all systems, the magnitudes of BLA's increase with the size of unit cell. For example, the addition of fluorene group changes BLA from -0.006 Å to -0.017 Å from OxF_1 to OxF_3. Again, the negative sign of BLA's of fluorene-based polymers indicates the aromatic structure in fluorene-based unit cells and in contrast to the magnitudes of BLA's, E_{gap}'s of PA isomers are smaller than E_{gap}'s of fluorene-based polymers.

Table 7.2: E_{total}, IP, EA, E_{gap}, max-gap and BLA values of PA and fluorene-based polymers at O3LYP/6-31G* level. E_{total} is in hartree, BLA is in Aand all other energies are in eV. Aromatic cis-PA and $TPAF_1$ isomer 1 are listed. The experimental values are available shown in the brackets.

Molecular	E_{total}	IP	EA	E_{gap}	max-gap	BLA
trans-PA	-77.38	3.86	3.06	0.80 (1.80)	11.39	0.040
cis-PA	-154.75	4.18	2.87	1.31	8.72	0.060
meta-PA	-309.51	4.00	3.00	1.01	5.09	0.060
OxF_1	-916.45	5.24	2.53	2.70	4.47	-0.006
OxF_2	-1572.46	5.06 (5.73)	2.26 (2.79)	2.80 (2.94)	3.57	-0.014
OxF_3	-2228.44	5.04 (5.61)	2.04 (2.58)	3.00 (3.03)	3.31	-0.017
$TPAF_1$	-1324.44	4.50	1.53	2.96	3.31	-0.015
$TPAF_2$	-2052.19	4.65 (5.16)	1.83 (2.27)	2.82 (2.89)	2.94	-0.015
$TPAF_3$	-2629.76	4.56 (5.21)	1.79 (2.32)	2.77 (2.89)	2.86	-0.019

In all cases, O3LYP underestimates the E_{gap}'s in comparison to the experimental

values by nearly 1 eV for trans-PA and approximately 0.1 eV for OxF_2, OxF_3, $TPAF_2$, and $TPAF_3$. Again, the E_{width}'s of trans-PA and cis-PA are similar in magnitude (4-5 eV) whereas the E_{width} of meta-PA is smaller (closer to 2 eV) due to its larger unit cell. As before, for the fluorene-based polymers, the band widths are quite flat (less than 0.7 eV). The IP is 5.24 eV for OxF_1, 5.06 eV for OxF_2 and 5.04 for OxF_3 which should be compared with the experimental 5.73 eV and 5.61 eV for OxF_2 and OxF_3 respectively. For O3LYP, the IP differences are of the order of 0.6 eV which are somewhat larger than for B3LYP. EA is 2.53 eV for OxF_1, 2.26 eV for OxF_2 and 3.00 eV for OxF_3 which should be compared with the experimental 2.79 eV and 2.58 eV for OxF_2 and OxF_3 respectively. The EA differences are of the order of 0.5 eV which are comparable to those for the IP and are smaller than those for B3LYP. The IP is 4.50 eV for $TPAF_1$, 4.65 eV for $TPAF_2$ and 4.56 eV for $TPAF_3$ which should be compared with the experimental 5.16 eV and 5.21 eV for $TPAF_2$ and $TPAF_3$ respectively. Again, the IP differences are in the range 0.3-0.5 eV which is comparable to B3lYP result. EA is 1.58 eV for $TPAF_1$, 1.83 eV for $TPAF_2$ and 1.79 eV for $TPAF_3$ which should be compared with the experimental 2.27 eV and 2.32 eV for $TPAF_2$ and $TPAF_3$ respectively. Hence, the EA differences are of the order of 0.5 eV which are similar to those for the IP and again are smaller than those for B3LYP. For the fluorene based polymers, it appears that O3LYP gives better agreement with experimental values for both the band gaps and EAs (for IPs the discrepancies are similar). This is clearly illustrated in Figure 7.1 where the magnitudes of the differences between the experimental and theoretical band gaps for B3LYP and O3LYP are displayed.

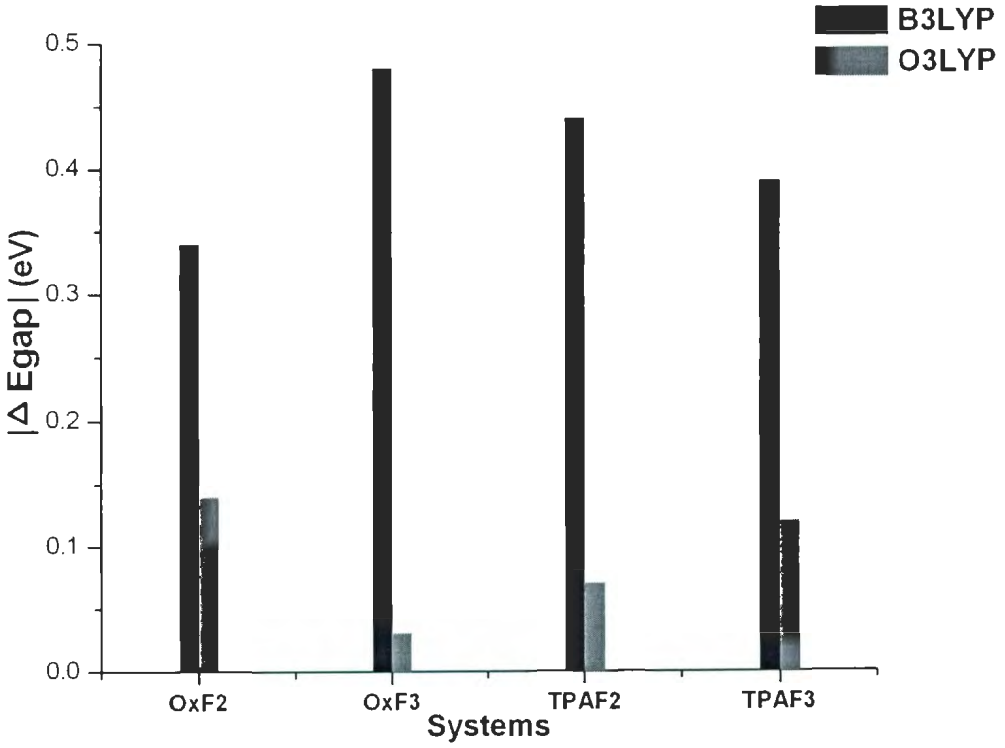

Figure 7.1: The magnitudes of band gap differences (between the experimental and theoretical values), $|\Delta E_{gap}|$'s for OxF_2, OxF_3, $TPAF_2$ and $TPAF_3$ at B(O)3LYP/6-31G* levels and 32 k-points are displayed.

Table 7.3: E_{total}, IP, EA, E_{gap} and max-gap values of trans-PA and fluorene-based polymers as obtained from 12 and 32 k-point 1D solid state DFT calculations. E_{total} is in hartree and all other energies are in eV.

Molecular	$\mathbf{E_{total}}$	**IP**	**EA**	$\mathbf{E_{gap}}$	**max-gap**
12 points					
trans-PA					
B3LYP/6-31G*	-77.41	4.31	2.69	1.62	12.03
O3LYP/6-31G*	-77.38	4.01	2.90	1.12	11.39
OxF_1					
B3LYP/6-31G*	-918.39	5.50	2.29	3.21	4.92
O3LYP/6-31G*	-916.45	5.24	2.53	2.70	4.43
OxF_2					
B3LYP/6-31G*	-1575.88	5.31	2.02	3.28	4.01
O3LYP/6-31G*	-1572.46	5.06	2.27	2.79	3.54
OxF_3					
B3LYP/6-31G*	-3000.13	4.88	1.46	3.42	3.55
O3LYP/6-31G*	-2228.44	5.04	2.04	3.00	3.31
$TPAF_2$					
B3LYP/6-31G*	-2999.75	4.75	1.45	3.30	3.52
O3LYP/6-31G*	-2055.88	4.50	1.65	2.85	2.97
32 points					
trans-PA					
B3LYP/6-31G*	-77.41	4.12	2.88	1.24	12.03
O3LYP/6-31G*	-77.38	3.86	3.06	0.80	11.39
OxF_1					
B3LYP/6-31G*	-918.39	5.50	2.30	3.20	4.92
O3LYP/6-31G*	-916.45	5.24	2.53	2.70	4.47
OxF_2					
B3LYP/6-31G*	-1575.88	5.31	2.02	3.28	4.03
O3LYP/6-31G*	-1572.46	5.06	2.26	2.80	3.57
OxF_3					
B3LYP/6-31G*	-2233.34	5.29	1.78	3.51	3.80
O3LYP/6-31G*	-2228.44	5.04	2.04	3.00	3.31
$TPAF_2$					
B3LYP/6-31G*	-2056.63	4.94	1.57	3.37	3.48
O3LYP/6-31G*	-2052.19	4.53	1.74	2.79	2.92

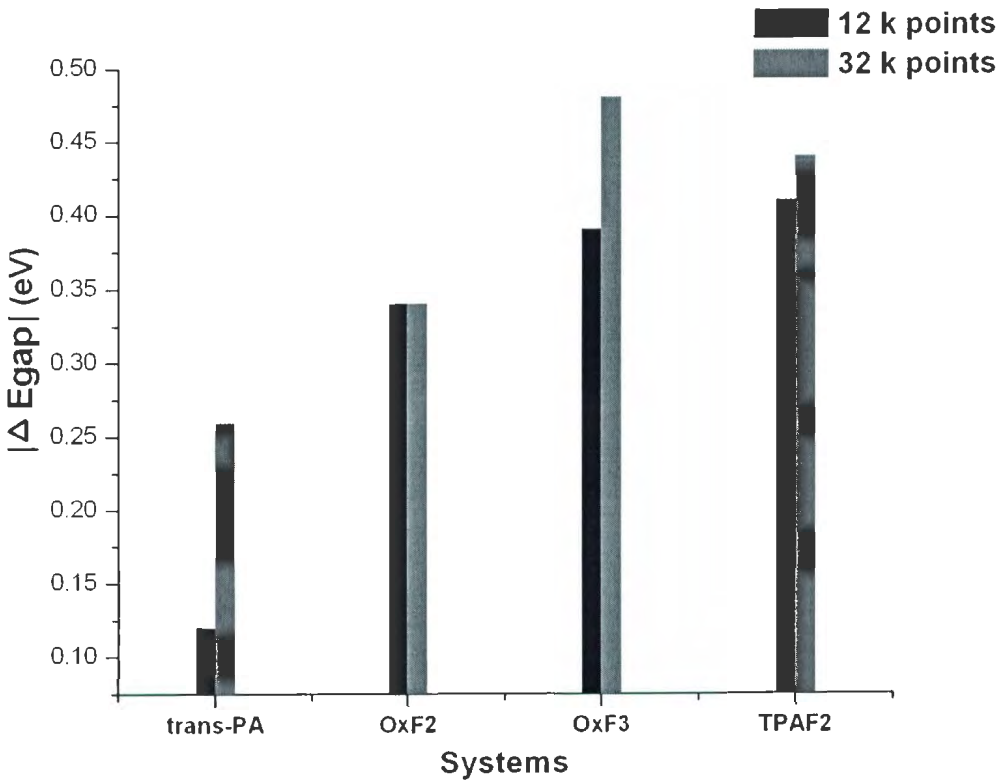

Figure 7.2: The magnitudes of band gap differences (between the experimental and theoretical values), $|\Delta E_{gap}|$'s for trans-PA, OxF_2, OxF_3 and $TPAF_2$ at B3LYP/6-31G* level with 12 and 32 k-points.

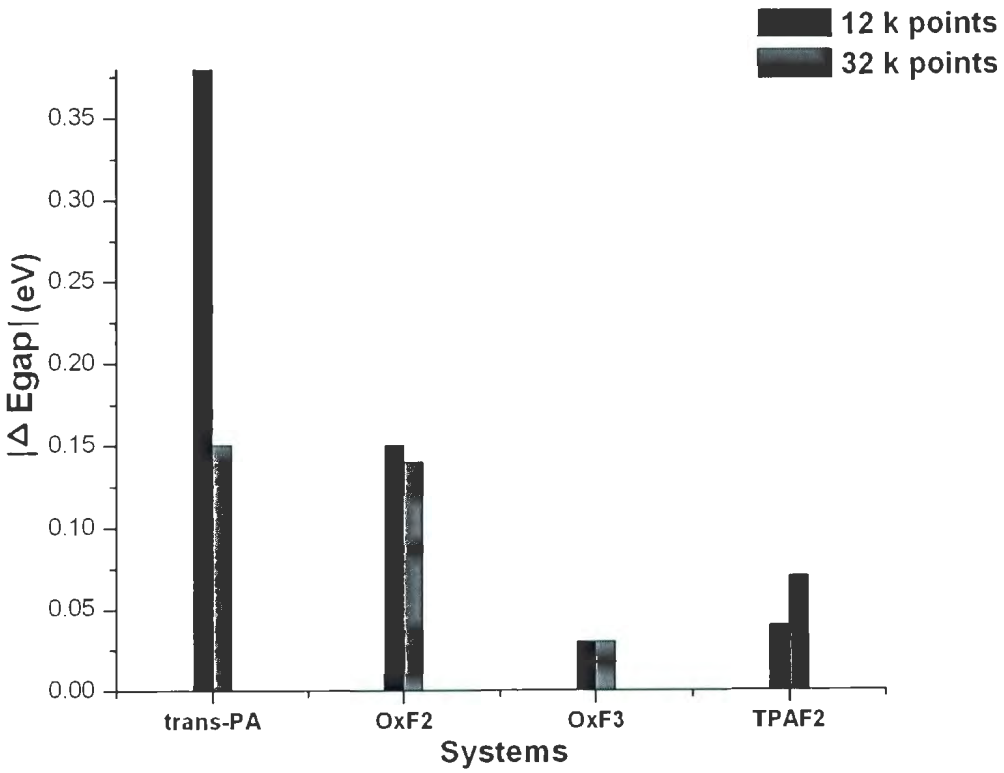

Figure 7.3: The magnitudes of band gap differences (between the experimental and theoretical values), $|\Delta E_{gap}|$'s for trans-PA, OxF_2, OxF_3 and $TPAF_2$ at O3LYP/6-31G* level with 12 and 32 k-points.

7.3 k-points Effect

Table 7.3 gives the actual values for IPs, EAs, E_{gap}'s and max-gaps for 12 and 32 k points 1D solid state B3LYP and O3LYP calculations. Figures 7.2 and Figure 7.3 show the $|\Delta E_{gap}|$'s for trans-PA, OxF_2, OxF_3 and $TPAF_2$ also for 12 and 32 k points 1D solid state calculations respectively. The differences for $|\Delta E_{gap}|$'s between 12 and 32 k points are only significant for PA, for the fluorene-based polymers the deviations from the experimental band gaps are nearly the same for both the 12 and 32 k points. This is due to the fact that fluorene-based polymers have much larger unit cells.

7.4 -H vs -OH End Group Effect

In $TPAF_1$ isomers' calculations, it was shown that the inclusion of -OH group on the one of fluorene side chains makes the compound more polar and introduces significant dipole moment component not only along the chain backbone but also in the transverse direction in the plane of the molecule.

7.5 Conclusions

We summarize the energy and the geometry structure results as obtained from the 1D DFT calculations for all compounds studied in this thesis. For all compounds studied, the magnitudes of BLA's correlate well with the size of the band gaps, that is, the bigger the magnitude of BLA, the larger the E_{gap}. For Tv's, there does not seem to be a significant correlation between their magnitudes and the size of the E_{gap}'s. All fluorene-based polymers are nonplanar. In all compounds, the largest dipole moment component is along Tv direction. For the fluorene-based polymers,

the inter-ring bonds are mostly C-C single bonds which means that their unit cells have aromatic structures. Oxadiazole group in OxF_n ($n = 1-3$) lowers EA bands thus increases the electron-transporting efficiency of PLED. The energy levels of $TPAF_n$ ($n = 1-3$) contribute in two ways in increasing the performance of PLED: first, their IPs are raised (relative to other conjugated polymers) and hence increase their hole-transport properties, and second, their EAs are also raised and enhance their electron blocking property. The combined effect of the inclusions of these two materials is a more efficient PLED. DFT computations performed in this thesis reproduced well the trends as observed in E_{gap}'s, EAs and IPs for the fluorene-based polymers. In the best cases involving B3LYP and O3LYP DFT approximations, the E_{gap}'s are reproduced to within less than 0.5 eV in most cases. It should be pointed out that the experimental results are for 3D bulk systems, whereas computations are for 1D polymers. It is known that (just as in the case of trans-PA) the 3D E_{gap}'s would need to be increased by approximately 0.2 eV to obtain the corresponding 1D E_{gap}'s. This would give even better agreement between theory and experiment for the band structures for the fluorene-based polymers. For EAs and IPS, the disagreement between the theory and experiment is in the range of 0.3-0.8 eV. All E_{gap}'s are direct. For all fluorene-based polymers, due to their large unit cells, their E_{width}'s are narrow and the band structures have the appearance of molecular energy levels rather than broad energy bands. In general, DFT gives reasonably good results for the electronic band structures for the fluorene-based polymers. O3LYP appears to give the best agreement with experimental values.

Chapter 8

Appendix-Bond lengths of OxF_n and $TPAF_n$

Table A-1: CC and CN, NN bond lengths of OxF_1 unit cell as obtained from 32 k-point 1D solid state DFT calculations. All bond lengths are in Å.

No. of CC	B3LYP	O3LYP	OB95	PBEPBE	PBE1PBE	TPSSTPSS
1	1.4100	1.4034	1.4101	1.4177	1.4047	1.4166
2	1.3810	1.3759	1.3826	1.3871	1.3786	1.3863
3	1.4174	1.4110	1.4172	1.4257	1.4125	1.4241
4	1.4701	1.4582	1.4609	1.4684	1.4651	1.4694
5	1.4113	1.4051	1.4107	1.4196	1.4065	1.4180
6	1.3786	1.3733	1.3805	1.3844	1.3760	1.3839
7	1.4091	1.4025	1.4090	1.4167	1.4040	1.4156
8	1.4571	1.4464	1.4519	1.4551	1.4529	1.4557
9	1.4584	1.4474	1.4520	1.4552	1.4548	1.4557
8	1.4571	1.4464	1.4519	1.4551	1.4529	1.4557
BLA	-0.0075	-0.0062	-0.0058	-0.0030	-0.0086	-0.0042
C-N,N-N,C-N						
10	1.3050	1.3036	1.3142	1.3196	1.3011	1.3164
11	1.3719	1.3535	1.3560	1.3724	1.3598	1.3785
12	1.3052	1.3535	1.3144	1.3198	1.3013	1.3166

Table A-2: CC and CN, NN bond lengths of OxF_1 unit cell as obtained from 12 k-point 1D solid state DFT calculations. All bond lengths are in Å.

No. of CC	B3LYP	O3LYP	OB95
1	1.4099	1.4034	1.4101
2	1.3811	1.3759	1.3827
3	1.4173	1.4110	1.4172
4	1.4700	1.4582	1.4609
5	1.4113	1.4051	1.4107
6	1.3786	1.3733	1.3806
7	1.4091	1.4025	1.4090
8	1.4572	1.4464	1.4519
9	1.4588	1.4474	1.4520
8	1.4572	1.4464	1.4519
BLA	-0.0075	-0.0062	-0.0058
C-N,N-N,C-N			
10	1.3050	1.3036	1.3142
11	1.3720	1.3535	1.3561
12	1.3051	1.3037	1.3144

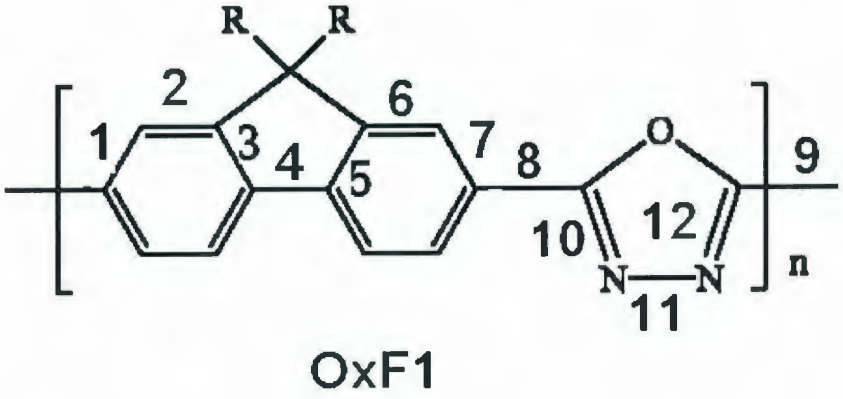

OxF1

Figure A-1: Chemical structure of OxF_1 unit cell.

Table A-3: CC and CN, NN bond lengths of OxF_2 unit cell as obtained from 32 k-point 1D solid state DFT calculations. All bond lengths are in Å.

No. of CC	B3LYP	O3LYP	OB95	PBEPBE	PBE1PBE	TPSSTPSS
1	1.4095	1.4029	1.4099	1.4170	1.4043	1.4161
2	1.3854	1.3799	1.3894	1.3911	1.3825	1.3845
3	1.4098	1.4036	1.4157	1.4181	1.4052	1.4180
4	1.4606	1.4497	1.4537	1.4598	1.4563	1.4697
5	1.4124	1.4065	1.4069	1.4208	1.4079	1.4206
6	1.3913	1.3857	1.3894	1.3970	1.3882	1.3912
7	1.4115	1.4048	1.4099	1.4187	1.4063	1.4158
8	1.4844	1.4732	1.4788	1.4833	1.4785	1.4871
9	1.4106	1.4039	1.4113	1.4180	1.4056	1.4170
10	1.3883	1.3825	1.3925	1.3937	1.3853	1.3923
11	1.4066	1.4007	1.4127	1.4150	1.4021	1.4007
12	1.4604	1.4497	1.4529	1.4596	1.4561	1.4555
13	1.4156	1.4094	1.4092	1.4240	1.4110	1.4019
14	1.3885	1.3829	1.3871	1.3944	1.3857	1.3894
15	1.4100	1.4036	1.4096	1.4178	1.4048	1.4153
16	1.4570	1.4461	1.4513	1.4539	1.4531	1.4582
17	1.4566	1.4458	1.4506	1.4498	1.4600	1.4559
16	1.4570	1.4461	1.4513	1.4539	1.4531	1.4582
BLA	-0.0162	-0.0143	-0.0138	-0.0104	-0.0173	-0.0153
C-N,N-N,C-N						
17	1.3034	1.3021	1.3130	1.3180	1.2997	1.3157
18	1.3878	1.3672	1.3699	1.3876	1.3736	1.3829
19	1.3035	1.3022	1.3130	1.3181	1.2998	1.3152

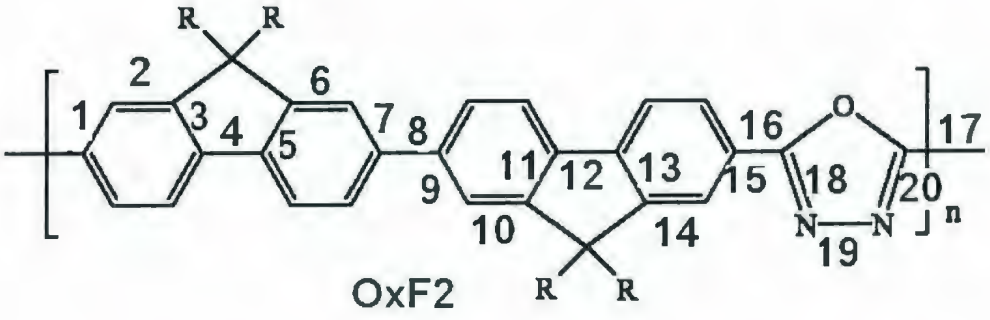

Figure A-2: Chemical structure of OxF_2 unit cell.

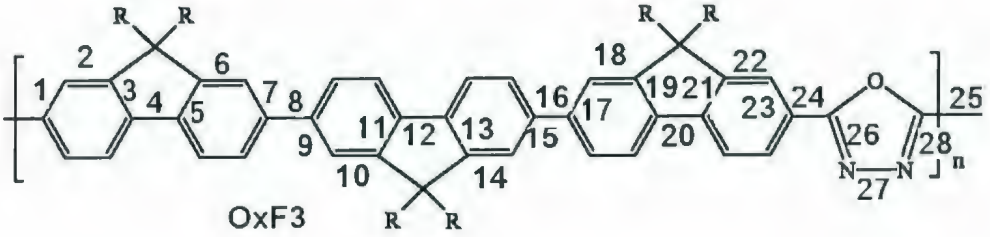

Figure A-3: Chemical structure of OxF_3 unit cell.

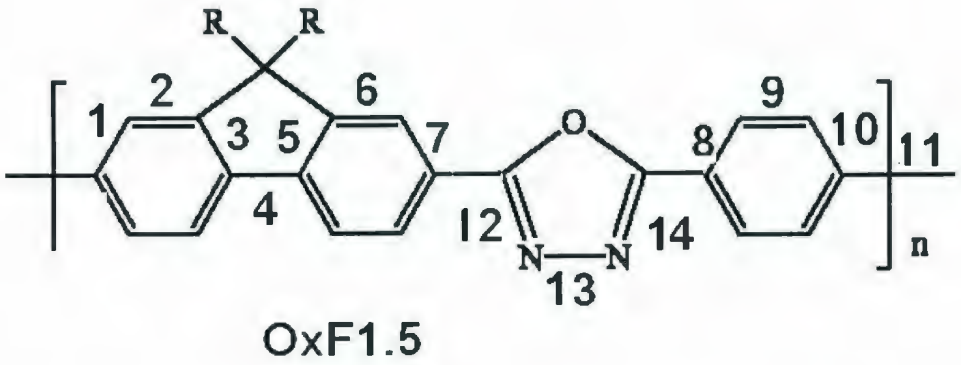

Figure A-4: Chemical structure of $OxF_{1.5}$ unit cell.

Table A-4: CC and CN, NN bond lengths of OxF_3 unit cell as obtained from 32 k-point 1D solid state DFT calculations. All bond lengths are in Å.

No. of CC	B3LYP	O3LYP	OB95	PBEPBE	PBE1PBE	TPSSTPSS
1	1.4093	1.4030	1.4095	1.4168	1.4096	1.4157
2	1.3934	1.3877	1.3941	1.3996	1.3941	1.3988
3	1.4131	1.4070	1.4130	1.4213	1.4130	1.4195
4	1.4583	1.4475	1.4512	1.4574	1.4512	1.4582
5	1.4063	1.4004	1.4065	1.4147	1.4065	1.4131
6	1.3921	1.3862	1.3930	1.3978	1.3930	1.3973
7	1.4100	1.4035	1.4097	1.4173	1.4097	1.4162
8	1.4855	1.4743	1.4805	1.4843	1.4804	1.4858
9	1.4100	1.4034	1.4095	1.4170	1.4095	1.4160
10	1.3875	1.3819	1.3892	1.3931	1.3893	1.3924
11	1.4139	1.4077	1.4138	1.4221	1.4138	1.4207
12	1.4688	1.4577	1.4607	1.4686	1.4604	1.4696
13	1.4078	1.4017	1.4075	1.4161	1.4075	1.4143
14	1.3842	1.3786	1.3861	1.3896	1.3863	1.3891
15	1.4089	1.4022	1.4081	1.4159	1.4082	1.4148
16	1.4856	1.4743	1.4803	1.4841	1.4799	1.4857
17	1.4107	1.4042	1.4104	1.4181	1.4107	1.4169
18	1.3954	1.3894	1.3959	1.4012	1.3955	1.4003
19	1.4119	1.4059	1.4125	1.4204	1.4124	1.4187
20	1.4583	1.4476	1.4512	1.4575	1.4515	1.4587
21	1.4074	1.4015	1.4074	1.4157	1.4075	1.4142
22	1.3906	1.3847	1.3914	1.3963	1.3913	1.3956
23	1.4088	1.4025	1.4092	1.4164	1.4089	1.4151
24	1.4592	1.4486	1.4549	1.4574	1.4547	1.4584
25	1.4612	1.4499	1.4553	1.4579	1.4550	1.4582
24	1.4592	1.4486	1.4549	1.4574	1.4547	1.4584
BLA	-0.0184	-0.0165	-0.0162	-0.0134	-0.0162	-0.0150
C-N,N-N,C-N						
26	1.3026	1.3162	1.3162	1.3172	1.3118	1.3139
27	1.3840	1.4426	1.4426	1.3830	1.3665	1.3894
28	1.3023	1.3027	1.3027	1.3170	1.3116	1.3140

Table A-5: CC and CN, NN bond lengths of $OxF_{1.5}$ unit cell as obtained from 32 k-point 1D solid state DFT calculations. All bond lengths are in Å.

No. of CC	B3LYP	O3LYP	OB95	PBEPBE	PBE1PBE	TPSSTPSS
1	1.4568	1.4517	1.4518	1.4683	1.4685	1.4692
2	1.4065	1.4093	1.4098	1.4160	1.4159	1.4149
3	1.3876	1.3835	1.3837	1.3991	1.3991	1.3986
4	1.3996	1.4095	1.4095	1.4152	1.4152	1.4136
5	1.4421	1.4578	1.4572	1.4569	1.4569	1.4576
6	1.4025	1.4143	1.4139	1.4185	1.4185	1.4167
7	1.3900	1.3893	1.3894	1.4049	1.4049	1.4042
8	1.4068	1.4105	1.4106	1.4158	1.4159	1.4149
9	1.4754	1.4782	1.4782	1.4905	1.4904	1.4925
10	1.3977	1.4095	1.4079	1.4100	1.4100	1.4090
11	1.4038	1.3843	1.3933	1.4048	1.4048	1.4041
10	1.4259	1.4071	1.4049	1.4100	1.4100	1.4089
BLA	0.0257	0.0184	0.0205	0.0269	0.0269	0.0285
C-N,N-N,C-N						
12	1.3128	1.2956	1.3129	1.3153	1.3152	1.3121
13	1.3626	1.3666	1.3625	1.3809	1.3810	1.3870
14	1.3137	1.2956	1.3136	1.3168	1.3168	1.3137

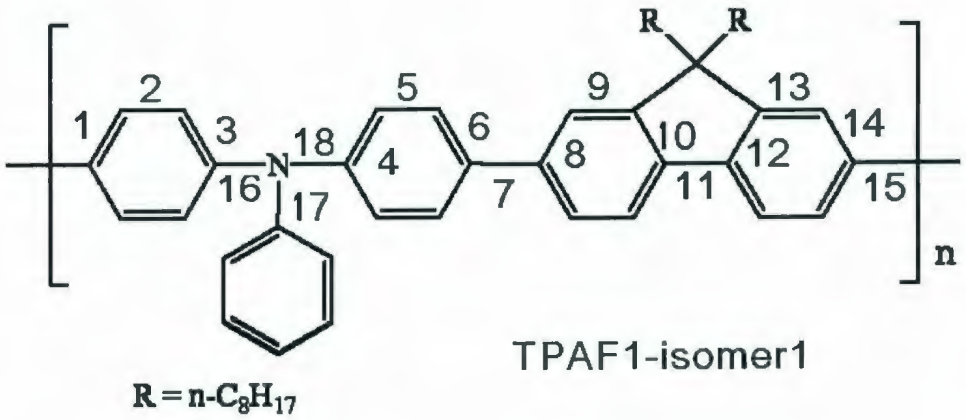

Figure A-5: Chemical structure of $TPAF_1$ isomer 1 unit cell.

Table A-6: CC and CN bond lengths of $TPAF_1$ isomer 1 unit cell as obtained from 32 k-point 1D solid state DFT calculations. All bond lengths are in Å.

No. of CC	B3LYP	O3LYP	OB95	PBEPBE	PBE1PBE	TPSSTPSS
1	1.4015	1.4025	1.4030	1.4088	1.3976	1.4075
2	1.3930	1.3897	1.3893	1.3955	1.3864	1.3947
3	1.4052	1.4059	1.4066	1.4130	1.4014	1.4118
4	1.4854	1.4855	1.4805	1.4844	1.4796	1.4861
5	1.4093	1.4092	1.4088	1.4162	1.4043	1.4151
6	1.3878	1.3891	1.3892	1.3935	1.3847	1.3931
7	1.4098	1.4095	1.4097	1.4180	1.4052	1.4162
8	1.4636	1.4625	1.4580	1.4650	1.4611	1.4661
9	1.4094	1.4090	1.4092	1.4175	1.4048	1.4160
10	1.3871	1.3882	1.3884	1.3927	1.3839	1.3923
11	1.4108	1.4111	1.4106	1.4179	1.4057	1.4168
12	1.4848	1.4828	1.4774	1.4818	1.4792	1.4834
13	1.4053	1.4064	1.4068	1.4145	1.4008	1.4120
14	1.3921	1.3924	1.3913	1.3934	1.3894	1.3973
15	1.4055	1.4067	1.4077	1.4137	1.4015	1.4110
14	1.3931	1.3924	1.3913	1.3934	1.3894	1.3973
BLA	-0.0159	-0.0153	-0.0129	-0.0100	-0.0165	-0.0130
C-N						
16	1.4125	1.4095	1.4046	1.4131	1.4033	1.4175
17	1.4261	1.4246	1.4187	1.4256	1.4162	1.4293
18	1.4287	1.4248	1.4219	1.4301	1.4199	1.4321

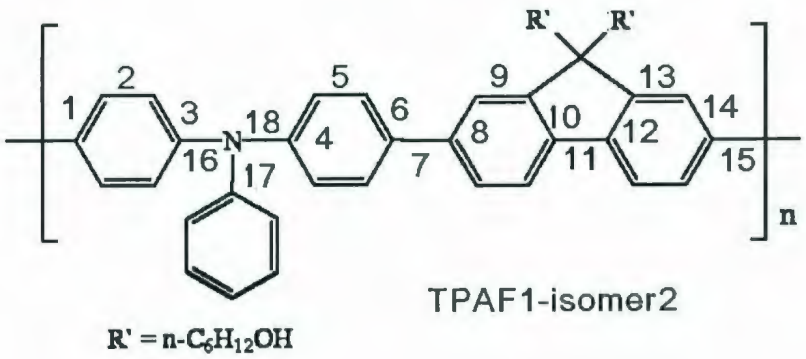

Figure A-6: Chemical structure of $TPAF_1$ isomer 2 unit cell.

Table A-7: CC and CN bond lengths of $TPAF_1$ isomer 2 unit cell as obtained from 32 k-point 1D solid state DFT calculations. All bond lengths are in Å.

No. of CC	B3LYP	O3LYP	OB95	PBEPBE	PBE1PBE	TPSSTPSS
1	1.4028	1.4014	1.4028	1.4087	1.3975	1.4071
2	1.3945	1.3947	1.3894	1.3956	1.3864	1.3949
3	1.4059	1.4053	1.4067	1.4131	1.4015	1.4120
4	1.4853	1.4852	1.4804	1.4842	1.4793	1.4860
5	1.4093	1.4094	1.4088	1.4162	1.4044	1.4151
6	1.3871	1.3857	1.3873	1.3915	1.3825	1.3908
7	1.4075	1.4077	1.4076	1.4158	1.4032	1.4141
8	1.4626	1.4657	1.4581	1.4652	1.4613	1.4663
9	1.4069	1.4072	1.4071	1.4152	1.4027	1.4135
10	1.3861	1.3849	1.3864	1.3906	1.3816	1.3899
11	1.4111	1.4108	1.4106	1.4178	1.4059	1.4167
12	1.4827	1.4848	1.4772	1.4818	1.4773	1.4831
13	1.4064	1.4072	1.4068	1.4131	1.4010	1.4120
14	1.3925	1.3877	1.3915	1.3978	1.3894	1.3973
15	1.4068	1.4063	1.4078	1.4130	1.4015	1.4114
14	1.3925	1.3877	1.3915	1.3978	1.3894	1.3973
BLA	-0.0158	-0.0151	-0.0129	-0.0114	-0.0162	-0.0129
C-N						
16	1.4130	1.4095	1.4047	1.4136	1.4037	1.4162
17	1.4251	1.4235	1.4180	1.4248	1.4152	1.4279
18	1.4295	1.4260	1.4230	1.4309	1.4207	1.4347

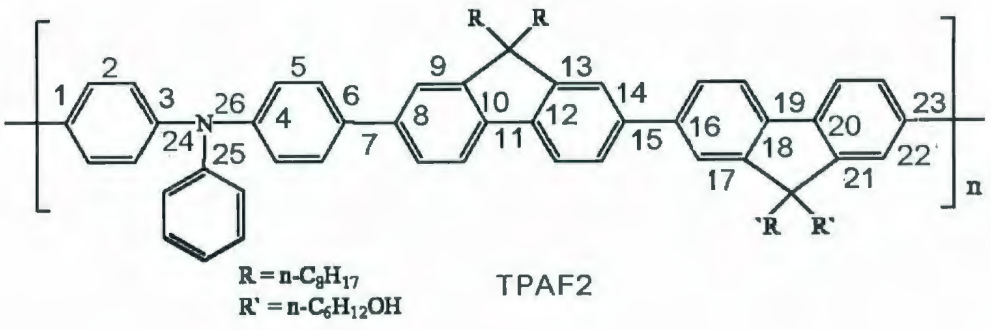

Figure A-7: Chemical structure of $TPAF_2$ unit cell.

Table A-8: CC and CN bond lengths of $TPAF_2$ unit cell as obtained from 32 k-point 1D solid state DFT calculations. All bond lengths are in Å.

No. of CC	B3LYP	O3LYP	OB95	PBEPBE	PBE1PBE	TPSSTPSS
1	1.3941	1.3940	1.4026	1.4088	1.3957	1.4072
2	1.3824	1.3825	1.3876	1.3926	1.3853	1.3920
3	1.4022	1.4022	1.4096	1.4160	1.4039	1.4150
4	1.4744	1.4745	1.4790	1.4836	1.4797	1.4851
5	1.4056	1.4055	1.4120	1.4197	1.4072	1.4186
6	1.3840	1.3840	1.3917	1.3960	1.3867	1.3956
7	1.3889	1.4021	1.3964	1.4012	1.3907	1.4007
8	1.4492	1.4493	1.4612	1.4587	1.4556	1.4597
9	1.4026	1.4025	1.4085	1.4168	1.4042	1.4152
10	1.3852	1.3851	1.3925	1.3972	1.3879	1.3968
11	1.4037	1.4037	1.4103	1.4176	1.4053	1.4166
12	1.4737	1.4736	1.4795	1.4839	1.4790	1.4854
13	1.4029	1.4029	1.4095	1.4168	1.4049	1.4158
14	1.3790	1.3790	1.3861	1.3899	1.3812	1.3893
15	1.3927	1.3926	1.4006	1.4056	1.3944	1.4050
16	1.4584	1.4584	1.4612	1.4693	1.4648	1.4704
17	1.4067	1.4067	1.4119	1.4201	1.4072	1.4184
18	1.3814	1.3814	1.3860	1.3899	1.3817	1.3892
19	1.4013	1.4012	1.4088	1.4154	1.4035	1.4143
20	1.4721	1.4721	1.4773	1.4836	1.4797	1.4851
21	1.3980	1.3980	1.4056	1.4123	1.3991	1.4110
22	1.3796	1.3796	1.3863	1.3917	1.3825	1.3909
23	1.4027	1.4028	1.4077	1.4141	1.4038	1.4125
22	1.3796	1.3796	1.3863	1.3917	1.3825	1.3909
BLA	-0.0165	-0.0154	-0.0160	-0.0136	-0.0189	-0.0150
C-N						
24	1.3962	1.3965	1.4072	1.4141	1.4034	1.4170
25	1.4156	1.4155	1.4173	1.4272	1.4179	1.4304
26	1.4208	1.4204	1.4218	1.4275	1.4238	1.4317

Table A-9: CC and CN bond lengths of $TPAF_3$ unit cell as obtained from 32 k-point 1D solid state DFT calculations. All bond lengths are in Å.

No. of CC	B3LYP	O3LYP	OB95	PBEPBE	PBE1PBE	TPSSTPSS
1	1.4028	1.3972	1.4040	1.4106	1.3991	1.4087
2	1.3881	1.3816	1.3875	1.3928	1.3844	1.3924
3	1.4075	1.4018	1.4089	1.4154	1.4031	1.4145
4	1.4833	1.4721	1.4775	1.4818	1.4772	1.4833
5	1.4115	1.4050	1.4112	1.4188	1.4064	1.4179
6	1.3891	1.3831	1.3903	1.3945	1.3860	1.3938
7	1.3949	1.3897	1.3974	1.4023	1.3915	1.4020
8	1.4651	1.4508	1.4543	1.4608	1.4570	1.4622
9	1.4090	1.4029	1.4089	1.4173	1.4046	1.4158
10	1.3896	1.3837	1.3909	1.3951	1.3864	1.3946
11	1.4102	1.4034	1.4097	1.4173	1.4051	1.4160
12	1.4842	1.4732	1.4796	1.4828	1.4783	1.4844
13	1.4103	1.4035	1.4093	1.4175	1.4054	1.4162
14	1.3866	1.3811	1.3891	1.3932	1.3834	1.3919
15	1.3964	1.3912	1.3989	1.4046	1.3930	1.4033
16	1.4667	1.4557	1.4585	1.4669	1.4621	1.4672
17	1.4123	1.4061	1.4121	1.4183	1.4078	1.4189
18	1.3900	1.3844	1.3915	1.3925	1.3869	1.3954
19	1.4068	1.4012	1.4085	1.4150	1.4027	1.4135
20	1.4844	1.4732	1.4794	1.4834	1.4785	1.4846
21	1.4099	1.4032	1.4097	1.4166	1.4048	1.4158
22	1.3876	1.3819	1.3890	1.3933	1.3844	1.3927
23	1.3966	1.3914	1.3994	1.4042	1.3932	1.4036
24	1.4651	1.4541	1.4574	1.4647	1.4607	1.4654
25	1.4093	1.4032	1.4092	1.4175	1.4048	1.4160
26	1.3870	1.3812	1.3881	1.3925	1.3839	1.3922
27	1.4091	1.4035	1.4107	1.4166	1.4048	1.4158
28	1.4833	1.4725	1.4769	1.4817	1.4791	1.4829
29	1.4056	1.3999	1.4072	1.4135	1.4011	1.4126
30	1.3922	1.3853	1.3906	1.3972	1.3887	1.3963
31	1.4055	1.4001	1.4077	1.4127	1.4013	1.4112
30	1.3922	1.3853	1.3906	1.3972	1.3887	1.3963
BLA	-0.0211	-0.0185	-0.0174	-0.0158	-0.0211	-0.0171
C-N						
32	1.4142	1.4012	1.4057	1.4169	1.4062	1.4183
33	1.4230	1.4104	1.4177	1.4224	1.4131	1.4266
34	1.4265	1.4131	1.4191	1.4266	1.4169	1.4296

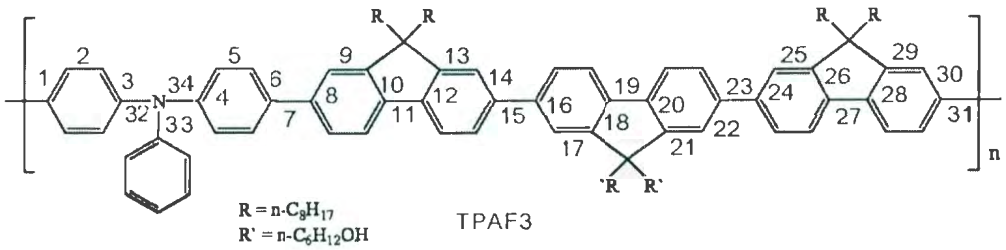

Figure A-8: Chemical structure of $TPAF_3$ unit cell.

Bibliography

[1] J. Lu, Y. Jin, J. Ding, Y. Tao, and M. Day, *J. Mater. Chem.* **16**, 593-601 (2005).

[2] G. Detriau, *J. Chem. Phys.* **33**, 587-625 (1936).

[3] M. Pople, H.P. Kallman, and P. Magnante, *J. Chem. Phy.* **38**, 8 (1963).

[4] L. Lyon, *Mol. Cryst. Liq. Cryst.* **171**, 53 (1989).

[5] D. Bradley, *Synth. Met.* **54**, 401 (1993).

[6] K. Tada, T. Sonoda, Y. Yokota, K. Kobashi, and K. Yoshino, *J. Appl. Phys.* **84**, 5635-8 (1998).

[7] M. Yoshida, A. Fujii, Y. Ohmori, and K. Yoshino, *Appl. Phys. Lett.* **69**, 6 (1996).

[8] J.H. Burroughes, D.D.C. Bradley, A.R. Brown, R.N. Marks, K. Mackay, R.H. Friend, P.L. Burns, and A.B. Holmes, *Nature* **347**, 539 (2000).

[9] C.K. Chiang, Y.W. Park, and A.J. Heeger, *J. Chem. Phy.* **69**, 11 (1978).

[10] Y. Yang and A.J. Heeger, *Appl. Phys. Lett.* **64**, 1245-7 (1994).

[11] M. Fukuda, K. Sawada, S. Morita, and K. Yoshino, *Synth. Met.* **41**, 855 (1991).

[12] D.D.C. Bradley, *Synth. Met.* **54**, 401-15 (1993).

[13] J. Kalinowski, *In Organic Electroluminescent Materials and Devices.* (Ed. S. Miyata and H.S. Nalwa), Gordon and Breach, London, Chap. 1 (1997).

[14] R.H. Friend, R.W. Gymer, A.B. Holmes, J.H. Burroughes, R.N. Marks, C. Taliani, and D.D.C. Bradley, *Nature* **397**, 121-8 (1999).

[15] a)F. Cacialli, *Math. Phys. Engng. Sci.* **358**, 173-92 (1999). b)F. Cacialli, *Curr. Opin. Colloid. Interf. Sci.* **4**, 159-64 (1999).

[16] N. Leventis and L. Huang, *Polym. News.* **20**, 307-13 (1995).

[17] Y. Mori, *Organic EL Materials and Devices.* (Ed. S. Miyata and H.S. Nalwa), Gordon and Breach, London, p. 391 (1997).

[18] L.J. Rothberg and A.J. Lovinger, *J. Mater. Res.* **11**, 3174-87 (1996).

[19] J.R. Sheats, Y. Chang, D.B. Roitman, and A. Socking, *Acc. Chem. Res.* **32**, 193-200 (1999).

[20] a) H. Ohnishi, *Ann. Rev. Mater. Res.* **19**, 83-101 (1989). b) S. Matsumoto, *Electronic Display Devices* New York, Chapt. 5, p. 180 (1990).

[21] H. Hong, D. Davidov, M. Tarabia, H. Chayet, I. Benjamin, E.Z. Faraggi, Y. Avny, and R. Neumann, *Synth. Met.* **85**, 1265 (1997).

[22] M. Ferreira, J. Cheung, and M.F. Rubner, *Thin Solid Films* **244**, 806-9 (1994).

[23] Z. Zhang, X. Jiang, S. Xu, T. Nagamoto, and S. Miyata, *Organic Electroluminescent Materials and Devices.* (Ed. H.S. Nalwa), Gordon and Breach, Netherlands, (1997).

[24] L. Akcelrud, *Prog. Polym. Sci.* **28**, 875-962 (2002).

[25] T.A. Skotheim, *Handbook of Conducting Polymers. Marcel Dekker Inc.*, New York, p. 272. (1986).

[26] G.G. Malliar and J.C. Scott, *Appl. Phys.* **83**, 5399-403 (1998).

[27] P.W.M. Blom, M.J.M. de Jong, and S. Breedijk, *Appl. Phys. Lett.* **71**, 930-2 (1997).

[28] H. Bassler, *Polym. Adv. Technol.* **9**, 402-18 (1998).

[29] M. Ozaki, D. Peebles, and B.R. Ikeda, *Makro. Chem.* **179**, 1565-1573 (1978).

[30] T. Bohr and S.A. Brazovski, *J. Phys. C.* **16**, 1189 (1983).

[31] D. Baeriswyl, G. Harbeke, H. Kiess, and W. Meyer, *Electronic Properties of Polymers.* (Ed. J. Mort and G. Pfister), John Wiley and Sons, New York, 267-326 (1982).

[32] J. Chen and A.J. Heeger, *Snyth. Met.* **24**, 311-327 (1988).

[33] H.G. Kiess, *Conjugated Conducting Polymers.* Springer-Verlag Berlin Heidelberg, New York, (1992).

[34] M. Springborg, *Phys. Rev. B.* **33**, 12 (1986).

[35] S. Sabyasachi and C. Swapan, *J. Chem. Phys.* **124**, 3 (2006).

[36] P. Ramiro and G.E. Scuseria, *J. Chem. Phy.* **121**, 16 (2004).

[37] E. Lewars, *Computational Chemistry: Introduction to the Theory and Applications of Molecular and Quantum Mechanics.* London, (2003).

[38] W.J. Hehre, L. Radom, P.V.R. Schleyer and J.A. Pople, *Ab Initio Molecular Orbital Theory.* New York, Chap. 2 (1986).

[39] M.J.S. Dewar, *Molecular Orbital Theory of Organic Chemistry.* McGraw-Hill, New York, (1969).

[40] D.R. Hartree, *Proc. Camb. Phil. Soc.* **24**, 189 (1928).

[41] a) J.C. Slater, *Phys. Rev. B.* **35**, 210 (1960). b) V. Fock and Z. Physik, *Phys. Rev. A.* **61**, 126 (1930).

[42] I.N. Levine, *Quantum Chemistry.* Prentice Hall, Engelwood Cliffs, New Jersey, (2000).

[43] J.A. Pople and D.L. Beveridge, *Approximation Molecular Orbital Theory.* McGraw-Hill, New York, Chap. 1 and 2 (1970).

[44] A.K. Rappe and C.L. Casewit, *Molecular Mechanics across Chemistry.* Sausalito, CA, (1997).

[45] U. Burkert and N.L. Alligner, *Molecular Mechanics., American. Chemical. Society.* Washingtong, DC, (1982).

[46] a) C.C.J. Roothaan, *Rev. Mod. Phys.* **23**, 69 (1951). b) G.G. Hall, *Proc. Roy. Soc.* **A205**, 541 (1951).

[47] Y. Jean and F. Volatron, *An Introduction to Molecular Orbitals.* Oxford University Press, New York, (1993).

[48] J.B. Foresman and A. Frisch, *Exploring Chemistry with Electronic Structure Methods.* Gaussian Inc. (1994).

[49] R.F.W. Bader, *Atoms in Molecules.* Oxford University Press, New York, (1990).

[50] R.G. Parr and W. Yang, *Density-Functional Theory of Atoms and Molecules.* Oxford University Press, New York, p. 53 (1989).

[51] a)E. Wilson, *Chem. Eng. News.* **12**, 330 (1988). b)D. Malakoff, *Science* **282**, 610 (1998).

[52] a) I.N. Levine, *Quantum Chemistry.*, Prentice Hall, New Jersey, Saddle River, (2000). b) P. Hohenberg and W. Kohn, *Phys. Rev. A.* **140**, 1133 (1965).

[53] W, Kohn and L.J. Sham, *Phys. Rev. A.* **140**, 1133 (1965).

[54] J.W. Mintmire and C.T. White, *Phys. Rev. B.* **35**, 8 (1987).

[55] a)A. Whitaker, *Einstein, Born and the Quantum Dilemma.* Cambridge University Press, Cambridge, (1996). b)V.J. Stenger, *The Unconsious Quantum.* Prometheus, Amherst, New York, (1995).

[56] F. Jensen, *Introduction to Computational Chemistry.* New York, **101**, 208 (1997).

[57] S.H. Vosko, L. Wilk, and M. Nusair, *Can. J. Phys.* **58**, 1200 (1980).

[58] A. Kraft, A.C. Grimsdale and A.B. Holmes, *Angew. Chem. Int. Ed.* **37**, 402-428 (1998).

[59] P.J. Stephens, F.J. Devlin, C.F. Chablowski, and M.J. Frisch, *J. Phys. Chem.* **98**, 11623 (1994).

[60] C. Lee, W. Yang, and R.G. Parr, *Phys. Rev. B.* **37**, 785 (1988).

[61] A. Frisch and M.J. Frisch, *Gaussian 03 User's Reference.* Carnegie Mellon University, (2003).

[62] N.C. Handy and A.J. Cohen, *Mol. Phys.* **99**, 403 (2001).

[63] J.C. Garcia, *J. Chem. Phy.* **121**, 3096 (2004).

[64] J. Baker and P. Pulay, *J. Chem. Phy.* **117**, 4 (2002).

[65] A.D. Becke, *J. Chem. Phys.* **104**, 1040 (1996).

[66] a) J.P. Perdew, K. Burke, and M. Ernzerhof, *Phys. Rev. Lett.* **77**, 3865 (1996). b) J.P. Perdew, K. Burke, and M. Ernzerhof, *Phys. Rev. Lett.* **78**, 1396 (1997).

[67] V.N. Staroverov, G.E. Scuseria, J. Tao, and J.P. Perdew, *J. Chem. Phys.* **119**, 12129 (2003).

[68] J.P. Perdew, K. Burke, and M. Ernzerhof, *Phys. Rev. B.* **77**, 18 (1996).

[69] N.W. Ashcroft and N.D. Mermin, *Solid State Physics*. Cornell University, (1976).

[70] C. Pisani, R. Dovesi, and C. Roetti, *Lecture Notes in Chemistry*. Springer-Verlag, (1988).

[71] U. Salzner, J.B. Lagowski, P.G. Pickup, and R.A. Poirier, *J. Phys. Chem.* **A**, 2572-2578 (1997).

[72] A.K. Bakhshi and P. Rattan, *J. Chem. Soc.* **94**, 2823-2826 (1998).

[73] Y.Q. Ding, D.C. Feng, S.Y. Feng, J. Zhang, and J. Xie, *Polymer.* **47**, 3681-3688 (2006).

[74] A.J. Revision, M.J. Frisch, G.W. Trucks, H.B. Schlegel, G.E. Scuseria, M.A. Robb, I.R. Cheeseman, J.A. Montgomery, T. Vreven, K.N. Kudin, J.C. Burant, J.M. Millam, S.S. Iyengar, J. Tomasi, V. Barone, B. Mennucci, M. Cossi, G. Scalmani, N. Rega, G.A. Petersson, H. Natatsuji, M. Hada, M. Ehara, K. Toyota, R. Fukuda, J. Hasegawa, M. Ishida, T. Nakajima, Y. Honda, O. Kitao, H. Nakai, M. Klene, X. Li, J.E. Knox, H.P. Hratchian, J.B. Cross, C. Adamo, J.

Jaramillo, R. Gomperts, R.E. Stratmann, O. Yazyev, A.J. Austin, R. Cammi, C. Pomelli, J.W. Ochterski, P.Y. Ayala, Morokuma, G.A. Voth, P. Salvador, J.J. Dannenberg, V.G. Zakrzeski, S. Dapprich, A.D. Daniels, M.C. Strain, O. Farkas, D.K. Malick, A.D. Rabuck, K. Raghavachari, J.B. Foresman, J.V. Ortiz, Q. Cui, A.G. Baboul, S. Clifford, J. Cioslowski, B.B. Stefanov, G. Liu, A. Liashenko, P. Piskorz, I. Komaromi, R.L. Martin, D.J. Fox, T. Keith, M.A. Al-Laham, C.Y. Peng, A. Nanayakkara, M. Challacombe, P.M.W. Gill, B. Johnson, W. Chen, M.W. Wong, C. Gonzalc, and J.A. Pople, Gaussian 03. Guassian Inc. Pittsubrg, PA, (2003).

[75] K.N. Kudin and G.E. Scuseria, *Phys. Rev. B.* **61**, 24 (2000).

[76] W.J. Hehre, L. Radom, V.R. Paul, P. Schleyer, and J.A. Pople, Ab Initio *Molecular Orbital Theory.* Wiley-Interscience, New York, (1985).

[77] A.D. Becke, *Phys. Rev. A.* **38**, 3098 (1988).

[78] N.R. Carlsen, *Chem. Phys. Lett.* **51**, 192 (1977).

[79] A.E. Frisch, R.D. Dennington II, T.A. Kieth, A.B. Nielsen, and A.J. Holder, *GaussView Reference Manual.* Gaussian Inc. Pittsburgh, PA, (2003).

[80] a) K.N. Kudin and G.E. Scuseria, *Chem. Phys. Lett.* **289**, 611 (1998). b) K.N. Kudin and G.E. Scuseria, *Chem. Phys. Lett.* **283**, 61 (1998). c)K.N. Kudin and G.E. Scuseria, *Phys. Rev. B.* **61**, 16440 (2000). d)O.V. Yazyev, K.N. Kudin, and G.E. Scuseria, *Phys. Rev. B.* **65**, 205117 (2002).

[81] C. Kittel, *Introduction to Solid State Physics.* New York, (1996).

[82] J.C. Garcia, *J. Chem. Phy.* **121**. 3096 (2004).

[83] S. Suhai, *Int. J. Quantum. Chem.* **42**, 193 (1992).

[84] S. Suhai, *J. Phys. Lett.* **B27**, 3506 (1983).

[85] C.S. Yannoni and T.C. Clarke, *Phys. Rev. Lett.* **51**, 1191 (1983).

[86] D.S. Qin and Y. Tao, *J. App. Phys.* **97**, 044505 (2004).

[87] D. Jacquemin, B. Champagne, and J.M. Andre, *J. Chem. Phys.* **108**, 3 (1998).

[88] J.W. Mintire and C.T. White, *Phys. Rev. B.* **35**, 8 (1987).

[89] A.V. Mitin, J. Baker, and P. Pulay, *J. Chem. Phy.* **118**, 17 (2003).

[90] A.J. Rocke, *Annals of Science.* **42**, 355-81 (1985).

[91] W.R. Salaneck, H.R. Thomas, C.B. Duke, A. Paton, E.W. Plummer, and B.H. Tonner, *Phys. Rev. L.* **49**, 801-804 (1982).

[92] U. Salzner, P.G. Pickup, R.A. Poirier, and J.B. Lagowski, *J. Phys. Chem.*, **102**, 2572-2578 (1998).

[93] D. Chakraborty and J.B. Lagowski, *J. Chem. Phys.* **115**, 1 (2001).

[94] T. Mark, M. Inbasekaran, J.O. Brien, and W.S. Wu, *Adv. Mater.* **12**, 23 (2000).

[95] M.S. Miao, P.E.V. Camp, and V.E.V. Doren, *Phys. Rev. B.* **54**, 15 (1996).

[96] P. Pulay, *Chem. Phy. Lett.* **73**, 393 (1980).

[97] S. Hirata, H. Torii, and M. Tasumi, *Phys. Rev. B.* **57**, 19 (1998).

[98] J. Ding, Y. Tao, M. Day, J. Roovers, and M.D. Iorio, *J. Opt. A.* **4**, (2002).

[99] B. Norden and E. Krutmeijer, *The Royal Swedish Academic of Science.* (2002).

[100] L. Akcelrud, *Prog. Polym. Sci.* **28**, (2003).

[101] J. Ding, M. Day, G. Robertson, and J. Roovers, *Macromolecules.* **35**, 3474-3483 (2002).